NATURAL ABUNDANCE ^{13}C KIES ON GLUCOSIDE HYDROLYSIS BY NMR

USING NMR SPECTROSCOPY TO MEASURE NATURAL ABUNDANCE ^{13}C KINETIC ISOTOPE EFFECTS ON THE ACID CATALYZED AND ENZYMATIC HYDROLYSIS OF METHYL GLUCOSIDES

By

JASON K. LEE B.SC.

A thesis submitted to the faculty of graduate studies in the partial fulfillment of the requirements for the degree of Master of Sciences

McMaster University

Title: Using NMR Spectroscopy to Measure Natural Abundance ^{13}C Kinetic Isotope Effects on the Acid Catalyzed and Enzymatic Hydrolysis of Methyl Glucosides.

Author: Jason K. Lee B.Sc. (University of Waterloo, Ontario, Canada)

Supervisor: Dr. Paul J. Berti

Number of Pages: 146

Abstract:

Kinetic isotope effect (KIE) study of enzymatic mechanisms has the potential for aiding the design of tight binding inhibitors, but is hampered by the need for isotopically labeled substrates. Recently, however, methods for measuring ^{13}C and ^{2}H KIEs at natural abundance by NMR spectroscopy have been developed, allowing KIEs to be measured at every NMR resolvable nucleus without isotopic substitution. Until this study, this technique had yet to be applied to an enzymatic system. KIEs provide information about transition states (TS) and since enzymes tightly bind structures resembling the TS, TS analogs can be used as powerful inhibitors and potential drugs. Glycosidases are enzymes that hydrolyze the acetals of carbohydrates. Inhibition of glycosidases has a large potential for therapeutic value. Methyl glucoside hydrolysis was used as a model substrate in the measurement of natural abundance KIEs. ^{13}C KIEs were successfully measured on the acid and glucosidase catalyzed hydrolysis of methyl glucosides. The values of the primary ^{13}C KIEs show that hydrolysis of β-methyl glucoside by β-glucosidase a more concerted A_ND_N reaction. KIEs on the corresponding α-anomer suggest the opposite result, a $D_N{}^*A_N$ reaction. The experimental KIEs also matched well with calculated equilibrium isotope effects, lending support for the accuracy of the measurements.

Acknowledgments:

I would like to thank Dr. Paul Berti for giving me the opportunity to come to McMaster and work on this project. The project would not have been possible without the help of Dr. Alex Bain who provided much advice in all things NMR. As well, I would like to thank Brian Sayer and Dr. Donald Hughes of the McMaster University NMR facility. As well as, Joe McCann and Bartosz Byczynski for constant ideas and support. Finally, I would like to thank my wife Kathleen for unending encouragement and support.

Abbreviations:

ALPH - antiperiplanar lone pair hypothesis.

COSY - correlation spectroscopy (NMR)

EDTA - ethylene diamine tetra acetic acid

EIE - equilibrium isotope effect

EM - exponential multiplication

FID - free induction decay

GM - Gaussian multiplication

GB - Gaussian broadening

HSQC - homonuclear single quantum correlation (NMR)

KIE - kinetic isotope effect

LB - line broadening

NOE - nuclear Overhauser effect

NMR - nuclear magnetic resonance (spectroscopy)

RF - radio frequency

SDS-PAGE - sodium dodecyl sulfate –polyacrylamide gel electrophoresis

TLC - thin layer chromatography

TS - transition state

VD-Variable delay

ZPE - zero point energy

Table of Contents

1 Introduction:

By definition, enzymes stabilize the transition states of reactions; lowering the activation energy to catalyze reactions. It is imperative to understand the transition state of the reaction because (1) it allows an understanding of the enzyme mechanism and (2) enzyme inhibition by transition state analogs is a common technique for drug design. However, the transition state lasts only on the order of femtoseconds. Kinetic isotope effects (KIEs) are used to study the transition states of reactions because they reflect the change in bonding forces in going from the reactant state to the transition state. Using KIEs and transition state analysis, the transition state can be experimentally determined.

1.1 Isotope Effects:

A kinetic isotope effect (KIE) is the ratio of two reaction rate constants; where one reactant is isotopically substituted with a heavy atom (an isotopologue) and the other reactant does not contain heavy atom substitution. By convention, the KIE is always defined as:

$$KIE = {}^{light}k / {}^{heavy}k \qquad (1)$$

If the KIE is greater than 1.0, the KIE is called a *normal* kinetic isotope effect and if the KIE is less than 1.0, it is called an *inverse* kinetic isotope effect.

An isotope effect at one of the atoms where chemistry is occurring (i.e. an atom to which bonds are being formed or broken) is called a primary isotope effect. Isotope effects on any other atoms are referred to as secondary isotope effects. Isotope effects can also be measured on equilibrium processes, equilibrium isotope effects (EIE). EIEs are defined as:

$$EIE = {}^{light}K_{eq} / {}^{heavy}K_{eq} \quad (2)$$

1.2 The source of KIEs:

A simple model of a chemical bond is a spring that connects two spheres (or balls) in a system that behaves as a perfect harmonic oscillator. Such a model is poor at predicting chemical reactivity but it is an excellent model for describing how molecules vibrate. Quantum chemical programs such as *Gaussian* treat molecules as harmonic oscillators. Because IEs are vibrational phenomena, it is convenient and effective to treat molecules as harmonic oscillators.[1] The vibrational energy of a harmonic oscillator is defined by the equation:[2]

$$E_v = (v + ½)h/2\pi\,(k/\mu)^{1/2} \quad (3)$$

Where v is the vibrational quantum number (0,1,2,3...), k is the force constant of the spring and μ is the reduced mass of the spheres (m1*m2 / (m1+m2)).

The KIE is the product of three values:[3,4] the masses and moments of inertia (MMI), the zero point energy (ZPE) and the excited-state energy (EXC).

$$KIE = MMI*ZPE*EXC \quad (4)$$

Usually, the largest contribution to the KIE is differences in vibrational zero point energy (ZPE) for different isotopologues. The ZPE is the vibrational energy contained in a bond at the lowest energy level (when ν, the vibrational quantum number is zero) and its value depends on two factors, the mass of the atoms (μ) and the force constant (or strength) of the spring (k) in (3). When a reactant proceeds from the reactant state to the transition state, differences in ZPE cause differences in activation energy (E_a) for various isotopologues and hence changes in the corresponding reaction rates (Figure 1).

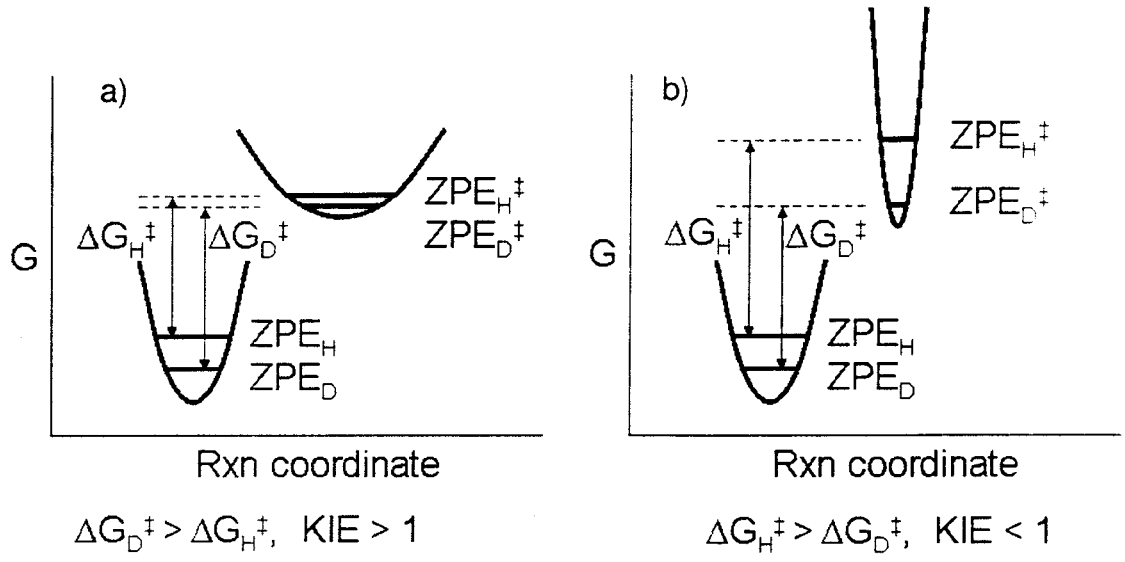

Figure 1. Potential energy curves of a C-H or C-D bond on going from the reactant state to the transition state. Secondary KIEs are shown. Differences in ZPE result from heavy atom substitution and changes in bonding force constants, (a) shows a normal isotope effect and b) shows an inverse isotope effect. The value of the KIE provides information on the vibrational environment at the transition state of reaction. A normal isotope effect implies a "looser" vibrational environment (a weakening bond) and an inverse isotope effect implies a "tighter" vibrational environment (a strengthening bond).

The value of the KIE (magnitude and inverse verses normal) provides information on the vibrational environment (bonding force constants and frequencies of the normal vibrational modes) of the atom for which the KIE is being measured. A normal isotope effect occurs when the ZPE difference is smaller at the TS than at the reactant state and indicates that the vibrational environment is "looser" at the transition state than the reactant state. An inverse isotope effect occurs when the ZPE

difference is larger at the TS than the reactant state, and indicates that the vibrational environment is "tighter" at the transition state.

1.3 Measuring KIEs:

The most common way of measuring KIEs is to use radioisotope labeled substrates and use scintillation counting to measure the relative amounts of labeled and unlabeled products. A reactant is synthesized with the heavy isotope (e.g., ^{3}H) at the site of interest. The light isotope at the position of interest (^{1}H in this case) is not radioactive, so a radioactive reporter label (^{14}C in this case) is introduced.

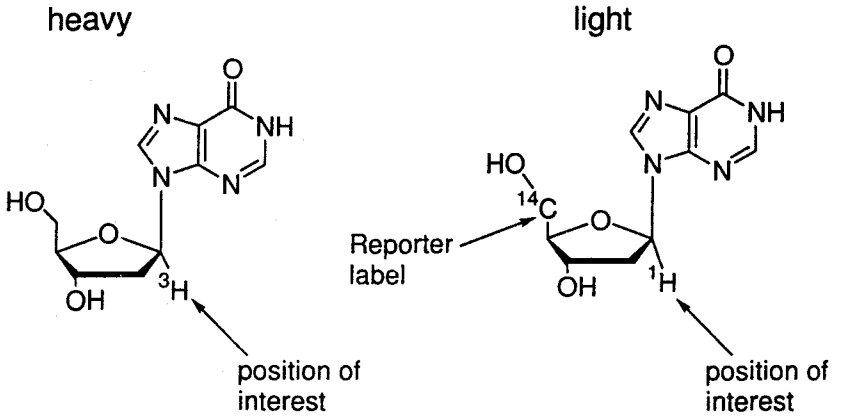

Figure 2. . The use of reporter labels allows quantification of the heavy and light products by scintillation counting and the determination of the ^{3}H KIE at the anomeric carbon. A reporter label is required for the light isotopologue because the light proton is not radioactive and cannot be measured by scintillation counting.

A significant amount of time in KIE measurement is devoted to synthesizing labeled substrates at every position for which a KIE is to be

measured. For accurate TS determination, a large number of labels are required. These syntheses require a great deal of research time; 2 years is not an unusual time for the synthesis of a complete set of isotopologues.

1.3.1 Competitive vs. noncompetitive KIE experiments:

In a competitive experiment, the two isotopologues are reacted concurrently in the same reaction vessel. In a noncompetitive experiment, the reactions of the different isotopologues are carried out independently, the kinetic constants are determined, and the KIE calculated as a ratio of these rate constants.

The accuracy of non-competitive KIEs is limited by the accuracy with which individual rate constants are known, typically ~5%. In competitive experiments, it is the ratio of rate constants for molecules reacting in the reaction mixture that is measured. This eliminates the largest source of experimental error and allows KIEs to be measured with accuracy of ±0.002 to ±0.005 (i.e., 0.2 to 0.5%).[5]

In a multi-step reaction, competitive experiments measure the KIE up to the first irreversible step of the reaction. Beyond this step, there is no more differentiation between isotopologues and no more information about the reaction is represented in the KIE. For enzymatic reactions, competitive experiments give KIEs that reflect the second order rate

constant (often called the specificity constant), k_{cat}/K_M.[6] However, noncompetitive KIE experiments can provide information on the every kinetic parameter (k_{cat}, K_M and k_{cat}/K_M).[5]

1.3.2 Commitment to catalysis:

In enzymatic reactions, "external commitment to catalysis" is important to the interpretation of KIEs. "External commitment to catalysis" occurs when an enzyme is so efficient that every molecule of substrate which binds to the enzyme is converted to products. In this situation, the first irreversible step of the reaction is substrate binding, not the chemical steps of catalysis and the KIEs will not contain information about the chemical steps of the reaction. To obtain information on the chemical step of the enzymatic reaction, the first irreversible step must also be the chemical step on the reaction. This is necessary to obtain any mechanistic information about catalysis and to measure KIEs for transition state (TS) analysis. Commitment to catalysis, that is, the contribution of substrate binding on the KIE can be measured by the isotope trapping methodologies of Rose.[7,8]

If substrate binding is kinetically significant then steps can be taken to make the chemical step of the reaction the first irreversible step, such as using unnatural substrates or changing reaction conditions, such as pH

or temperature. This can be an important consideration in multi-step reactions.

1.4 Measuring KIEs by NMR:

As early as 1981, natural abundance ^{2}H NMR has been used in determining the source and chemical history of molecules because of the unique distribution of deuterium atoms.[9,10] Using this idea, Pascal and coworkers showed the utility of natural abundance ^{2}H NMR for measuring KIEs by measuring a primary ^{2}H KIE on the elimination reaction of 2-bromoethyl benzene[11] and a number of other reactions including a secondary KIE on the dimerization of ketene.[12] Since that time, Zhang and coworkers have demonstrated: the simultaneous measurement of primary and secondary KIEs,[13,14] the use of internal and external references[13,15] and the measurement of equilibrium isotope effects (EIE) by ^{2}H NMR. The measurement of KIEs was not precise enough to be used in ^{13}C KIE measurement.

By carefully considering the errors involved in KIE measurement, Singleton introduced a simple method for the measurement of high precision ^{13}C and ^{2}H KIEs.[16] This is a competitive experiment; the KIEs measured in this manner represent the first irreversible step of the reaction. Rather than synthesizing isotopologues needed for the KIE measurement, the experiments are carried out at natural abundance.

Nature provides the substitution of heavy atoms at all possible positions in the molecule. As a reaction proceeds, the starting material will become enriched in the slower reacting isotopes and when the reaction nears completion, the enrichment of slower reacting isotopes will be sufficient to be measured by NMR (Figure 3).

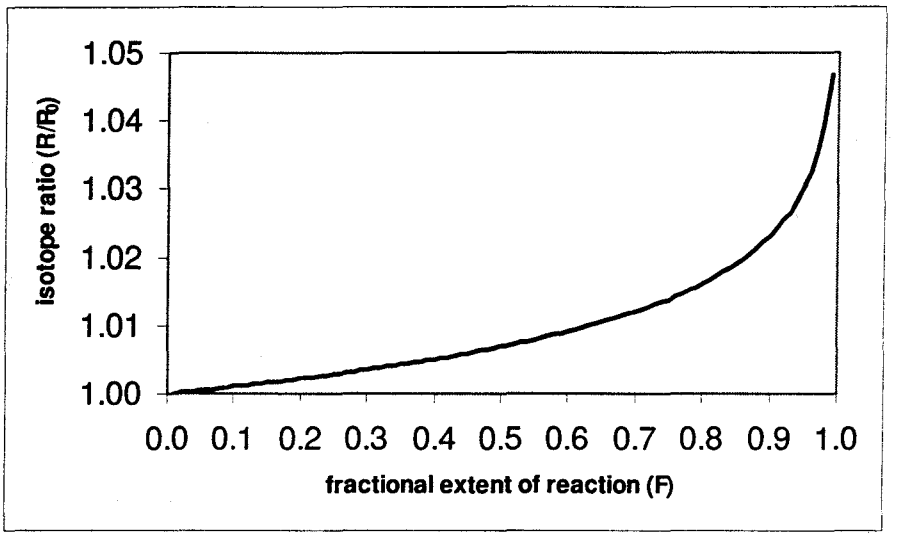

Figure 3. The enrichment of slower reacting isotopes in the starting material over the course of a reaction is the basis for the measurement of small KIEs by NMR at natural abundance. At 90% completion (F=0.9), a 1% isotope effect (1.01) gives an isotope enrichment of greater than 2%.

In a typical experiment, a reaction is carried to 90% completion and the remaining 10% reactant is re-purified. The enriched reactant is compared to the non-enriched reactant and the relative ^{13}C and ^{2}H peak areas are used to determine the isotope ratio (R/R_0). Using the isotope ratio and the extent of the reaction (F), the KIE is calculated:

$$KIE = \ln (1-F) / \ln[(1-F)R/R_0] \quad (5)$$

All peak areas are referenced to a remote atom, away from the site of chemistry, where no KIE is expected. The experimental KIEs are measured relative to this reference atom. The most obvious advantage of this type of KIE measurement is that isotopic substitution is not necessary and that the KIEs can be measured on all NMR resolvable nuclei simultaneously! Limitations to the technique include the fact that the KIEs are limited to NMR active nuclei (primarily ^{13}C, ^{2}H), which provide smaller KIEs compared to ^{14}C and ^{3}H. Cost is also a potential limitation. The reactions must be inexpensive enough to provide enough enriched starting material that an NMR spectrum with a good signal to noise can be acquired. The technique also requires that the small amount of residual reactant must be isolatable from a large amount of product. Finally, there is a limit on the molecular weight of the reactant because: (1) the probability of having more than one heavy atom in the substrate increases with molecule size, leading to an increasing probability of a molecule being doubly-labeled and (2) molecules of smaller molecular weight will have a larger NMR signal because a higher concentration can be attained in the NMR sample.

Since the initial paper in 1995, Singleton and coworkers have gone on to study a large number of reactions, including: Diels-Alder, ester aminolysis, ene reactions and Claisen rearrangements.[17,18,19,20] He has also described simultaneous determinations of intermolecular and

intramolecular ^{13}C and ^{2}H KIEs,[21] measured ^{17}O KIEs,[20] and described a new type of isotope effect on dynamic effects.[22] As powerful as this technique is, however, it has yet to be used to measure KIEs for enzyme catalyzed reactions.

1.5 Quantitative NMR:

In the presence of a magnetic field (B_o), a spin 1/2 nucleus orients itself into 2 energy levels by attempting to align its magnetic moment with the direction of the magnetic field, like a bar magnet in the presence of the Earth's magnetic field, **Figure 4**(a). At equilibrium, the populations of nuclei distributed between the two energy levels are determined by the Boltzman distribution, with slightly more in the lower energy (α) state. The application of a radiofrequency (RF) pulse to the nuclei causes the transition of the nuclear spin from the lower energetic state (α) to the higher energetic state (β). Since NMR samples are composed of many nuclei, it is the differences in the α and β populations are represented by the macroscopic magnetization vector (M). Diagrammatically, the NMR experiment is represented by the flipping of the macroscopic magnetization vector (M) from the z-axis towards the y-axis, **Figure 4**(b).

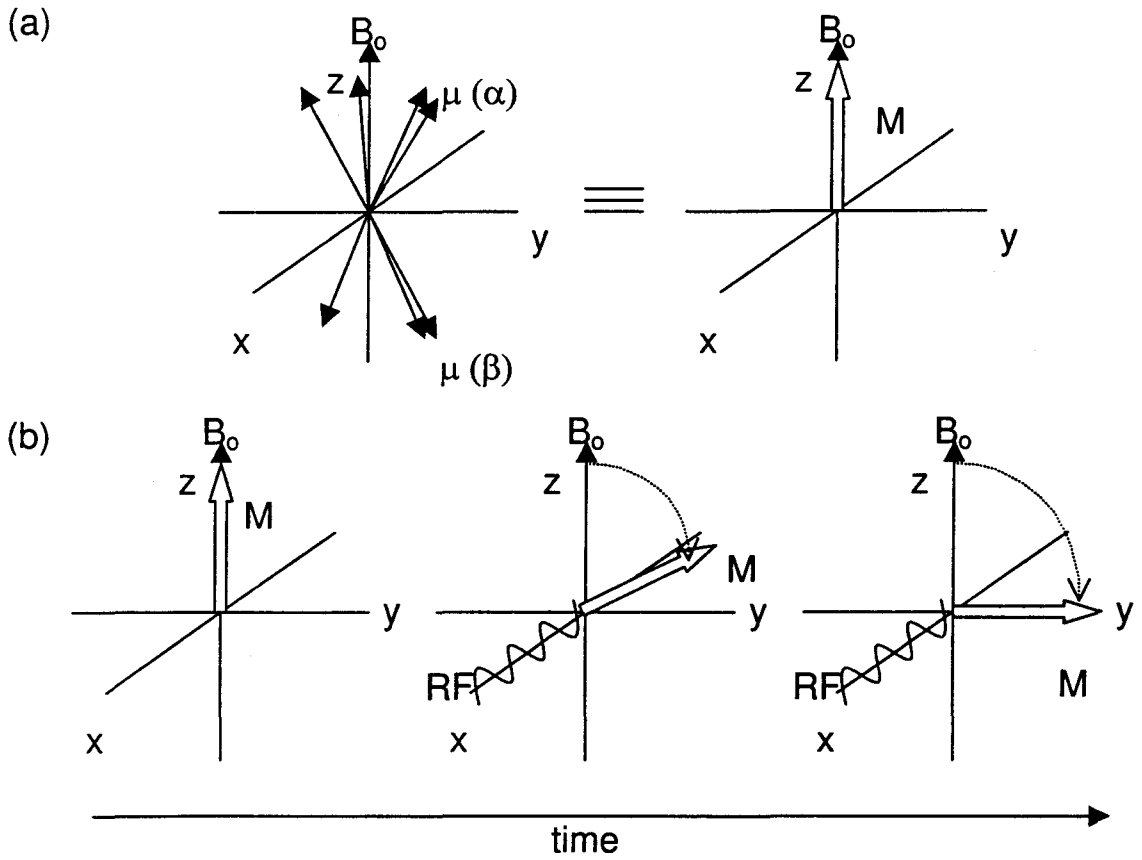

Figure 4. (a)The magnetic moments of the nuclei are distributed between the α and β spin states in magnetic field (B_o) (b) The macroscopic magnetization vector (M) flips in an NMR experiment, representing increases in the population of nuclei in the higher (β) energetic state.

The relaxation of nuclei back to the lower energetic state, called free induction decay (FID), generates an electromotive force in the instrument receiver coils observing the contribution of M in the x,y plane. Usually, one NMR pulse is insufficient to achieve a sufficient signal to noise ratio for quantitative peak measurement. A number of NMR pulses are applied with a delay (D1) between pulses to ensure relaxation of nuclei before the

next RF pulse. After the acquisition of the FID, the data is mathematically converted from the time domain to the frequency domain by Fourier transformation, giving the NMR spectrum.

In principle, the area of the peak in the NMR spectrum corresponds to the relative amount of the nucleus measured (i.e. ^{13}C in ^{13}C NMR) in a given position of the molecule. To achieve truly quantitative measurements, however, three criteria must be met.[23],[24] The first criterion relates to the relaxation of the nuclei. The relaxation of nuclear spin was first modeled by Bloch, who assumed that relaxation was a first-order process. He described the relaxation with three equations (known as the Bloch equations), which relate relaxation to two lifetimes T1 and T2. The relaxation times T1 and T2 are known as the spin-lattice (longitudinal) and spin-spin (transverse) relaxation times, respectively. The relaxation times are the lifetimes for first order decay, i.e. the inverse of the first-order rate constant for exponential decay. In general, T1 is the longest relaxation time and is important to quantitative NMR because complete relaxation of nuclei to the equilibrium populations between RF pulses is needed. If inadequate time is allowed between RF pulses, loss of signal intensity in the NMR peaks will occur. As a general rule, 5 to 10 times the longest T1 (the T1s of nuclei in a molecule differ according to substitution and motion) is needed for complete relaxation. To determine T1 relaxation times of the nuclei, the *inversion-recovery* method is used with the pulse sequence

180°- VD –90°-AQ. The nuclei are given a 180° pulse and allowed to relax for a variable delay (VD) at which time a 90° is applied and the FID acquired (AQ). The result is a first-order (exponential) increase in peak area as a function of delay time, which provides the decay rate and relaxation time T1.

The second criterion needed for quantitative NMR is elimination of the Nuclear Overhauser Effect (NOE). Peaks (specific nuclei) in the NMR spectrum can be selectively saturated by irradiation of the NMR sample at the resonance frequency for the particular nucleus, which equalizes the α and β populations. The NOE occurs when the saturation of one peak causes the increase or decrease in intensity of another peak in the NMR spectrum. The nuclei that are affected by the NOE are usually close in space to the suppressed nuclei. This is because the NOE occurs through dipolar interactions that depend on distance. However, this change in intensity is not reliable and must be eliminated if quantitative peak measurement is required.

In the case of ^{13}C NMR, the suppression of the proton peaks by broad-band decoupling causes (1) the collapse of the coupled peaks into singlets when applied during the acquisition (2) an increase in peak intensity due to the NOE when applied during the RF pulse. To eliminate NOEs, decoupling must be on only during the acquisition, and is termed

inverse-gated decoupling. This is because decoupling only during the acquisition does not give enough time for the NOE to develop.

Lastly, digital resolution is important. To properly define the shape of a peak, enough points should be collected such that information (peak area) is not lost at the top of the peak. If the digital resolution is greater than 0.4 of the peak width, then the maximal error on the integration will be only 0.1%.[25] For example, for a peak width of 1 Hz, a digital resolution of 0.4 Hz/point is needed for an error of better than 0.1%.

1.5.1 Apodization or window functions

An apodization function is a mathematical function that is used to alter the FID, and therefore the appearance of the transformed spectrum. The shape of the peaks in the spectrum relates to decay characteristics of the FID and mathematically results from the Fourier Transformation. By manipulating the FID, the appearance of the transformed spectrum can be improved. The integral information (area) is related to the first few points in the FID. Ideally, the apodization function should alter the shape of the FID and transformed spectrum, but keep the area information intact. The benefits of using apodization functions are improved signal to noise ratio and improved peak resolution. Two commonly used apodization functions are *exponential multiplication* and *Gaussian multiplication.*

Exponential multiplication is normally used and the exponential decay of the FID gives Lorentzian line shapes. The exponential function is manipulated with a parameter called line broadening (LB) which is measured in Hz and can have any positive or negative value (but 0 to 5 Hz is most commonly used). Higher values of LB give better signal to noise in the spectrum, but also cause the broadening of peaks. Therefore, a balance must be found that gives good signal to noise, but also adequate peak resolution. The drawback of using Lorentzian line shapes for quantitative NMR is that the Lorentzian line shapes are broad along the baseline, meaning that peaks with similar chemical shifts may be difficult to completely resolve.

Gaussian peak shapes, on the other hand, are much narrower at the baseline and are better suited for resolution of closely spaced peaks. The Gaussian multiplication is composed of two functions. The first parameter used is LB, as in the exponential function, but negative values of LB are used. The effect of a negative value of LB is to cause the peaks in the spectrum to narrow, giving superior peak resolution. However, a negative LB also causes an increase in the noise. To counteract the increased noise, a second function imposes a decay to the FID which suppresses the noise and gives a Gaussian shape to the NMR peaks. The Gaussian function is manipulated by a variable called Gaussian broadening (GB) which has values between 0 and 10. The GB represents the fraction of

the FID to which the Gaussian function is applied and therefore it determines the point in the FID where the function reaches a maximum before Gaussian decay. Gaussian functions can introduce artefacts in the FID and affect the intensity of sharp peaks in the spectrum. By using a very small value of GB and small negative value of LB, these artefacts are avoided.

1.6 Using KIEs to study enzymatic reaction mechanisms:

A large number of techniques are employed to probe mechanisms of enzymatic catalysis. Characterization of rate limiting steps by Bronsted relationships, the contribution of non-covalent interactions to catalysis (i.e. binding energy) by point mutations and covalent intermediate trapping are just a few. The only technique that allows the direct determination of transition state structures is by measuring multiple KIEs. Furthermore, KIEs provide information on the environments of single atoms, (i.e. high resolution data) as opposed to Bronsted analyses or transition state analog studies from which one can only infer the overall nature transition state structures. Therefore, KIE studies have played an important role in elucidating enzymatic mechanisms; but have also contributed to the design of transition state analogues, which are used as therapeutics and in x-ray crystallographic studies.

1.61 Use of KIEs in drug design:

Transition state theory states that the reaction rate enhancement imparted by enzymes is approximately equal to the affinity of the enzyme for the transition state structure over the reactant-state structure (or substrate).[26]

$$k_e/k_n \approx K_T/K_S \quad (6)$$

Where k_e and k_n are the reaction rate constants for the enzymatic and spontaneous reactions respectively. K_T and K_S are the equilibrium constants for enzymatic binding of the transition state and substrate respectively. Rate enhancements on the order of 10^{17} fold over non-enzymatic reactions have been observed. In other words, enzymes can bind the transition state on the order of 10^{17}-fold more tightly than the substrate. The design of transition state mimics is an important aspect of drug design, as an overwhelmingly large number of drugs either inhibit or modify enzyme activity by binding and blocking the enzyme active site. Penicillin, an antibiotic, works by inhibition of transpeptidases, enzymes involved in the production of bacterial cell walls. PROZAC™, a common anti-depressant drug affects brain chemistry by inhibiting the reuptake of the neurotransmitter serotonin, thereby prolonging its effect.[27]

The power of KIEs to study enzymatic reactions is clear. The ability to experimentally determine the transition state structure of an enzymatic reaction leads directly to the design of target transition state mimics for synthesis. The synthesis of gigantic molecular libraries coupled to high through-put screening methodologies can be costly, time-consuming and may not even lead to a useable molecule. If the enzymatic TS is known, it becomes possible to use more specific, targeted, libraries of compounds, increasing the probability of success

Already, KIE techniques have been used in the study of: diphtheria toxin,[28] pertussus toxin,[29] ricin,[30,31] sialyl transferases,[32] malic enzyme,[33,34,35,36] nucleoside hydrolases,[37] cholera toxin[38] and uracil DNA glycosylase.[39] Also, KIE study of inosine hydrolysis by purine nucleoside phosphorylase (PNP) yielded a transition state structure in atomic detail. From these studies, nanomolar RNA stem loop inhibitors of ricin[40] and immucilin-H[41,42] (for PNP) were synthesized. The design of immucilin-H included the replacement of the ribose oxygen with a positively charged nitrogen atom (mimicking the build up of positive charge at the transition state) and a non-hydrolyzable carbon-carbon bond to the nitrogenous base (Figure 5). It is a picomolar inhibitor that is currently in clinical trials for treatment of T-cell lymphoma.

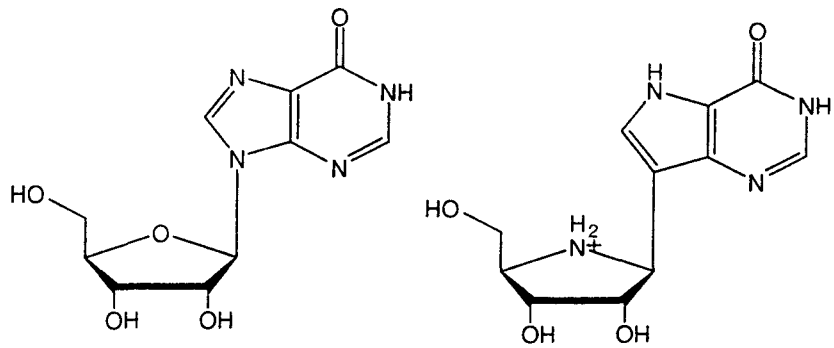

Figure 5. The picomolar enzyme inhibitor immucilin H (right) mimics the TS of inosine (left) hydrolysis by purine nucleoside phosphorylase and was designed through KIE study of the enzyme mechanism. It is a potential therapeutic for T-cell lymphoma and is currently undergoing clinical trial.

1.7 The chemistry of glycosides:

An *O*-glycosidic bond is the exocyclic carbon-oxygen bond of an acetal; the condensation product of the anomeric carbon of a carbohydrate, such as glucose (the glycone) with an alcohol (the aglycone). The aglycone can be a carbohydrate, as is the case for maltose **1** (a disaccharide containing two glucose units). The aglycone can also be an alkyl alcohol such as methanol, giving methyl glucopyranoside **α-2**, **β-2**.

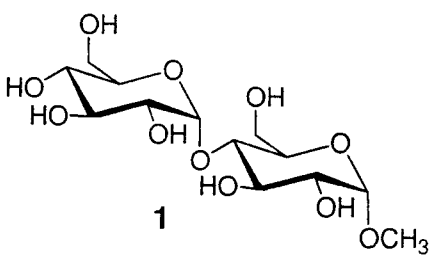

1

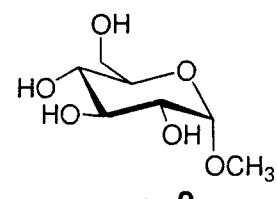

α–2

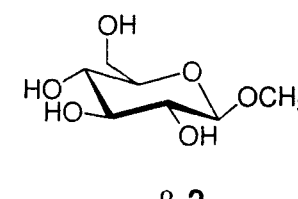

β-2

Glycosides occur widely in nature and have also been utilized in pharmaceuticals. For example, salicilin, a hydroxymethylphenol glucoside is naturally produced in the bark of willow trees and has been a known analgesic since the time of ancient Greece.[46] Digitoxin is another example, having uses in regulating heart rate and rhythm. Moreover, cellulose consists of repeating glucose units and is likely the most abundant organic substance on Earth.[46]

The glycosidic bond is one of the most stable biopolymer linkages in nature. For example, methyl glucoside has a half-life of over 4.5 million years for spontaneous hydrolysis at room temperature and neutral pH.[43] This is a tremendous amount of time when considering that nucleic acid and peptide bonds have half lives of 140 000 and 460 years, respectively.[44,45] Of course, Nature has found other ways to overcome the seemingly indestructible bond by enzymatic catalysis.

In solution, monosaccharides exist in equilibrium between straight chain (aldehyde) and closed (hemiacetal) cyclic forms (pyranose or furanose). There are two stereochemical outcomes of ring closure, which result in the formation of the α- and β-anomers. The α-anomer has the C1 hydroxyl in an axial position and the β anomer with an equatorial hydroxyl. Since an *O*-glycoside is an acetal, the α/β anomers can only epimerize at acidic pHs, resulting in two isolatable anomers having different

properties.[46] To explain the differences on α/β reactivity, the anomeric effect and the anti-periplanar lone pair hypothesis (ALPH) have been invoked.

The anomeric effect[47,48] is a term that is used to describe the preponderance of α-glycosides over β-glycosides despite conventional wisdom that would predict a more stable equatorial β-anomer because of a smaller amount of steric hindrance. The effect is explained in two ways: (1) unfavorable electrostatic interactions between the endo and exocyclic oxygen lone pair electrons in the β-anomer (but not α-)[49] and (2) the O5 lone pair electrons are positioned to donate electron density (hyperconjugate) to the σ* anti-bonding molecular orbital of the C1-exocyclic bond only in the α-anomer. This would tend to weaken and therefore, lengthen the α- C1-O bond, providing a lower energy structure.[50]

The anti-periplanar lone pair hypothesis (ALPH) is a stereo-electronic model that has been used to predict the geometry of acetal hydrolysis.[51,52] In the case of glucoside hydrolysis, the hypothesis states that the C1-LG bond must hydrolyze such that it is anti-periplanar to the ring oxygen lone pair electrons. The conformational implications are that **α-2** should hydrolyze as a $^4C_1$ chair (*vide infra*) and the **β-2** should hydrolyze by a

transition state resembling a boat in order to fulfill the stereoelectronic requirement.

Pyranoses can exist in a number of possible ring conformations (Figure 6). The conformations: chair, boat, half-chair and skew are represented by the single letters C, B, H and S respectively. Superscripted numbers on the left of the letter, represent carbons that are above the plane of the ring, while subscripted numbers to the right of the letter represent the carbons that are below the plane of the ring. For example, $^{4}C_{1}$ is a chair conformation with the number 4 carbon (C4) above the plane of ring and the number 1 carbon (C1) below the plane of the ring.

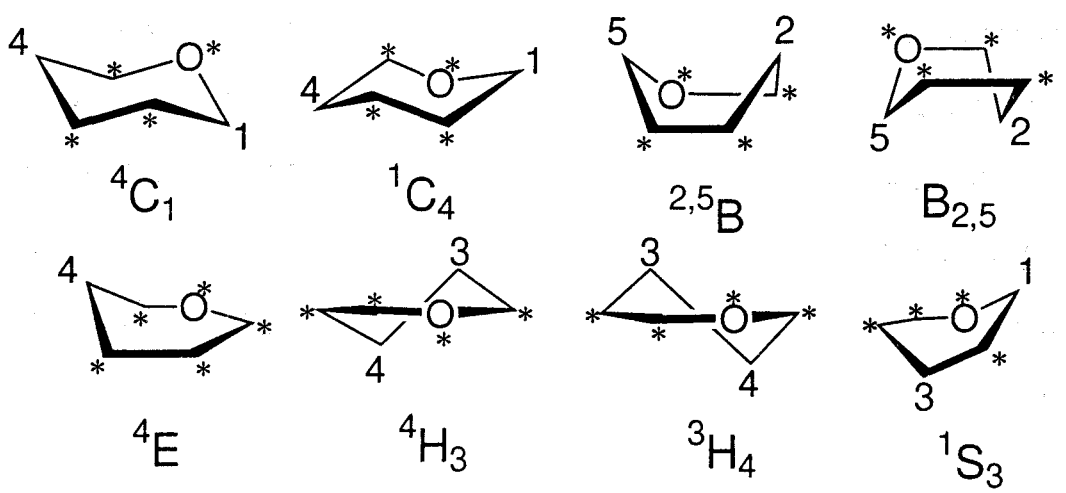

Figure 6. Some possible conformations of pyranoses: chair (C), boat (B), envelope (E), half-chair (H) and skew (S). The hydroxyl and hydroxyl-methyl groups have been omitted for clarity. The coplanar atoms are indicated by the asterisks. Superscripted numbers indicate atoms that are above the plane and subscripted numbers show atoms below the plane.

1.8 Glycosidases (glycoside hydrolyases):

Glycosidases (or glycoside hydrolases) are enzymes that hydrolyze o-glycosidic bonds. Recently, the structural and sequence-based information available on such enzymes has increased astronomically, and as of 1999, over 2000 predicted glycosidase sequences were available.[53] A number of recent reviews have been written on the subject of glycosidases and glycosyl transferases.[54,55,56,57,58]

The interest in glycosidases has arisen for a number of reasons. First, the rate enhancement imparted by glycosidases when compared to spontaneous hydrolysis is quite astounding, reaching rate enhancements of 10^{17} fold,[55] attracting interest from enzymologists who wish to study the mechanistic and structural reasons for such rate enhancements. Second, glycosyl transferases and glycosidases have been utilized by bio-organic chemists to synthesize increasingly complex carbohydrates.[59] Third, glycosidases have a diverse physiological importance, having roles in everything from carbohydrate digestion to glycoprotein processing (and/or post-transiational modifications).

It is the large physiological scope of glycosidases that has captured the attentions of many researchers, in the hopes of treating a large number of diseases.[60] For example, glycosidase inhibitors have the potential for treatment of: cancer metastasis,[61] viral infections (HIV and

hepatitis)[62,63] and metabolic disorders (lysosomal storage diseases and diabetes).[64] Therefore, much interest has been associated with glycoside inhibition.[65, 66, 67, 68, 69]

1.8.1 Glycosidase classification:

There has been a recent move to classify glycosidases by 3D structural and sequence based similarity.[53,*] The enzymes have been classified into 70 families and also further grouped in "clans" that share similarities in their 3D structure.

Almond β-glucosidase, one of the enzymes used in this study, has been recently identified as a family 1 glucosidase by labeling of the active site nucleophile, digestion and peptide sequencing.[70] The assignment was based on the sequence similarity to clover[71] and *Agrobacterium faecalis*[72] β-glucosidases, both family 1 glycosidases. Family 1 glycosidases are characterized by a conserved $(\alpha/\beta)_8$ fold, a structural motif in the protein composed of repeating α-helices and β-sheets.

Glycosidases are commonly classified by two mutually independent criteria. The first criterion is based on the anomeric stereochemistry of

---

* The current information on glycosidases can be accessed at http://www.expasy.org/cgi-bin/lists?glycosid.txt.

substrates. Glycosidases are classified as either *α* or *β*, depending if they hydrolyze α- or β- glycosides. The second criterion is mechanism-based, and describes whether the anomeric stereochemistry is *retained* or *inverted* (Figure 7).

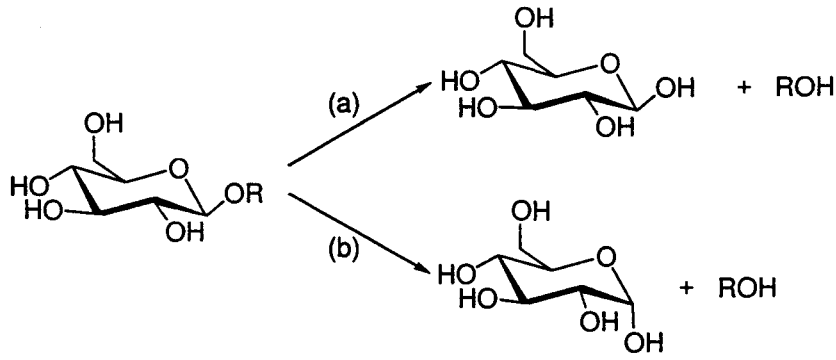

Figure 7. The products of (a) retaining and (b) inverting β-glucosidases.

1.8.2 Glycosidase mechanisms, inversion and retention:

As there are two possible stereochemical outcomes of the hydrolysis reaction (inverting or retaining), there must be two distinct mechanisms to account for this observation. A common feature of all glycosidases is the positioning of two carboxyl-containing amino acid side chains (glutamate or aspartate) above and below the site of glycoside hydrolysis in the enzyme active site. These carboxyls act as either a nucleophile or a general acid/base.

Inverting glycosidases use the carboxyls in a single-displacement mechanism, and are spaced 10.5 Å apart such that a water molecule can

fit between the substrate and the side chain, facilitating hydrolysis.[73] The reaction proceeds through a transition state that has oxocarbenium ion character, which contains a partial positive charge on the endocyclic carbohydrate oxygen and a bond order of >1 between the anomeric carbon and the endocyclic oxygen (Figure 8).

Retaining glycosidases, have carboxyls that are spaced ~5 Å, closer together than inverting enzymes,[73] which does not allow sufficient space for a nucleophilic water molecule in the active site in addition to the substrate. The reaction proceeds through a double-displacement mechanism.[73] Again, both reactions (glycosylation and deglycosylation) proceed through transition states containing oxocarbenium ion **3** character (Figure 8).

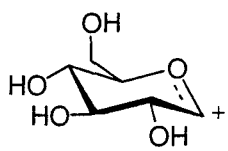

3

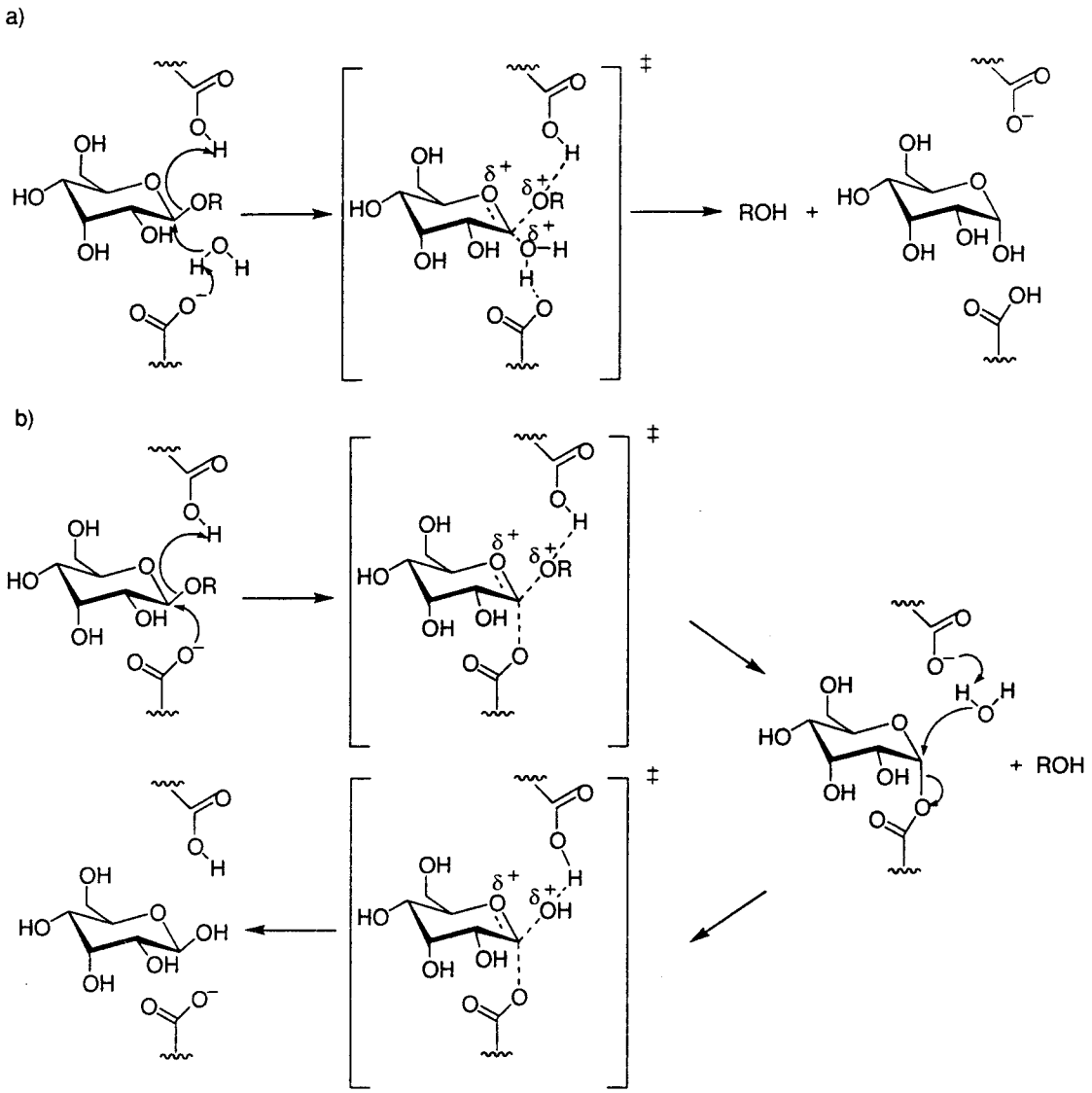

Figure 8. Proposed mechanism of a) inverting and b) retaining glucosidases. A glucosyl oxocarbenium ion is shown in c). The transition states of the glucosidase mechanisms are thought to resemble the oxocarbenium ion **3**.

The mechanism first proposed by Koshland[74] for retaining glycosidases has since been shown to be largely correct.[55,75] The mechanism is shown in Figure **8** b and is characterized by having an

enzyme-bound intermediate as opposed to the Philips mechanism in which a free oxocarbenium ion **3** is stabilized by electrostatic interactions to an active site nucleophile. Glycosidase mechanisms have been a point of controversy, however, in that the exact nature of the transition state, though known to be oxocarbenium ion-like, is not entirely understood. A number of questions remain: (1) what is the extent of nucleophilic involvement at the transition state (does the reaction go through an A_ND_N or $D_N{}^*A_N$[†,76] mechanism)? (2) What is the ring conformation at the transition state? (3) Is a discrete oxocarbenium ion formed and what is the bond order of the C1-endocyclic oxygen bond? (4) To what extent is the C1-leaving group bond broken? (5) What is the timing of the bond making and bond breaking process? Over the last two decades, a substantial amount of work has attempted to answer these questions, a large part of which includes KIE studies.

[†] The notation A_ND_N refers to a bimolecular mechanism (S_N2, where A = association, D = dissociation and N = nucleophile). $D_N{+}A_N$ refers to a stepwise mechanism (S_N1) where the cation is stable enough to completely dissociate whereas in a $D_N{}^*A_N$ mechanism, the cation is too unstable to diffuse completely.

1.8.3 Lifetime of glycosyl oxocarbenium ions:

Jencks and coworkers first estimated the lifetime of glucosyl oxocarbenium ions **3** to be on the order of 10^{-11} to 10^{-15} s by trapping of the oxocarbenium ion using a sulfite dianion and by structure/activity relationships.[77] They later refined the estimated lifetime of the glycosyl oxocarbenium to be ~10^{-12} s.[78] A lifetime on this order is only slightly longer than a single bond vibration (10^{-13}s), but is nonetheless a finite lifetime. A major conclusion from these studies was that the glucosyl oxocarbenium ion can exist in solution for a finite lifetime, but only in the absence of good nucleophiles. Support for this conclusion was also noted by Zhang *et al*[85] who found a much larger α-^{13}C KIE for the fluoro-glucoside hydrolysis compared to methyl-glucoside hydrolysis.[84] This result indicates that the glucosyl oxocarbenium ion can exist in the presence of the neutral methanol leaving group, but not the anionic fluoride. Therefore, $D_N{}^*A_N$ reactions are possible for methyl glucosides which have neutral leaving groups.

1.8.4 KIE studies:

The meaning of KIEs measured on glycosides:

The magnitude of the primary ^{13}C KIE (C1 or anomeric carbon) is a direct indication of nucleophilic involvement at the TS and therefore the type of hydrolysis mechanism ($D_N{}^*A_N$ or A_ND_N). A primary ^{13}C KIE in the

range of 1.00-1.01 indicates a $D_N{}^*A_N$ mechanism, whereas a KIE in the range of 1.03-1.08, indicates an A_ND_N mechanism.[79] There is a difference in isotope effects between the two mechanisms because there is a contribution to the isotope effect from the reaction coordinate motion in addition to the ZPE.[5,80]

The α-secondary ^2H KIE cannot be used to distinguish $D_N{}^*A_N$ and A_ND_N reactions as previously thought. At one time, a large KIE at this position was used to support an $D_N + A_N$ reaction for glucoside hydrolysis because a large value would indicate the formation of a discrete oxocarbenium ion and the accompanying change in the C1-endocyclic oxygen bond hybridization from sp^3 to sp^2. To date, large isotope effects have been measured at the α- secondary-^2H position, regardless of mechanism and the interpretation of the KIE is tenuous.[81,82]

The β-secondary ^2H KIE provides hyperconjugative arguments used to derive conformational information at the TS. Hyperconjugation is donation of electron density from a valence orbital (of a C-H bond) that has π-type symmetry to a vacant p-orbital on C^+. While stabilizing the carbocation, the electron donation causes a weakening of the C-H bond, which changes the vibrational environment of the proton and causes a KIE. The value of the KIE depends on the angular geometry of the C2 proton to the positively charged p-orbital on C1.[83]

The glucoside oxygen atom KIEs also provide a lot of information. The leaving group KIE (^{18}O) results from bond order changes to C1 and the value can give information on the extent of glycone-aglycone bond cleavage. Endocyclic ^{18}O KIEs result from bond order changes to C1. The positive charge, however, tends to remain on the C1 and not the O atom.[5]

1.8.5 Acid catalyzed and spontaneous hydrolysis of glycosides:

A number of glucoside hydrolysis reactions including methyl (**2**)[84] , fluoro (**4**)[85], isoquinolinium-glucosides (**5**)[86] as well as methyl-xylosides (**6**)[87] have been examined. KIEs on methyl-5-thioxylopyranoside (**7**) hydrolysis have also been measured.[87] The KIE results are summarized (Table 1).

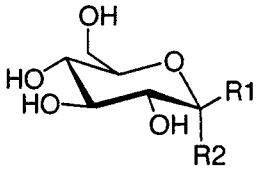

R1=H,R2=F α-**4**
R1=F,R2=H β-**4**

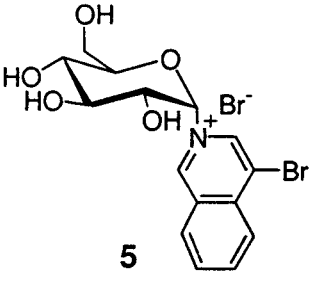

5

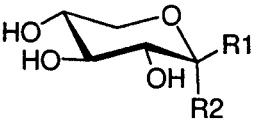

R1=H,R2=OMe α-**6**
R1=OMe,R2=H β-**6**

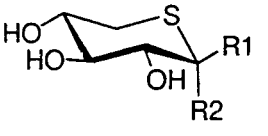

R1=H,R2=OMe α-**7**
R1=OMe,R2=H β-**7**

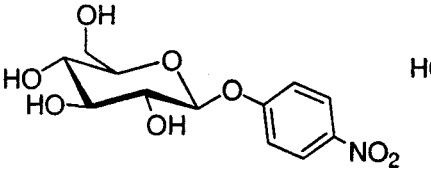

8

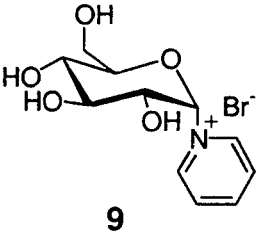

9

Table 1. A summary KIEs measured on acid catalyzed reactions of various glucosides.

pyranoside	C1 ^{13}C	α-^{2}H	β-^{2}H	γ-^{2}H	Endo ^{18}O	Exo ^{18}O
α-2[84]	1.007	1.137	1.073	0.987	0.996	1.026
β-2[84]	1.011	1.089	1.045	0.971	0.991	1.024
α-4[84]	1.032	1.142	1.067	0.979	0.984	-
β-4[84]	1.016	1.105	1.059	0.981	0.988	-
5[86]	1.005	1.189	1.094	-	-	1.015 (^{15}N)
α-6[87]	1.006	1.128	1.088	0.986	0.983	1.023
β-6[87]	1.006	1.098	1.042	0.967	0.978	1.023
α-7[87]	1.031	1.142	1.061	0.999	-	1.027
β-7[87]	1.028	1.094	1.018	0.986	-	1.035
8[88]	-	-	-	-	-	1.0355

Neutral Leaving Groups:

KIEs on the acid catalyzed hydrolysis of both α- and β- anomers of methyl glucoside **α-2** and **β-2** were measured by Bennet and Sinnott and the results are summarized in Table 1. The inverse IE for endocyclic (ring) oxygen confirms the double bond character to the anomeric carbon, which is consistent with formation of an oxocarbenium-like transition state. The magnitude of the exocyclic (aglycone) ^{18}O KIE suggests that the glycosidic bond is largely broken at the transition state. The ring conformation at the transition state for the α-anomer was deduced to be a $^{1}S_3$ skew boat and the β-anomer through a flattened $^{4}C_1$ chair TS, which contradicts the ALPH. The KIEs suggest that there is no nucleophilic assistance (the reaction is $D_N{}^*A_N$).

The KIEs measured on methyl xylosides (**6**) are similar to the methyl glucoside hydrolyses and thus afford the same conclusions: a largely broken glycone-aglycone bond at the TS, no nucleophilic assistance ($D_N{}^*A_N$) and the formation of oxocarbenium ion character. Larger inverse endocyclic ^{18}O KIEs for the xylosides suggest a greater development of positive charge on the ring oxygen and a more fully sp^2 hybridized C1-O bond.

The small primary ^{13}C KIE measured on *N*-glucosides (pyridinium **9** and isoquinolinium **5**) hydrolysis showed also that there was no nucleophilic assistance ($D_N{}^*A_N$ mechanism). The ^{15}N KIE shows significant C-N bond cleavage at the transition state and the β- secondary ^2H KIE shows more hyperconjugation than in the methyl-glucoside which indicates differences in TS geometry.

1.8.6 Anionic Leaving Groups:

The KIEs measured on the fluoro-glucosides[84] are in stark contrast to the glucosides with neutral leaving groups. The magnitude of the primary ^{13}C KIEs suggest nucleophilic assistance and A_ND_N (S_N2) reactions. The transition state was a $^4C_1$ chair, which also is different from the boat and skew conformations determined for the methyl glucosides.

In general, neutral leaving groups show a number of commonalities. There seems to always be a $D_N{}^*A_N$ mechanism and significant amount of

cleavage of the leaving group bond at the transition state. Anionic leaving groups hydrolyze by A_ND_N reactions.

1.8.7 Enzymatic hydrolysis of glycosides:

A number of KIEs on enzyme catalyzed reactions have been measured and are summarized (Table 2) including: β-4-nitrophenyl-glucoside (**8**)[88], fluoro-glucoside (**α-4**)[89] and pyridinium/isoquinolinium glucosides **5** and **9**.[86]

Table 2. A summary of KIEs measured on enzymatic hydrolyses of glycosides

Glucoside	C_1 ^{13}C	α ^3H	β ^3H	6-^3H	exo ^{18}O	exo ^{15}N	type	enzyme
α-4[89]	1.007[90]	1.103	1.039	1.033	-	-	k_{cat}/K_m	α-glucosidase (beet)
5[86]	1.019	-	1.106	-	-	0.985	k_{cat}	α-glucosidase (yeast)
8[91]	-	-	-	-	1.0377	-	k_{cat}/K_m	β-glucosidase
9[86]	1.027	-	1.115	-	-	1.019	k_{cat}	α-glucosidase (yeast)

The KIEs on the enzymatic hydrolysis of β-nitrophenyl-glucosides were measured by Rosenberg and Kirsch.[91] The large ^{18}O KIEs measured indicate that the C-O bond is being cleaved at the TS and is therefore the first irreversible step.

Enzymatic hydrolysis of **α-4** is more dissociative as indicated by the small primary ^{13}C KIE. The transition state determined for the hydrolysis

is a flattened $^4C_1$ chair. Surprisingly, Tanaka *et al.* found that the experimental transition state would be stable enough in the enzyme active site to be attacked after the fluoride has departed (supported by the KIEs) which is in contrast to the findings of fluoro-glucoside hydrolysis in solution.[89] Pyridinium glucosides which have neutral leaving groups showed A_ND_N mechanisms with a small amount of nucleophilic assistance.

The major conclusions are that the glucosides with neutral leaving groups occur by A_ND_N reactions and the glucosides with anionic leaving groups occur by $D_N{}^*A_N$ reactions.[5] The conclusion is the opposite of what occurs in the spontaneous and acid catalyzed reactions.

The major generalization noted by Bennet and coworkers is that the transition state of glucosidase catalyzed reactions is largely dependent on the nature of the leaving group (the aglycone) and that studies of nucleophilic assistance on the hydrolysis of unnatural substrates cannot be applied to the natural substrate of the enzyme.[86] Furthermore, Bennett states that the aglycone natural substrate will resemble a partially deprotonated alcohol, carrying partial negative charge on the oxygen, which is different from both the fluoro and pyridinium glucosides studied. Therefore, enzymatic catalysis of methyl glucoside, which has yet to be shown in the literature, should provide mechanistic information that is

closer to the reaction of the enzyme with its natural substrate (a secondary alcohol of a carbohydrate).

1.9 Project goals:

There were two main objectives in the project: (1) to develop NMR methods for measuring KIEs on glycoside hydrolysis reactions and (2) measure ^{13}C and ^{2}H KIEs on the acid catalyzed and glucosidase catalyzed hydrolyses of methyl glucoside and compare experimental KIEs to calculated EIEs to shed light on glucosidase mechanisms.

2 Experimental:

2.1 General:

Glucose oxidase (EC 1.1.3.4, Type X-S: from *A. niger*) and catalase (EC 1.11.1.6, from bovine liver), baker's yeast α-glucosidase (EC 3.2.1.20), recombinant *Saccharomyces cerevisiae* α-glucosidase (EC 3.2.1.20), and almonds β-glucosidase (EC 3.2.1.21, barley amylase (EC 3.2.1.1) and *Aspergillus niger* amyloglucosidase (EC 3.2.1.3) were also purchased from Sigma. All other chemicals were purchased from Aldrich or Bioshop. A Varian, CARY Bio 100, UV-VIS spectrophotometer was used for absorbance readings. A Bruker 200 MHz spectrometer was used for routine NMR analysis. Bruker 300, 500 and 600 MHz spectrometers were used for quantitative NMR data acquisitions and T1 measurements. In all cases, 5 mm NMR tubes (Wilmad) were used. Sealed 5mm NMR tubes were used for experiments involving isoprene and high temperatures. All acetylated methyl glucoside samples were prepared in D_6-acetone (1 g ampoules, 99.9%) and methyl glucoside in D_2O (99%, both from Cambridge Isotope Laboratories, Inc.).

2.2 Reducing sugar assay:[92]

To a 600 µL sample solution in a 1.5 mL microcentrifuge tube, 300 µL solution A (4% Na_2CO_3, 1.6% glycine, 0.045% anhydrous $CuSO_4$) and 300 µL solution B (0.12% 2,9-dimethyl-1,10-phenanthroline) were added. A blank solution was also prepared with the same proportions. The solutions were heated for 8 min at 95°C, allowed to cool and A_{450} was measured. This assay was linear between 0 and 100 µM glucose (Figure 9).

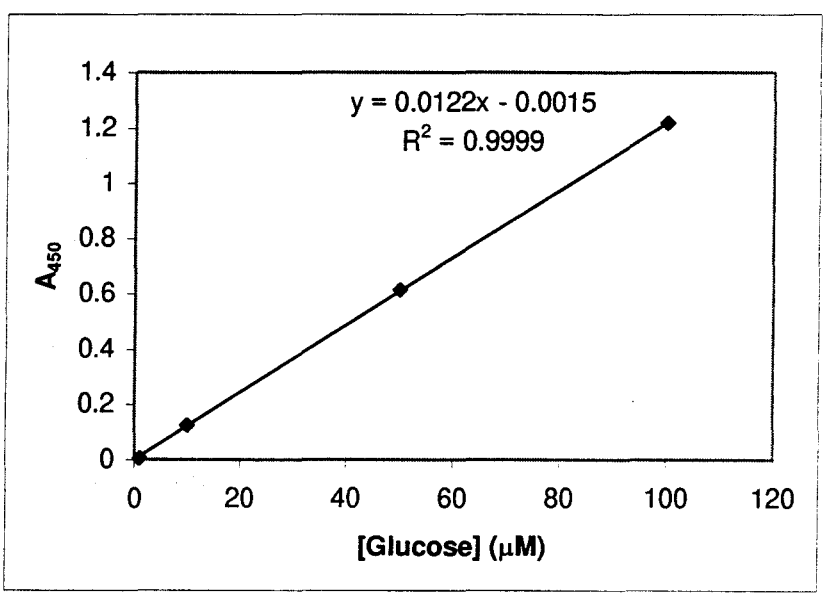

Figure 9. A typical standard curve for the reducing sugar assay.

2.3 Acid catalyzed hydrolysis:

1. Hydrolysis:, A 950 mL reaction mixture was prepared by pre-heating a 750 mL solution of 2 M $HClO_4$ to an internal temperature of 80°C in

a 1000 mL RBF in an 83-85°C oil bath. A separate 200 mL solution of 2 M $HClO_4$,190 mM methyl glucoside **2** and 25 mM sodium succinate was prepared. A 5 mL aliquot was removed for measurement of the extent of reaction (t = 0) and the remaining amount was added to the pre-heated solution. The temperature was allowed to equilibrate to 80°C, at which point, timing of the reaction began. The reaction ran 8.5 to 9 h for **α-2** and 4 to 4.5 h for the **β-2**, giving 90% hydrolysis to glucose, after which, the reaction was cooled on ice.

2. Extent of reaction:

The extent of reaction was determined over the course of the reaction using the reducing sugar assay. When an approximate reaction extent of 90% was measured, the reaction was stopped.

To more accurately determine the extent of the reaction, the unreacted (t = 0) solution, was cooled on ice and neutralized with 1 mL 10 M KOH, which was added dropwise with stirring and occasional cooling on ice. $KClO_4$ precipitated and was filtered off using a 10 mL syringe and 0.45 μm syringe filter. The filtrate was then concentrated *in vacuo*. The process was repeated for 50 mL of the 90% reacted solution, neutralizing with 10 mL 10 M KOH and filtering with a Buchner funnel. Both NMR samples were dissolved in

D_2O and extent of reaction was determined by comparing peak intensity of the succinate methylene (δ= 34 ppm) and C1 of **α-2** (δ= 99 ppm) or **β-2** (δ=105 ppm).

3. Solution Preparation for Purification: When the extent of the reaction was ~90%, the reaction solution was cooled on ice, neutralized with ~200 mL 2 M KOH, with cooling on ice as required. Precipitated $KClO_4$ was removed by filtration and the filtrate was divided between 2 Erlenmeyer flasks and diluted to a final volume of 600 mL.

4. Enzymatic oxidation of glucose: To each flask was added dibasic potassium phosphate (9.8 g, 0.056 mol) and monobasic potassium phosphate (0.43 g, 0.0032 mol). The solutions were stirred to promote dissolution and often filtration was required. The pH as adjusted with KOH to 8.5. To each flask, glucose oxidase (20 mg, 3150 U) and catalase (30 mg, 66000 U) and a solution of H_2O_2 (35% in H_2O, 1.7 mL) were added. The reactions were stirred uncovered overnight, quantitatively converting glucose to gluconic acid. (See Appendix 4 for a typical ^{13}C NMR spectrum of a complete reaction).

5. Anion exchange removal of gluconic acid: The reaction solutions were combined and reduced to a volume of 300 mL *in vacuo*. The solution was applied to an anion exchange column (750 mL, Dowex 1x4-200-400 mesh) in the acetate form. Flow through (300 mL) was

first collected from the column and discarded and then 80 10 mL fractions were collected with a flow of 100 mL/h. The fractions containing methyl glucoside were determined by TLC (R_f = 0.6) using silica plates, with 50:50 MeOH:EtOAc as mobile phase and phosphomolybdic acid (PMA) stain for development (5% solution in EtOH). The fractions containing methyl glucoside were pooled and concentrated to 300 mL *in vacuo*. The column was regenerated, then the procedure was repeated and the pooled sample was concentrated to dryness *in vacuo*.

6. Column generation / regeneration: The column was washed with 500 mL 3 M KCl with gravity flow. The column was then washed with 1000 mL dH_2O, 500 mL 3 M sodium acetate and 1000 mL dH_2O.

7. Acetylation of the 90% reacted methyl glucoside. The dried material containing **2** and sodium acetate was combined with 30 mL pyridine and 20 mL acetic anhydride. The mixture was stirred overnight. Solvent was then removed under reduced pressure until dry. Acetone (150-200 mL) was stirred with the acetylated solid for 1 h and the salt precipitate was removed by filtration and washed with acetone until white. The filtrate was concentrated and the process repeated with chloroform (50 mL). Acetylated methyl glucoside was

further purified by flash column chromatography using ethyl acetate as the mobile phase and the same TLC method as above.

8. Acetylation of unreacted methyl glucoside: Unreacted **2** (1.0 g) was added to pyridine (20 mL) and acetic anhydride (30 mL) and stirred overnight. The solution was reduced to dryness *in vacuo*.

2.4 T1 measurement by inversion-recovery:

T1 values were measured on Bruker 300 MHz and 600 MHz spectrometers. The 90° pulse was determined by locating the node (pulse that gives zero intensity) at 360° and dividing that time by 4 to give the 90° pulse. For ^{13}C NMR, the 90° pulse was 11.3 μS. For ^{2}H NMR, the 90° pulse was 83.0 μs. T1 was determined with a pulse sequence 180° - VD - 90° - AQ, where VD is a variable delay. Typically 10 values for VD were used. The intensity data was plotted with *Grafit* and the rate constant for the first-order increase in intensity was determined by non-linear fitting. The T1 value is the inverse of the rate constant.

2.5 NMR:

Sealing NMR tubes

Samples were prepared in sealed 5mm NMR tubes, modified with an 8cm (6mm OD) glass extension. Samples were frozen in liquid N_2 and

placed under high vacuum while still immersed in the liquid N_2. A stopcock was used to seal off the sample from the vacuum pump and the NMR tube was flame-sealed at the glass extension while under vacuum.

Quantitative ^{13}C NMR

NMR samples of both reacted and unreacted **2** were prepared in acetone-D_6 (50% w/w). The samples were run on a Bruker 600 MHz spectrometer using calibrated $\pi/2$ pulses, Waltz-super ^1H decoupling, SWH=36331.9 Hz, TD = 64 k and a D1 delay of 8.8 s (~10 x the longest T1) between pulses. FIDs were zero-filled to 256 K. Spectra (16 x 256 scans) were recorded successively as a 2D serial file and peak areas were averaged over the 16 spectra. A Gaussian apodization function was applied to the FID using LB = -0.06 and GB = 0.01. ^{13}C peak area, integrated +/- 4.98Hz about the centre of the peak was used to quantitate peaks (as opposed to peak intensity). All peak areas were calibrated to C4 of methyl glucoside.

The NMR data was analyzed using the Bruker software X-WINNMR. An AU (automation program) was written (in C) to convert the 2D serial file to 16 successive 1D Proc (processed) files (Appendix 6). The first spectrum was then integrated manually using X-WINNMR ($\pm$ 4.98 Hz from the peak maximum) and the integration region file was saved using the WMISC command. The integration regions were applied to the rest of the

16 spectra using the Bruker provided AU program called "multi_integ" which outputted a summary of the integrations as a text file. The text files were imported into Microsoft Excel, areas were averaged and the KIEs calculated from the averaged areas.

^{2}H NMR

Deuterium NMR spectra were collected on the 600 MHz spectrometer at 56°C in sealed NMR tubes. The samples were prepared as a 50% (w/w) solution in acetone (non-deuterated). Inverse decoupling, a pulse width of 83.0 μs, an acquisition time of 1.11 s and a delay (D1) of 1.0 s were used. The spectrum was acquired in 35000 scans.

2.6 Evaluation of enzymes for hydrolyzing methyl glucoside:

The enzymes were reacted with **α-2** and **β-2** (40 mM) and the production of glucose was monitored using the reducing sugar assay after a 1000-fold dilution. The reactions with amylase (3 mg, 91 U) and amyloglucosidase were on a 1 mL scale (0.1 M potassium phosphate buffer pH 4.5 or pH 6 at both 45°C and room temperature). The α- and β-glucosidases (0.8 mg/mL) were reacted with the methyl glucosides (40 mM) at room temperature and at 37°C in 0.1 M potassium phosphate buffer, pH 6.8. The extent of reaction was determined by comparison to a

concurrently run reaction containing 2 M $HClO_4$ at 95°C, which was assumed to go to 100% completion in 24 h

2.7 SDS-PAGE of enzymes:

SDS-PAGE of the enzymes were carried out in acrylamide gels by the method of Laemmli[93] (4% stacking, 10% resolving). A standard protein ladder (MBI Fermentas) was used containing: 121.6, 91.4, 46.8, 32.0, 24.5 and 20.2 kDa markers. Gels were stained with Coomassie blue stain (50% MeOH, 10% AcOH and 0.05% Coomassie brilliant blue R450) and destained in 5:5:1 MeOH: dH_2O: AcOH.

2.8 Enzymatic hydrolyses for KIE measurement:

The enzymatic reactions were carried out at a 300 mL scale with the following conditions. The reactions contained: 100 mM **α-2** of **β-2**), 50 mM potassium phosphate buffer at pH 6.8, 1 mM EDTA, 1 mg/mL bovine serum albumin (BSA), 30 μg/mL kanamycin, 50 μg/mL ampicillin at room temperature, 25°C. Potassium succinate (5 mL,1 M) was added to each reaction as the internal standard. Typically, 40 mg of solid enzyme was added to each reaction, but an additional 20-30 mg was added if the reaction appeared to be slowing. Reactions were followed by measuring the production of glucose using the reducing sugar assay until the reaction

was approximately 90% complete. The enzymatic reactions were purified using the same procedure as the acid catalyzed reactions.

2.9 Steady-state kinetics on β-glucosidase and recombinant α-glucosidase:

Steady-state kinetic parameters were determined for β-glucosidase and the recombinant α-glucosidase by measuring the production of glucose by the reducing sugar assay on a 1 mL scale. The reactions contained: 50 mM potassium phosphate buffer pH 6.8, 1 mM EDTA, 1 mg/mL BSA, at 25°C. **β-2** concentrations of 20 to 500 mM were used and of 0.125 mg/mL (1.55 U/mL) β-glucosidase. **α-2** concentrations of 5 to 500 mM were used with 0.1 mg/mL (2.8 U/mL) α-glucosidase. Reactions were initiated by the addition of enzyme and glucose concentration was determined every ten minutes. Rates were determined using linear regression and the kinetic constants were determined with non-linear fitting of the rates (Grafit) to the Michaelis-Menten equation.

$$v_0 = V_{max}[S] / (K_M + [S]) \quad (7)$$

2.10 Synthesis of CD_3-glucoside:

Glucose (0.6 g), 5 g D_4-methanol and 0.35 mL concentrated H_2SO_4 were refluxed for 2.5 h, then the reaction was neutralized with 10 M KOH. The reaction was dried in vacuo yielding a whitish solid. The solid was

combined with 15 mL pyridine and 20 mL acetic anhydride and stirred at room temperature overnight. Pyridine, acetic acid and excess acetic anhydride were removed under vacuum. The peracetylated product was used without further purification. The ^{13}C, ^{1}H, ^{2}H NMR spectra are shown in Appendix 5.

2.11 Computational EIE calculation:

Calculated EIEs were determined by optimizing the relevant structures quantum mechanically and calculating the vibrational frequencies. This was done using the electronic structure program Gaussian 98. EIEs were then calculated from the vibrational frequencies using *QUIVER*.[94]

In calculating EIEs, the effect of ring conformation was also examined. In **α-2**, **β-2** and **3**, all stable ring conformations were sought. This was done by starting with structures containing ring conformations that were expected to be stable (*e.g.*, $^{4}C_{1}$, $^{2,5}B$, $B_{2,5}$), then optimizing the structure at a low level of theory (RHF/3-21G**) with the dihedral angles in the sugar ring held fixed. The constraints were released and the structure fully optimized at the same level of theory. Finally, the structure was optimized using density functional theory with Becke's exchange functional[95] and Perdew and Wang's correlation fuctional[96] with the 6-

31+G** basis set (RB3PW91/6-31+G**). Vibrational frequencies were also calculated at this same level of theory.

Some ring conformations tested were unstable. That is, when the dihedral angle restraints were released after the first, constrained optimization, the ring conformation changed into a different, stable conformation. In this case, the structure with the stable conformation was retained and the starting structure was simply labeled as "unstable".

Oxocarbenium ion **3** ring conformations were sought first by progressively breaking the C1-O bond of **α-2** and **β-2** starting from different conformations. The C1-O bond was fixed at increasing bond lengths (corresponding to bond orders* $n_{C1\text{-}O}$ = 0.7 to 0.01) and the rest of the structure was re-optimized at each fixed bond length. After optimization at $n_{C1\text{-}O}$ = 0.1, the leaving group was removed altogether and **3** was fully optimized at RHF/3-21** level of theory, followed by (RB3PW91/6-31+G**). Finally, the vibrational frequencies were calculated.

---

* Pauling bond order: $n_{ij} = e^{(r_1 - r_{ij})/0.3}$ where r_{ij} is the bond length between atoms i and j and r_1 is the bond length of a single bond between i and j.[1]

In addition to the **3** ring conformations that arose directly from breaking the C1-O bond, other ring conformations for which there was literature precedent were sought as described for **2** above. That is, structures of **3** were created in the expected conformations, then optimized at a low level of theory with the ring conformation fixed before full optimization.

Fractionation factors (Φ) were calculated for each optimized conformation of **2** and **3** *QUIVER* with temperatures of 298 K for the glucosidase reactions or 353 K for the acid catalyzed reactions. ^{13}C and ^{2}H EIEs were calculated by dividing the fractionation factors for **2** by **3**, that is: $EIE = \Phi_2/\Phi_3$.

3 Results:

3.1 NMR validation

To validate NMR measurements, KIEs were measured on the Diels-Alder reaction of isoprene and maleic anhydride (Scheme 1). This was the system with which Singleton and co-workers developed the method of measuring KIEs by NMR.[16]

Scheme 1.

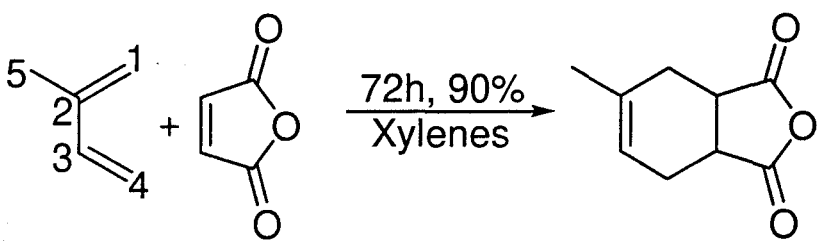

As discussed above, quantitative NMR requires a delay between pulses of 5-10 times the longest T1 relaxation time. The isoprene T1 relaxation times were measured (Table 3).

Table 3. ^{13}C T1 relaxation data for isoprene as measured by the inversion-recovery method.

Carbon Atom	T1 relaxation (s)
C1	13.0
C2	19.5
C3	16.4
C4	13.2
C5	13.4

As the longest T1 was 19.5 s, a delay of 120 s was used, the same as in the original NMR experiments.[16]

3.1.1 KIEs on isoprene Diels-Alder Rxn

The ^{13}C KIEs measured for isoprene are shown in comparison to the KIEs measured by Singleton (Table 4). The methyl ^{13}C peak (carbon 5) was used as the reference atom, so that the KIE at this position was 1.000 by definition. The experimental values were in good agreement with the literature values, with all KIEs within 0.002 of the reported values.

Table 4. The Experimentally determined KIEs for the Diels-Alder reaction of isoprene and maleic anhydride. KIEs were determined by peak areas.

Carbon Atom	Experimental ^{13}C KIE Exponential multiplication	Experimental ^{13}C KIE Gaussian Multiplication	Literature ^{13}C KIE
C1	1.021	1.022	1.022
C2	1.001	1.003	1.001
C3	0.999	0.999	1.000
C4	1.017	1.019	1.017
C5	1.000	1.000	1.000

3.2 KIE measurement

Accurate KIE measurement was affected by the width of the NMR peaks at the baseline because of peak overlap with impurity peaks as well as other peaks of interest. Therefore, Gaussian peak shapes were chosen over Lorenztian peak shapes because Gaussian peak shapes are narrower along the baseline. Effective quantitation of the NMR peaks was

found when the peaks were integrated to ±4.98 Hz. At this range, the experimental KIEs matched the literature KIEs for isoprene.

The peak-picking function in the X-WIN NMR fits the highest 3 points of the peak to a parabolic function to find the top of the peak. In doing so, intensity information is not lost when the highest point does not correspond to the top of the peak. When peak intensity was used to calculate the KIEs, the KIEs were affected by the value of LB used in the apodization function when processing spectra (Figure 10). In contrast, the value of LB did not affect the KIE values when peak area was used to quantitate the NMR peaks.

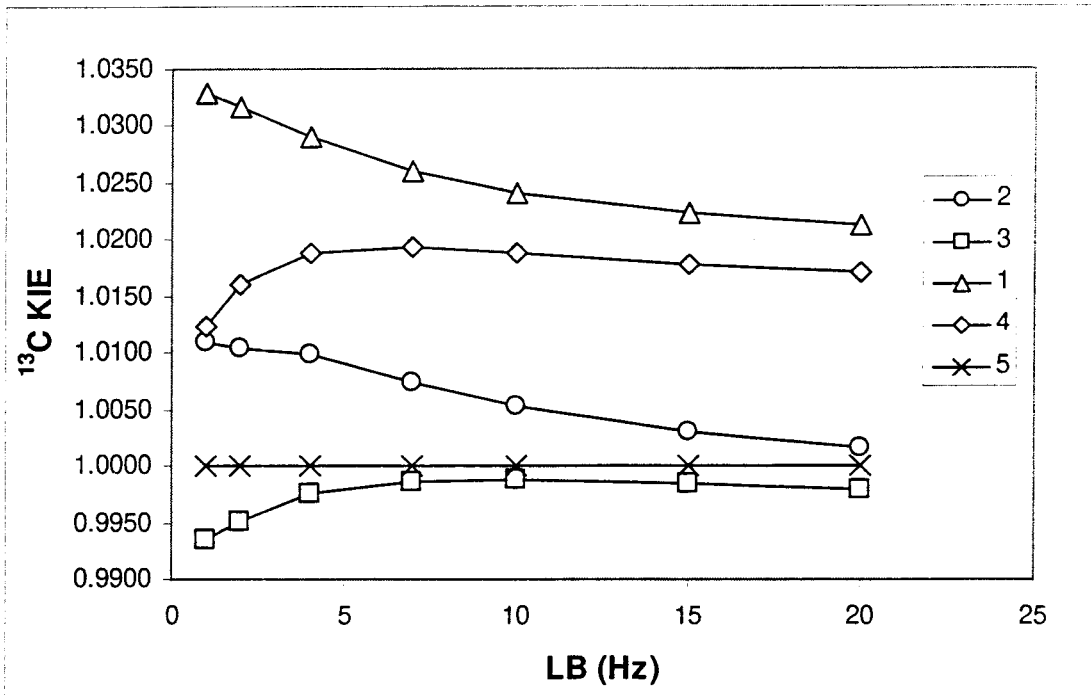

Figure 10. The LB affects the KIE value when peak intensity is used in peak quantitation.

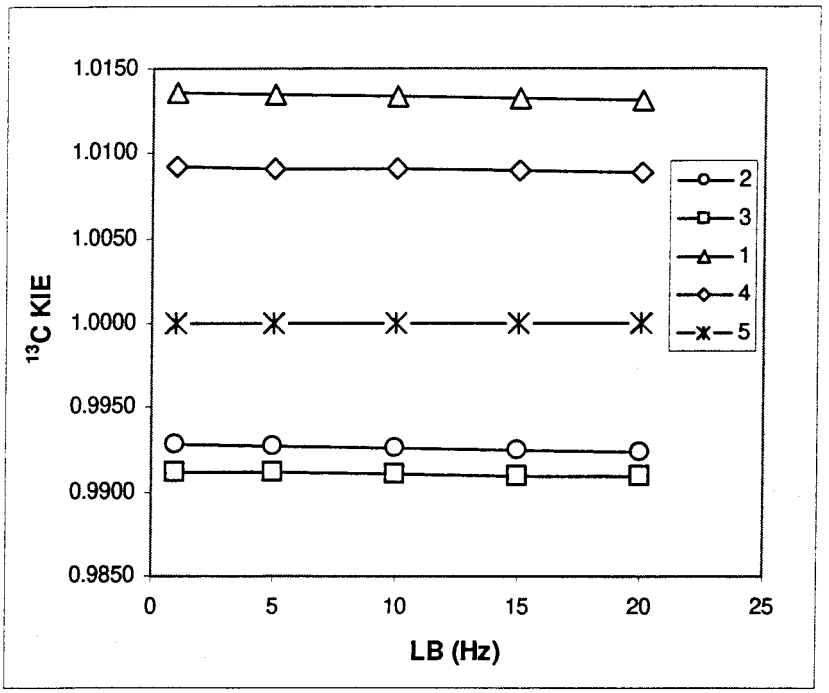

Figure 11. The LB has no effect on KIE measurement when peak area is used in peak quantitation.

3.3 KIEs on Methyl glucoside hydrolysis

Initial work focused on two areas: (1) developing a purification scheme for residual **2** and the scale up of all reactions involved and (2) determining the conditions necessary for quantitative NMR for methyl glucoside.

The purification scheme that was developed for the isolation of residual **2** from the glucose product involved (1) the oxidation of glucose to gluconic acid, and (2) the removal of the gluconic acid by anion exchange. Oxidation of glucose by the enzymes glucose oxidase and catalase was found to go to completion in 24 h when 0.1% H_2O_2 was added to the initial

reaction. Gluconic acid was found to only exchange on the resin for acetate and not for chloride (the form in which the resin was purchased).

Methyl glucoside was only sparingly soluble (mM range) in organic solvents (acetone, acetonitrile and methanol). Although it was soluble in water, it gave a viscous solution at higher concentrations and there was peak overlap in the ^{1}H NMR spectrum (potentially making ^{2}H NMR impossible). Viscosity was anticipated to be a problem, affecting peak width and peak resolution in the NMR spectra. Therefore, **2** was acetylated, which gave the desired solubility in organic solvent and dispersed the methyl glucoside proton peaks so that they were well resolved (See Appendix 1 and Appendix 2).

To ensure that isotopic fractionation did not occur, the acetylation reaction was taken to completion and the product purified in such a way that no losses occurred. The yield of the acetylated product a of 99.4% was achieved by vacuum removal of excess pyridine/acetic anhydride, which formed an azeotrope. Spectroscopic work was therefore focused on the acetylated methyl glucoside.

Peak assignments for acetylated methyl glucosides, COSY and HSQC NMR

The ^{13}C and ^{1}H peaks were assigned for both the α- and the β-peracetylated methyl glucosides by standard 2D NMR techniques including COSY (correlation spectroscopy), which correlates the 3-bond coupled protons in the HNMR spectrum and HSQC (homonuclear single quantum correlation), which correlates carbons to covalently bound protons.

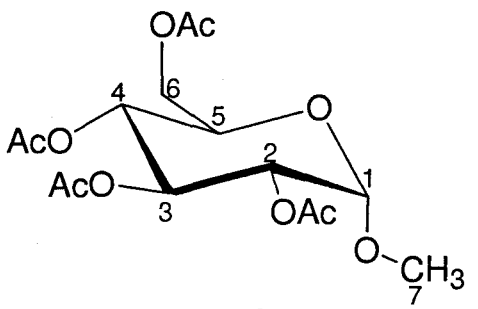

10

Table 5. ^{1}H and ^{13}C NMR peak assignments for peracetylated α-methyl glucoside.

Carbon	δ (ppm)	Proton	δ (ppm)
C1	97.3769	H1	4.9269
C2	71.2762	H2	4.8403
C3	70.5334	H3	5.3881
C4	69.3703	H4	5.0086
C5	67.9944	H5	3.9760
C6	62.6644	H6', H6"	4.2085, 4.0934
C7	55.4660	H7	3.4088

Table 6. ^{1}H and ^{13}C NMR peak assignments for peracetylated β-methyl glucoside.

Carbon	δ (ppm)	Proton	δ (ppm)
C1	101.9297	H1	4.6340
C2	71.9950	H2	4.9881
C3	73.4620	H3	5.2275
C4	69.3625	H4	5.0044
C5	72.2475	H5	3.9214
C6	62.6689	H6', H6"	4.2554, 4.1078
C7	56.8063	H7	3.4454

T1 measurement

As with the isoprene experiment, the first step was to measure the ^{13}C T1 relaxation times for **10**, (Table 7). The longest T1 was C7 (the methoxy carbon), 0.88 s. The D1 delay required for quantitative NMR was therefore 4.4-8.8 s. An 8.8 s delay was used throughout.

Table 7. The ^{13}C T1 data for peracetylated- α -methyl glucoside.

Carbon atom	T1 (s)
C1	0.29
C2	0.29
C3	0.28
C4	0.28
C5	0.29
C6	0.17
C7	0.88

Reaction kinetics

The pseudo-first-order rate constants were measured for the acid catalyzed hydrolysis of **α-2** and **β-2** (Table 8) and were in fair agreement

with the literature values. The reactions were found to remain first order up to the required 90% completion.

Table 8. A comparison of Pseudo-first order rate constants for the acid catalyzed hydrolysis of methyl glucosides in 2 M $HClO_4$ at 80°C with literature values.

	α-2	**β-2**
This work	6.8×10^{-5} s^{-1}	2.7×10^{-4} s^{-1}
Literature[84]	7.3×10^{-5} s^{-1}	1.4×10^{-4} s^{-1}

KIEs for Acid-catalyzed hydrolysis of methyl glucosides

^{13}C KIEs were measured on acid catalyzed hydrolysis of both the α- and β- methyl glucosides (Table 9, Table 10). Duplicate experiments were carried out in both cases.

Table 9. ^{13}C KIEs for the acid catalyzed hydrolysis of **α-2** in 2 M $HClO_4$ at 80°C.

carbon	Average	Range
1	1.007	0.002
2	1.013	0.005
3	1.010	0.003
4	1.000	0.000
5	1.008	0.002
6	1.005	0.002
7	1.007	0.011

Table 10. ^{13}C KIEs for the acid catalyzed hydrolysis of **β-2** in 2 M $HClO_4$ at 80°C.

carbon	Average	Range
1	1.010	0.006
2	1.007	0.006
3	0.998	0.002
4	1.000	0.000
5	1.005	0.003
6	0.999	0.005
7	0.999	0.004

KIEs were all referenced to C4, a site where little or no KIE was expected. Therefore, the ^{13}C KIE is 1.0, by definition. The standard deviation in the 16 spectra was found to be the same for the trials in Table 1 so the large range value was thought to result from differences in sample (i.e., different KIEs) and not errors in measurement.

3.3.1 Testing glycosidases for activity with methyl glucoside

Several commercially available glycosidases were tested for activity with **α-2** and **β-2** (Figure 12 and Figure 13). Of the enzymes tested, yeast α-glucosidase and the almond β-glucosidase had the highest activity and were chosen for the large scale reactions. Both enzymes are retaining glucosidases, giving products with retention of the anomeric stereochemistry.

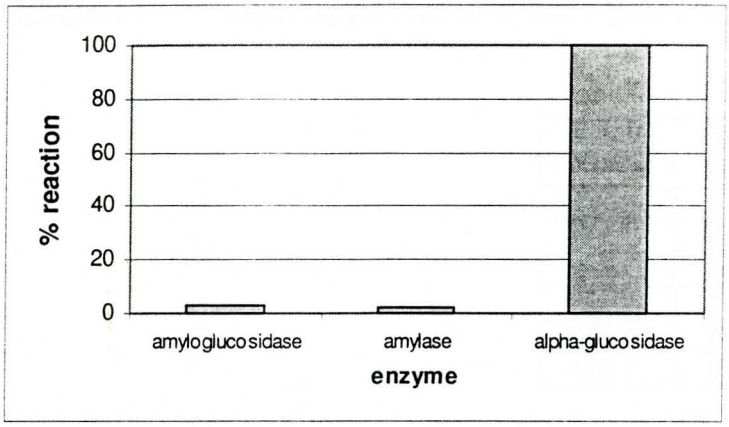

Figure 12. Activity of enzymes for α methyl glucoside hydrolysis. The reactions with amylase (3 mg, 91 U) and amyloglucosidase (10 μL, 60 U) were on a 1 mL scale (0.1 M potassium phosphate buffer pH 4.5 or pH 6 at both 45°C and room temperature). The α-glucosidases (0.8 mg/mL) were reacted with the methyl glucoside (40 mM) at 25° in 0.1 M potassium phosphate buffer, pH 6.8.

Amylase and amyloglucosidase showed a low level of activity with **α-2** and were never able to reach the required 90% completion, despite varying of a number of parameters in the reaction including pH, temperature, substrate concentration.

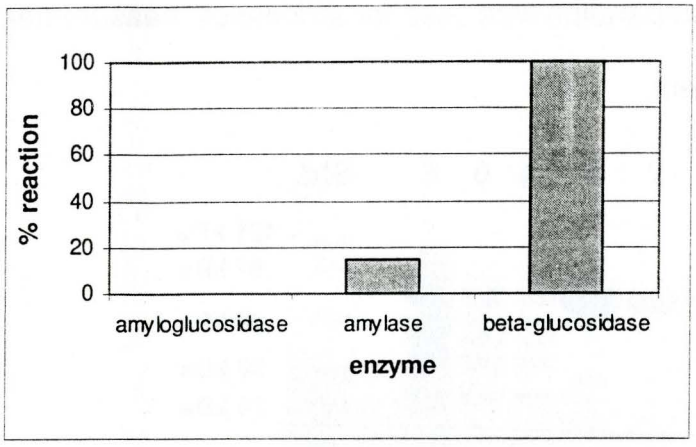

Figure 13. Activity of enzymes for β-methyl glucoside hydrolysis. The reactions with amylase (3 mg, 91 U) and amyloglucosidase (10 μL, 60 U) were on a 1mL scale (0.1 M potassium phosphate buffer pH 4.5 or pH 6 at both 45°C and room temperature). The α- and β-glucosidases (0.8 mg/mL) were reacted with the methyl glucosides (40 mM) at room temperature and at 37°C in 0.1 M potassium phosphate buffer, pH 6.8.

Similarly, amylase and amyloglucosidase showed lower activity with the **β-2** and the required 90% completion was never achieved. Therefore, the α-glucosidase and β-glucosidase were selected as the enzymes for use in KIE measurements of enzymatic methyl glucoside hydrolysis.

α- and β-glucosidases were purchased as "partially purified" preparations from Sigma chemical Co. The enzymes were examined by SDS-PAGE (Figure 14). Almond β-glucosidase appeared to be pure, with very little contaminating protein. This preparation was used throughout this study. Yeast α-glucosidase was a mixture, with only a small fraction of the protein being α-glucosidase. Recombinant yeast α-glucosidase appeared

pure (Figure 15). This preparation was used for all kinetics measurements and one KIE measurement.

Figure 14. SDS-PAGE (4% stacking, 10% resolving) of the commercially available α- and β-glucosidases. The β-glucosidase is shown in lanes 1 to 3 and the α enzyme in lanes 4 to 6 in increasing amounts from the left to right (5, 10 and 20 μg). The standard lane contains 121.6, 91.4, 46.8, 32.0, 24.5 and 20.2 kDa markers.

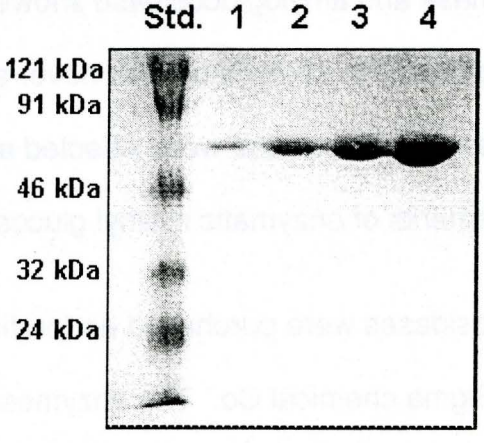

Figure 15. SDS-PAGE (4% stacking, 10% resolving) of recombinant yeast α-glucosidase with increasing amounts of the enzyme in lanes 1 to 4 (10, 20, 40 and 80 μg). The standard lane contains 121.6, 91.4, 46.8, 32.0, 24.5 and 20.2 kDa markers.

3.4 Steady State Kinetics on Recombinant α-glucosidase and β-glucosidase

Steady-state kinetic constants were measured on the β-glucosidase and the recombinant α-glucosidase catalyzed reactions and are shown in comparison to the kinetics on p-nitro-phenyl glucoside[97, 98, 99] which is a good substrate for the enzyme.

Table 11. Steady state kinetic constants with almond β-glucosidase

glucoside	k_{cat} (s^{-1})	K_M (mM)	k_{cat}/K_m ($M^{-1}s^{-1}$)
β-Methyl-[a]	0.90 ± 0.15	440 ± 13	2.0 ± 0.6
p-nitrophenyl-[b]	17.6	0.25	7040

[a] this work,[b] see 97,98

Table 12. Steady state kinetic constants for yeast α-glucosidase. Recombinant yeast α-glucosidase was used to measure the methyl glucoside kinetics.

glucoside	k_{cat} (s^{-1})	K_M (mM)	k_{cat}/K_M ($M^{-1}s^{-1}$)
α-Methyl-[a]	0.88 ± 0.05	61 ± 9	15 ± 0.2
p-nitrophenyl-[c]	20	0.30	$6.6x10^4$

[a] this work, [c]see 99

3.5 KIEs on the enzymatic hydrolysis of α- and β-methyl glucosides

KIEs were measured on the enzymatic reactions in the same manner as the acid catalyzed reactions, using the α-glucosidase with **α-2** and the β-glucosidase with **β-2** (Table 13 and Table 14).

Table 13. A summary of ^{13}C KIEs (4 trials) measured for the enzyme catalyzed hydrolysis of α-methyl glucoside. Trials 1 to 3 were measured with the crude α-glucosidase and trial 4 was measured with the recombinant α-glucosidase.

carbon	Average	Std. Dev.
1	1.010	0.004
2	1.011	0.004
3	1.002	0.007
4	1.000	0.000
5	1.003	0.001
6	1.007	0.004
7	1.007	0.003

Table 14. A summary of ^{13}C KIEs (2 trials) measured for the enzyme catalyzed hydrolysis of β-methyl glucoside.

carbon	Average	Range
1	1.032	0.001
2	1.007	0.003
3	0.999	0.001
4	1.000	0.000
5	1.013	0.002
6	1.003	0.001
7	0.999	0.005

3.6 Computational chemistry

Glycoside hydrolysis mechanisms are known to proceed on the borderline between highly dissociative A_ND_N mechanisms and true $D_N{*}A_N$ mechanisms with discrete oxocarbenium ion intermediates. In either case, the sugar ring will be highly oxocarbenium ion-like. It is possible, therefore, to interpret secondary KIEs on glycoside hydrolysis in terms of EIEs on oxocarbenium ion formation. This does not apply to primary KIEs, where the reaction coordinate motion contributes to the KIE. Therefore EIEs were calculated to help interpret ^{13}C KIEs at C2 to C6.

The geometries of four **α-2** starting conformations ($^{2,5}B$, $^{4}C_1$, $B_{2,5}$ and $^{1}S_3$) and three **β-2** structures ($^{2,5}B$, $^{4}C_1$, $B_{2,5}$) were computationally optimized with GAUSSIAN 98. The $^{4}C_1$ starting structures remained intact while optimizing the geometry of the molecule, but the boat structures ($^{2,5}B$ and $B_{2,5}$) became slightly skewed. The **α-2** and **β-2** with computationally optimized geometries were subjected to decreasing $n_{C1\text{-}O}$ bond orders and re-optimized. The methoxy group was then removed from the structure that had $n_{C1\text{-}O} = 0.1$ and re-optimized to give the oxocarbenium structure. The oxocarbenium ions all optimized to two basic ring conformations, despite beginning from different ring conformations. These were either a ^{3}E sofa, or an E_3 sofa conformation. A summary of the ring conformations for **α-2** and **β-2** are shown (Table 15) for the ten trials that were attempted.

Table 15. Conformations of **α-2** and **β-2** structures.

Trial		Starting conformation	oxocarbenium ion conformation
1	**α-2**	$^{2,5}B$	^{3}E
2	**α-2**	$^{4}C_1$	E_3
3	**α-2**	$B_{2,5}$	^{3}E
4	**α-2**	$^{1}S_3$	$^{4}H_3$
5	**β-2**	$^{2,5}B$	E_3
6	**β-2**	$^{4}C_1$	E_3
7	**β-2**	$B_{2,5}$	^{3}E
8	**α-2**	$^{2,5}B$	E_4
9	**α-2**	$^{4}C_1$	E_4
10	**α-2**	B2,5	E4

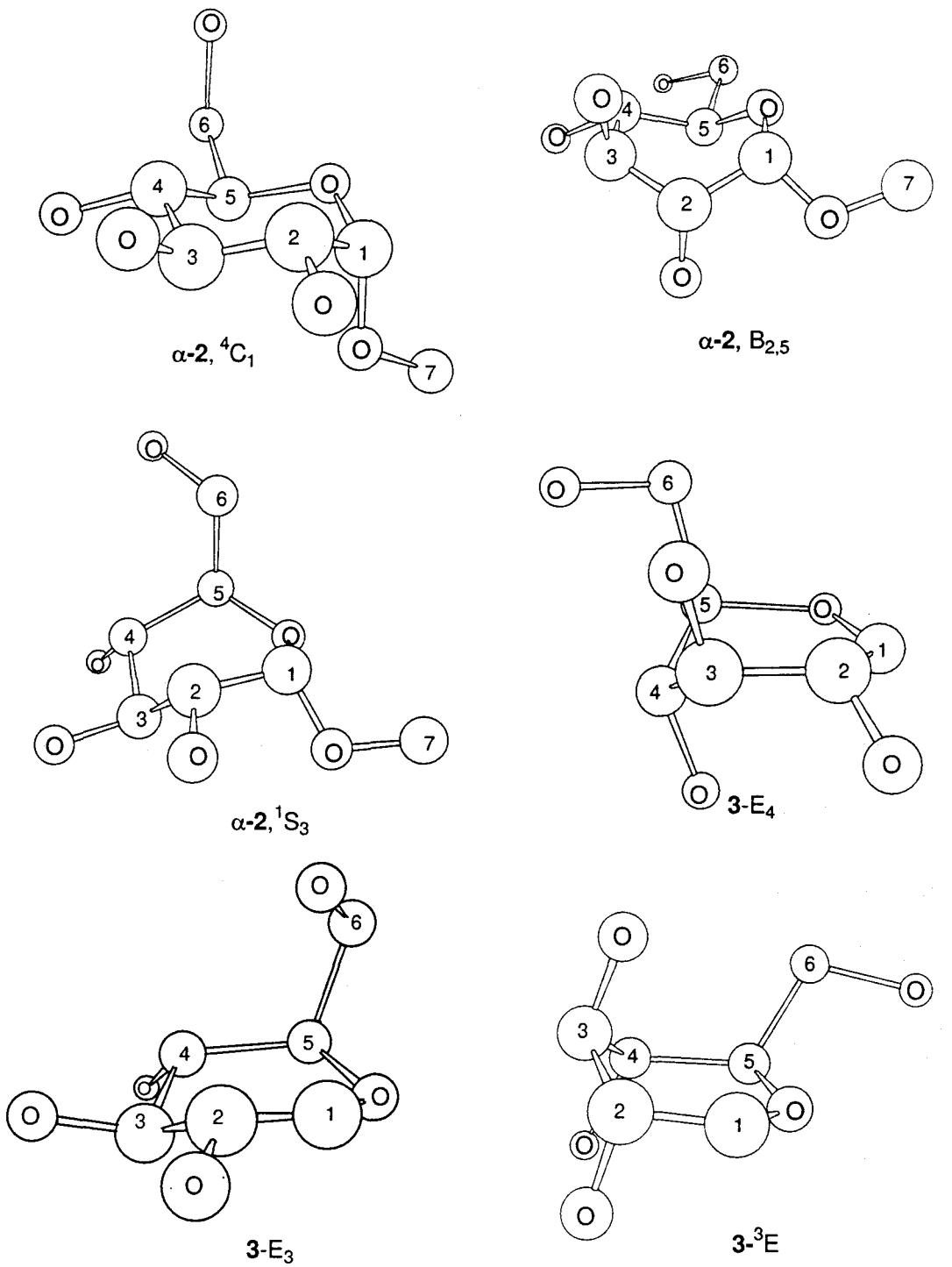

Figure 16. Examples of **α-2** and oxocarbenium ion structures. Hydrogens have been omitted for clarity.

Fractionation factors were calculated for each starting structure and oxocarbenium ion structure and were used to calculate EIEs (Table 16 and Table 17). The EIE for the acid catalyzed reactions were calculated for 80°C as isotope effects are temperature dependent (Table 18 and Table 19). Other conformations of **3** were sought to try to improve the fit of the calculated EIEs to the **α-2** experimental KIEs. This included an envelope (E_4) oxocarbenium structure (Table 20). The ^2H EIE isotope effects were also calculated for the different conformations of **2** and their respective oxocarbenium ions. The largest calculated ^2H EIEs were for the H1 and H2. The calculated H2 - ^2H EIE was sensitive to differences in ring conformation. The α-secondary EIE is smaller for the **β-2** anomer than for the **α-2** anomer (Table 21 to Table 24).

Table 16. The ^{13}C EIEs calculated for **α-2** starting structures at 25°C.

Carbon	$^{2,5}B$ to ^3E	$^4C_1$ to E_3	$B_{2,5}$ to ^3E	$^1S_3$ to $^4H_3$
C1	1.003	1.001	1.005	1.005
C2	1.006	1.010	1.008	1.014
C3	0.997	1.004	1.000	1.006
C4	1.000	1.000	1.000	1.000
C5	1.016	1.010	1.012	1.016
C6	1.000	0.998	1.001	1.004

Table 17. ^{13}C EIEs calculated for **β-2** at 25°C.

Carbon	$^{2,5}B$ to E_3	$^4C_1$ to E_3	$B_{2,5}$ to ^3E
C1	1.002	1.003	1.006
C2	1.010	1.011	1.007
C3	1.001	1.004	1.002
C4	1.000	1.000	1.000
C5	1.012	1.010	1.014
C6	1.000	0.998	1.003

Table 18. The calculated ^{13}C EIE for **α-2** hydrolysis at 80°C.

Carbon	$^{2,5}B$ to ^3E	$^4C_1$ to E_3	$B_{2,5}$ to ^3E	$^1S_3$ to $^4H_3$
C1	1.001	0.999	1.003	1.003
C2	1.005	1.007	1.006	1.011
C3	0.997	1.003	1.000	1.005
C4	1.000	1.000	1.000	1.000
C5	1.013	1.008	1.010	1.013
C6	1.000	0.998	1.001	1.003

Table 19. The calculated ^{13}C EIE for **β-2** hydrolysis at 80°C

Carbon	$^{2,5}B$ to E_3	$^4C_1$ to E_3	$B_{2,5}$ to ^3E
C1	1.0001	1.0006	1.0034
C2	1.0077	1.0085	1.0051
C3	1.0011	1.0028	1.0015
C4	1.0000	1.0000	1.0000
C5	1.0094	1.0082	1.0116
C6	0.9997	0.9980	1.0023

Table 20. The calculated ^{13}C EIEs for **α-2** hydrolysis using E_4 oxocarbenium ions

carbon	$^{2,5}B$ to E_4	$^4C_1$ to E_4	$B_{2,5}$ to E_4
C1	1.0072	1.0024	1.0054
C2	1.0140	1.0079	1.0135
C3	1.0023	1.0037	1.0051
C4	1.0000	1.0000	1.0000
C5	1.0111	1.0093	1.0133
C6	1.0029	1.0000	1.0038

Table 21. Calculated ^{2}H EIEs for **α-2** hydrolysis at 25°C.

Proton	$^{2,5}B$ to ^{3}E	$^{4}C_1$ to E_3	$B_{2,5}$ to ^{3}E	$^{1}S_3$ to $^{4}H_3$
H1	1.2547	1.2611	1.2706	1.1554
H2	1.0077	1.1614	1.0353	1.1143
H3	1.0107	1.0239	1.0530	0.9950
H4	1.0000	1.0000	1.0000	1.0000
H5	1.0179	0.9793	1.0154	1.0265
H6	1.0180	1.0290	1.0160	0.9448

Table 22. Calculated ^{2}H EIEs for **β-2** hydrolysis at 25°C.

Proton	$^{2,5}B$ to E_3	$^{4}C_1$ to E_3	$B_{2,5}$ to ^{3}E
H1	1.1696	1.1785	1.1631
H2	1.1468	1.1311	1.0258
H3	0.9376	1.0001	1.0420
H4	1.0000	1.0000	1.0000
H5	0.9625	0.9474	0.9991
H6	0.9981	1.0265	0.9529

Table 23. Calculated ^{2}H EIEs for **α-2** hydrolysis at 80°C

Proton	$^{2,5}B$ to ^{3}E	$^{4}C_1$ to E_3	$B_{2,5}$ to ^{3}E	$^{1}S_3$ to $^{4}H_3$
H1	1.1923	1.1947	1.2078	1.1132
H2	1.0047	1.1272	1.0294	1.0923
H3	1.0080	1.0185	1.0450	0.9956
H4	1.0000	1.0000	1.0000	1.0000
H5	1.0133	0.9804	1.0148	1.0204
H6	1.0145	1.0227	1.0157	0.9531

Table 24. Calculated ^{2}H EIEs for **β-2** hydrolysis at 80°C

Proton	$^{2,5}B$ to E_3	$^{4}C_1$ to E_3	$B_{2,5}$ to ^{3}E
H1	1.1246	1.1294	1.1213
H2	1.1183	1.1039	1.0212
H3	0.9465	0.9980	1.0347
H4	1.0000	1.0000	1.0000
H5	0.9666	0.9532	0.9984
H6	0.9462	1.0206	0.9952

3.7 ^{2}H NMR-Progress towards KIEs on ^{2}H

^{2}H KIEs measurements with natural abundance deuterium NMR were focused on the Diels-Alder reaction of isoprene. The existence of experimental values in the literature would allow validation of NMR acquisition and processing techniques.

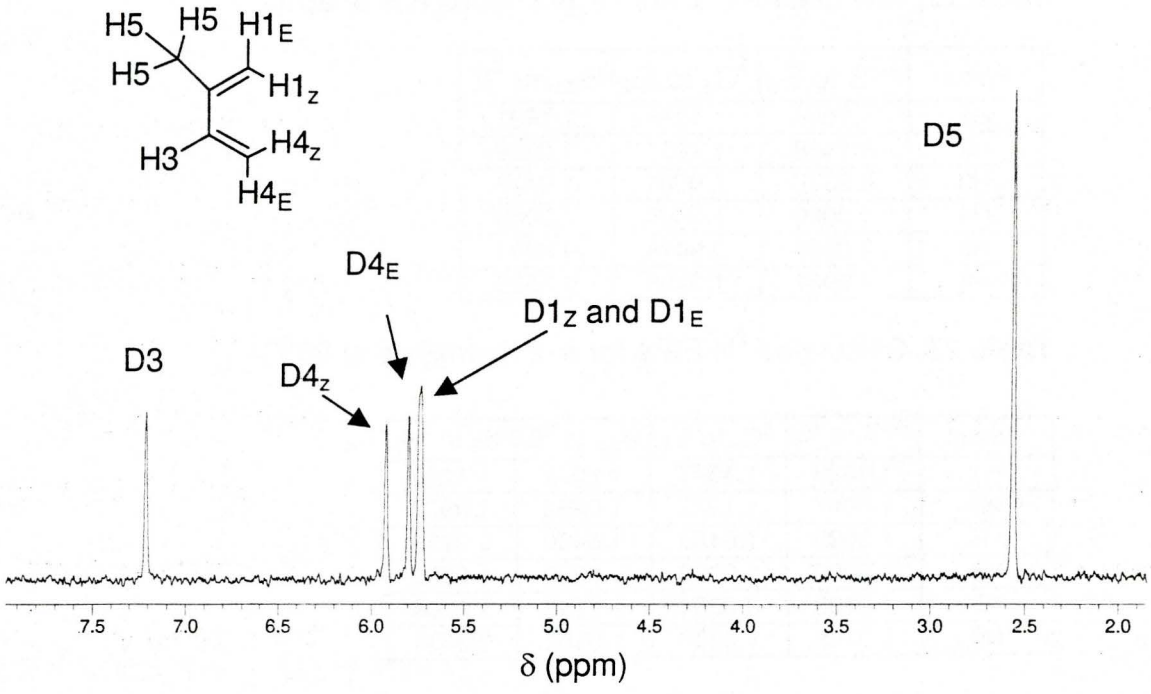

Figure 17. Proton-decoupled natural abundance 2H spectrum of isoprene was acquired on a 600MHz instrument.

The experimental ^{2}H KIE values were in reasonable agreement with the literature KIEs despite the peak overlap. Not all of the KIEs could be obtained, since the 1E and 1Z peaks were overlapped. The methyl peak is used as the internal standard, having a KIE = 1.0 by definition.

Table 25. ^{2}H KIEs measured for the Diels-Alder reaction of isoprene. The Experimental KIEs are shown in comparison to the literature values.[16]

^{2}H	Experimental KIE	Literature KIE
Average $D1_Z$ & $D1_E$	0.934	0.932
D3	0.984	0.990
$D4_Z$	0.925	0.938
$D4_E$	0.963	0.968
D5	1.000	1.000

Initial attempts to obtain ^{2}H NMR spectra for **β-2** gave spectra in which not all of the deuterons were visible. The methyl deuterons were clearly visible at 4.79 ppm as well as the acetyl deuterons (Figure 18). To improve both sensitivity and peak resolution, a number of parameters were changed. First, acetone, a less viscous solvent compared to chloroform was used for sample preparation. Secondly, proton decoupling was added. Finally, higher temperatures were used; 56°C rather than 25°C. The high temperature spectra were acquired on samples that were prepared at 50% (w/w) in non-deuterated acetone and sealed in modified NMR tubes. Spectra were run at 56°C. There was a dramatic effect of temperature on the sensitivity of the **β-2** ring deuterons. The spectrum shown in Figure 19 required 35000 scans and all ring deuterons are visible.

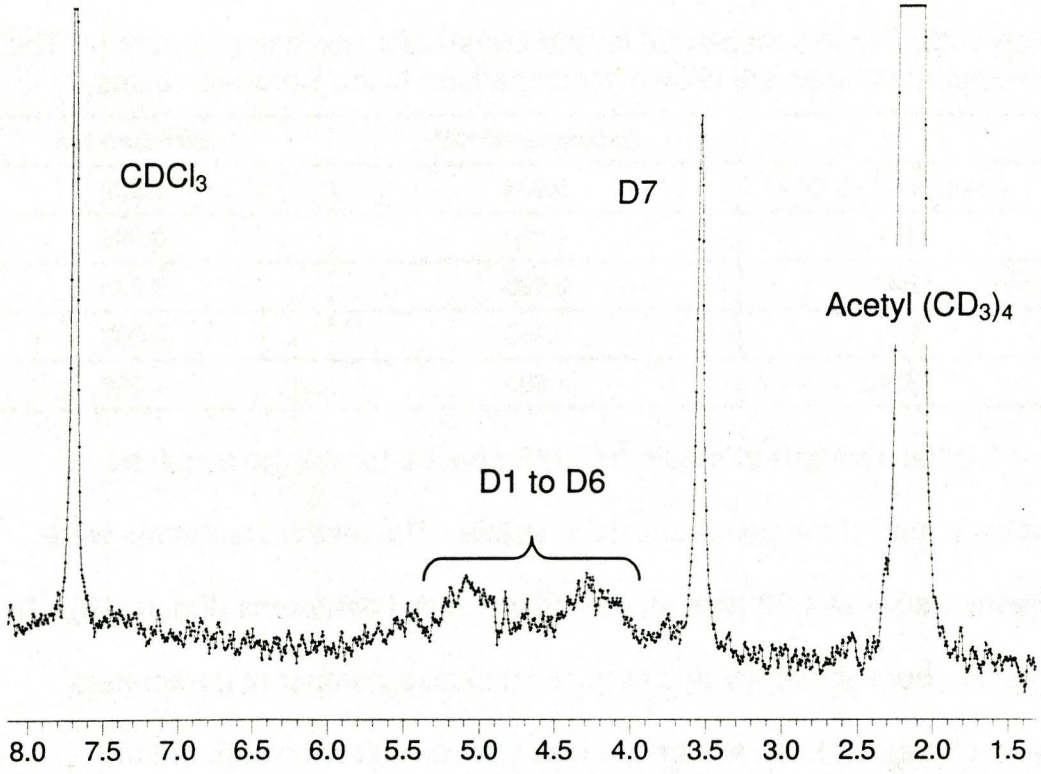

Figure 18. Initial natural abundance proton-decoupled ^2H spectra for methyl glucoside acquired on a 600 MHz instrument at 25°C.

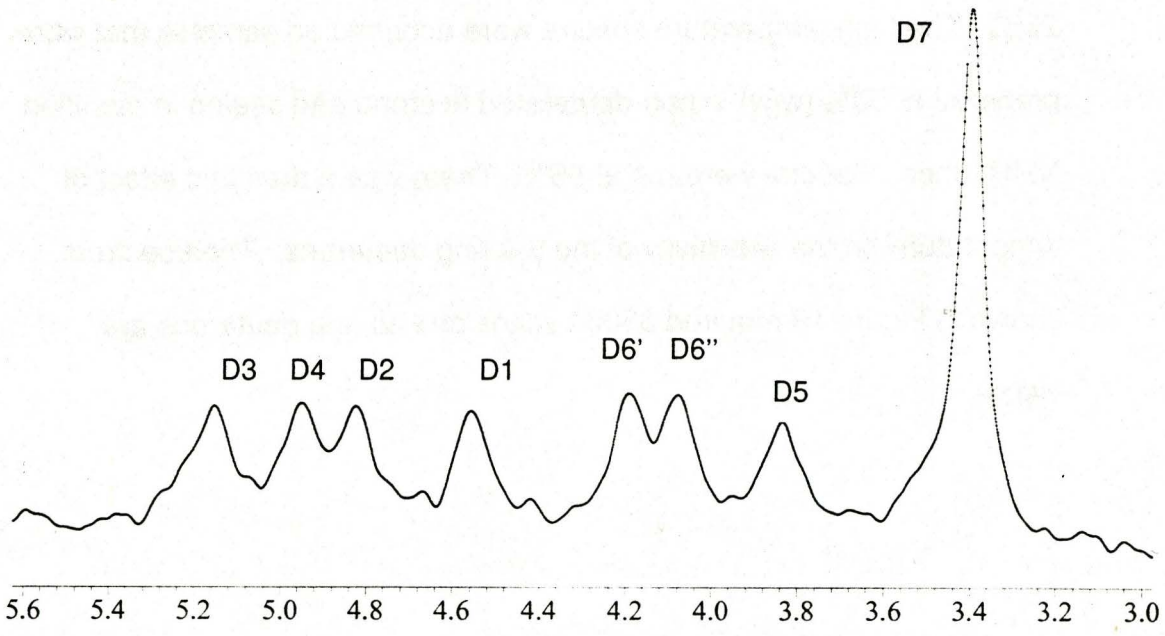

Figure 19. Natural abundance proton-decoupled ^{2}H NMR spectrum of **β-2** acquired at 56°C.

3.8 Synthesis of CD_3-glucoside

Acquisition of ^{2}H NMR spectra for **β-2** required a large number of scans, making it difficult to measure the ^{2}H T1 relaxation times at natural abundance. ^{2}H labeled methyl glucoside [7-$^{2}H_3$-2] was prepared as an anomeric mixture. The identity of the compound was shown by comparing ^{1}H and ^{13}C NMR spectra of labeled and unlabeled materials, which showed the deuterium split ^{13}C methoxy peak (see Appendix 5). The ^{2}H spectrum showed CD_3 deuterium peaks for both the β- and α- anomers (see Figure 20). This allowed quick determination of the T1 value for the $^{2}H7$, which would be the slowest based on the value of the ^{13}C T1s[23,100] (Table 7), and hence, the value needed to set the D1 delay time for quantitative NMR. The T1 relaxation data is shown in Figure 21.

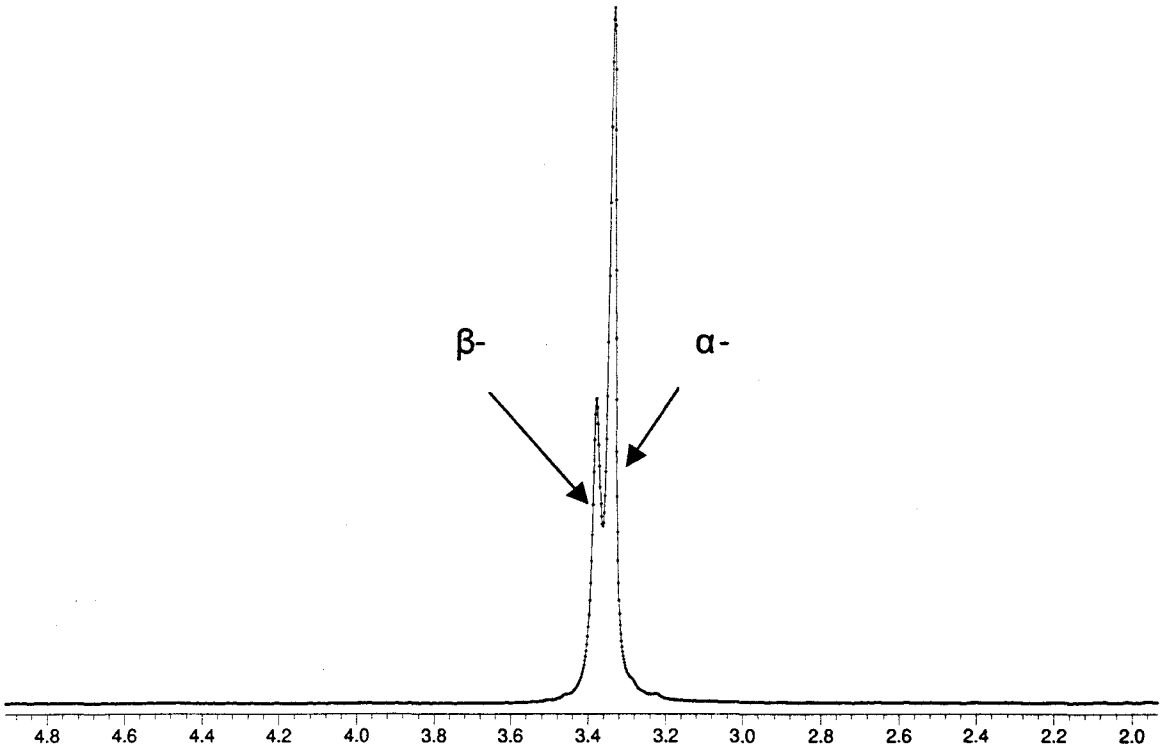

Figure 20. ^{2}H NMR spectrum of [7-$^{2}H_3$-2] acquired in 4 scans on a 600 MHz spectrometer.

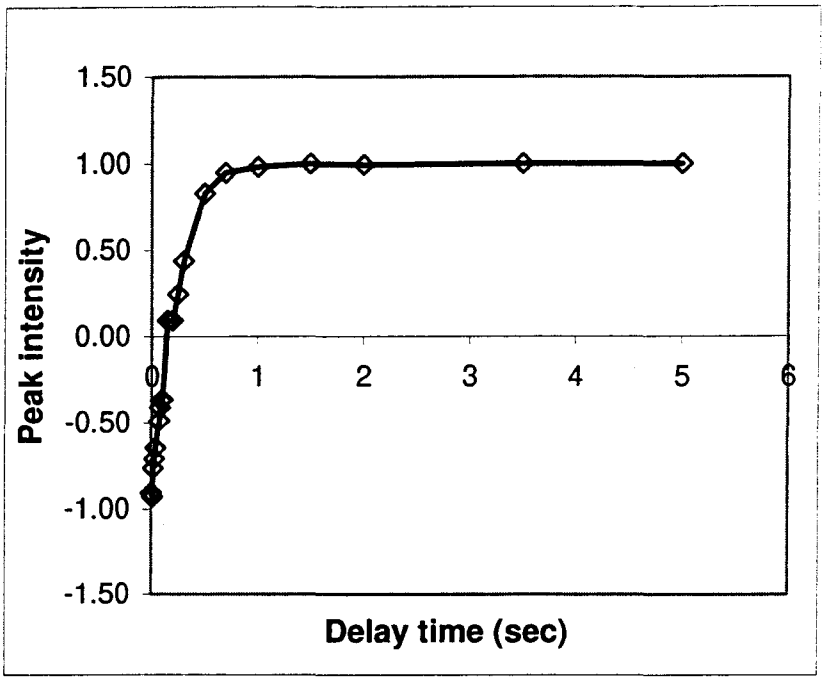

Figure 21. ^{2}H T1 relaxation data for CD3-glucoside gives a T1 value of 0.25 seconds.

A T1 value for the methyl glucoside relaxation was determined to be 0.25 s. For quantitative NMR, a 1.25 to 2.5 s delay is required for complete relaxation.

4 Discussion:

Acid catalyzed methyl glucoside hydrolysis occurs by specific acid catalysis; with a fast pre-equilibrium protonation of the exocyclic oxygen followed by rate determining cleavage of the C1-O bond. The enzymatic hydrolysis of glucosides by retaining glucosidases is thought to occur by a double displacement mechanism involving the oxocarbenium ion-like transition states. The Koshland mechanism[74] proposes an enzyme bound intermediate (Figure 8), whereas the Philips mechanism[101,102] proposes a discrete oxocarbenium ion that is stabilized electrostatically by an active-site carboxylate. In support for the Koshland mechanism, Withers and coworkers showed the production of an enzyme bound intermediate, using 2-deoxy-2-fluoro-glucoside, β-glucosidase and ^{19}F NMR.[72]

KIE experiments have been used to elucidate the mechanisms of enzymatic and non-enzymatic glycoside hydrolysis. These studies used a variety of substrates as shown in Table 1 and Table 2. It was found that the mechanism of the reactions changed, depending on the identity of the leaving group and mechanistic questions about the hydrolysis of the natural enzyme substrate remain.

For the acid-catalyzed and spontaneous hydrolyses of glucosides, it can be generalized that: glucosides with anionic leaving groups, such as **α-4**, are hydrolyzed by A_ND_N reactions while glucosides with neutral

leaving groups, such as isoquinolinium are hydrolyzed by $D_N{}^*A_N$ reactions. For enzymatic hydrolyses of α-glucosides, the opposite has been found. The glucosides with anionic leaving groups hydrolyze by $D_N{}^*A_N$ reactions and the neutral leaving groups hydrolyze by an A_ND_N mechanism.

Until now, the natural abundance measurement of KIEs on an enzymatic reaction was unprecedented. To date, no KIEs have been measured on the enzyme catalyzed hydrolyses of methyl glucosides, even though the methanol leaving group is closer to the natural substrate than other leaving groups such as: fluoro, pyridinium or phenyl groups. Therefore, the KIEs measured here have significance to the overall understanding of glucosidase mechanisms. Bennet and coworkers predicted that the leaving group of the natural substrate would be the partially deprotonated alcohol, carrying a partial negative charge at the transition state.

4.1 Primary ^{13}C KIEs:

The primary ^{13}C (or ^{14}C) KIE depends on the concertedness of the reaction.[79] $D_N{}^*A_N$ reactions have [1-^{13}C] KIEs in the range 1.00 to 1.01 and A_ND_N reactions are in the range 1.03 to 1.08. The differences in the KIEs result from differences in the reaction coordinate motion at the transition state.[5]

For the acid catalyzed hydrolysis of **2**, the measured primary ^{13}C KIEs match the values measured by Bennet and Sinnott.[84] This lends support for the accuracy of the KIEs measured here. The α-methyl glucoside ^{13}C KIE was 1.007, indicating that the reaction occurs by a $D_N{}^*A_N$ mechanism. Similarly, the 1-^{13}C KIE for **β-2** was 1.011, slightly larger than the **α-2** value, but still consistent with a $D_N{}^*A_N$ mechanism. Additional support for the $D_N{}^*A_N$ mechanism is the previous observation that adding of solutes of varying nucleophilicities has no effect on the rate of the reaction.[84]

The primary ^{13}C KIE for the α-glucosidase reaction showed a similar value to the acid catalyzed reaction, i.e. a small KIE indicating a $D_N{}^*A_N$ mechanism. It seems that as one possible catalytic strategy used by the enzyme, protonation of the exocyclic oxygen by the acid/base residue, is sufficient for the catalysis of the C-O bond cleavage, without the assistance by the nucleophilic carboxylate. Therefore, in this mechanism, the formation of the enzyme-bound glucosyl intermediate would occur following rate determining C-O bond cleavage. The result coincides with the prediction by Bennet and coworkers[86] that the methoxy leaving group with be a partially negatively charged species. The measured KIE of 1.008 was essentially the same value as for the anionic fluoro glucoside.

The primary ^{13}C KIE for the β-glucosidase reaction was 1.032, larger than the KIE for **α-2**. This value indicated that there is some nucleophilic involvement by the nucleophilic carboxylate for C-O bond cleavage. Nucleophilic assistance for **β-2** is consistent with previously reported evidence for nucleophilic participation in the hydrolysis of α-*N*-glucosides by an α-glucosidase.[86] The KIE indicated that the formation of the enzyme-bound intermediate occurs simultaneously with C-O bond cleavage. The nucleophilic assistance observed with β-**2** may arise, at least partly, from the difference in exocyclic bond lengths between α-**2** and β-**2** due to the anomeric effect. Electron donation from the C5 lone pairs to the C1-O σ* anti-bonding would weaken the C1-O bond, assisting leaving group departure. This may also explain why primary isotope effects are consistently larger for the β-glucosides compared to the α-anomers.

There is mounting evidence in support of the Koshland mechanism, in which the intermediate is an enzyme bound species and not an oxocarbenium ion stabilized by electrostatic interaction between the active site carboxyl and the positively charged oxocarbenium ion. For example, Withers and coworkers showed the production of an enzyme bound intermediate on an α-glucosidase. The β-glucosidase results, which show an A_ND_N mechanism are in support of the Koshland mechanism in which nucleophilic attack by a carboxylate leads directly to an enzyme bound

intermediate. The small KIEs from the α-glucosidase reaction (indicating an $D_N{}^*A_N$ mechanism) for methyl glucoside hydrolysis do not require the Philips (electrostatic) mechanism, however, because the active site nucleophile may attack the oxocarbenium ion following the departure of the methanol leaving group (i.e. after the rate determining step). Thus, those KIEs are also consistent with the Koshland mechanism.

From the values of the primary KIEs, it can be concluded that the α-methyl glucoside hydrolysis is more "oxocarbenium ion-like" compared to the β anomer (for both acid catalysis and enzyme catalysis). There is more oxocarbenium ion character to the acid catalysis compared to enzyme catalysis in the β-methyl glucoside hydrolysis.

4.2 Secondary ^{13}C KIEs

Historically, heavy atom (non ^2H or ^3H) secondary KIEs have generally not been measured because they were expected to be essentially unity. Large ^2H and ^3H KIEs are usually used to provide conformational information of the transition state. The determination of all the secondary ^{13}C KIEs is unprecedented for an enzymatic reaction, though Singleton and coworkers have done so for a number of organic reactions (see above).

The measurement of significant secondary ^{13}C KIEs at C2 and C5 of a glucoside hydrolysis reaction was unexpected. The largest α-secondary ^{13}C KIE measured to date on a glycosyl system, 1.037, was on hydrolysis of cytidine monophosphate N-acetylneuraminate (CMP - NeuAc).[103] Such a large α-secondary KIE, however, is a reflection of the electrostatic interaction between the carboxylate and the glycosyl cation, which Horenstein concluded was the source of the KIE as it would "drive open the OCO bond angle".[103] This KIE cannot be directly compared to the glucosyl ring ^{13}C KIEs in this study where there is not such a close juxtaposition of positive and negative charges.

In Singleton's study of the uncatalyzed decarboxylation of orotic acid, the α-secondary ^{13}C KIE was 1.004.[104] An α-secondary EIE of 1.0066 to 1.0113 for different temperatures, has been measured on the rearrangement of the 2,3,-dimethyl-2-butyl cation **11**.[105] The EIE was likely a result of both the inductive and hyperconjugative effects to the methyl group as well as the increase in vibrational freedom as a result of the planarity of the cation species.

11

Figure 22. α-secondary EIE for the rearrangement of 2,3-dimethyl-butyl cation.

The experimental KIEs for C2 in the methyl glucoside hydrolyses were in a similar range. The C2 KIE is expected to result from the same effects as for the dimethyl butyl cation, induction and hyperconjugation, which result in bond weakening and planarity of the oxocarbenium ion which increases out-of-plane bending motions. Therefore, it is not surprising that the values are similar.

The **α-2** reactions show some differences in secondary KIE when comparing the acid catalyzed reactions to the enzymatic reactions, most notably at C3, C5 and C6. Based on ^{13}C KIEs only, it is not possible to determine the exact difference in the structure between the acid catalyzed and the α-glucosidase catalyzed transition states at C3, C5, C6; however, the fact that the KIEs are different in these two reactions necessarily indicates that the enzyme is using binding energy to change the structure in this region and thereby promote catalysis.

The secondary KIEs for acid-catalyzed and enzyme catalyzed **β-2** hydrolysis differ at C5 and C6. The significance of these KIEs is the same as with **α-2** hydrolysis.

4.3 Computational EIEs:

Since the transition state of the reaction is expected to be similar (structurally and energetically) to an oxocarbenium ion, the KIEs can be

compared to the calculated EIEs. This does not apply to the primary ^{13}C KIE, however, because there is a contribution from the reaction coordinate motion.

Comparisons of the calculated EIEs and the measured KIEs are shown in Figure 23 to Figure 27. The experimental secondary KIEs for **β-2** hydrolysis match well with the calculated EIE providing confidence that the experimental KIEs are on the chemical step of the reaction. As well, similar secondary KIEs and calculated EIEs indicate that the transition state for the reaction is close in structure to the oxocarbenium ion.

4.3.1 ^{13}C EIEs

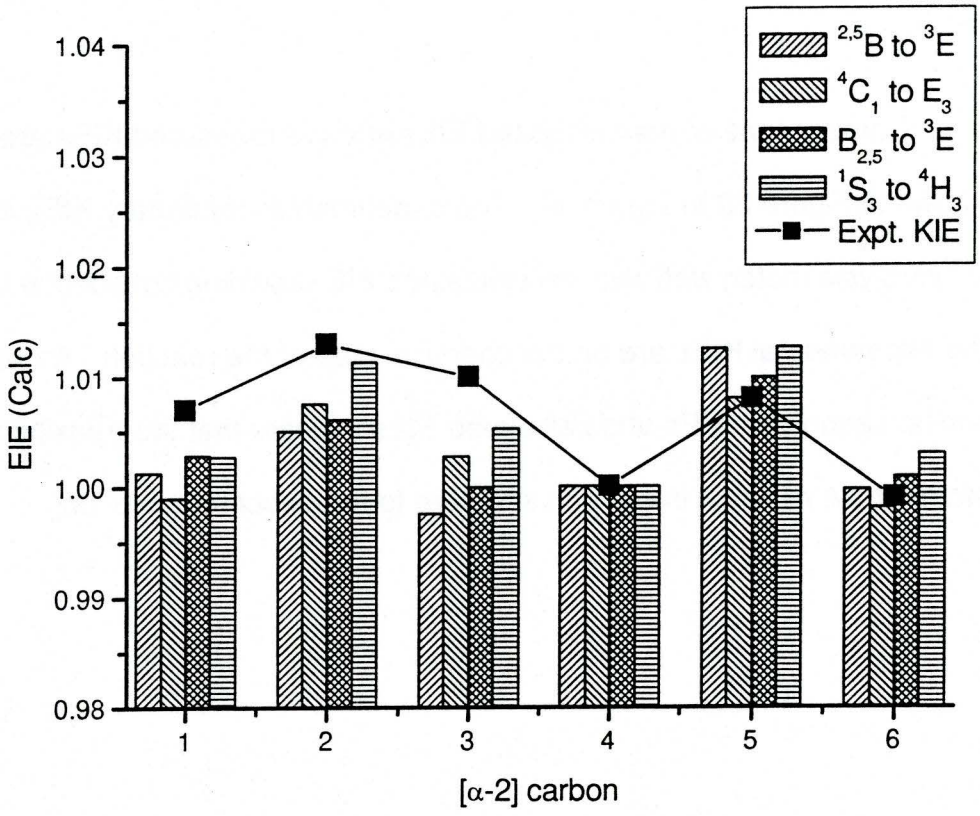

Figure 23. Comparison of experimental ^{13}C KIEs (lines and symbols) to calculated ^{13}C EIE (bars) acid catalyzed hydrolysis of **α-2**.

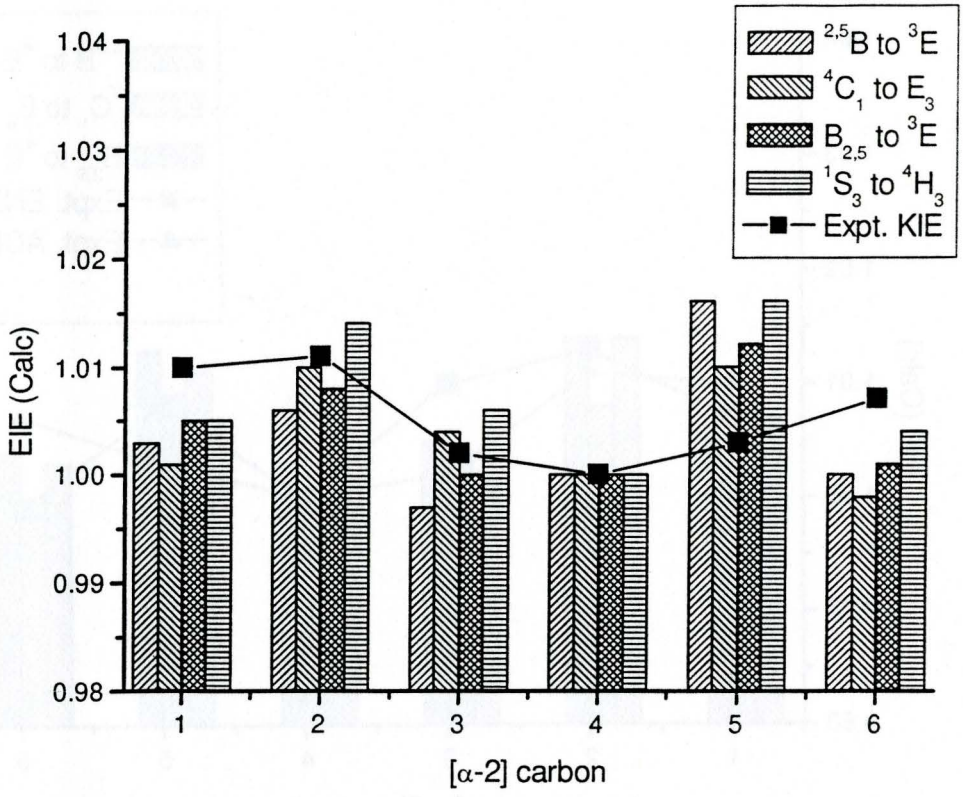

Figure 24. Comparison of experimental ^{13}C KIEs (lines and symbols) and calculated ^{13}C EIEs (bars) for α-glucosidase catalyzed **α-2** hydrolysis.

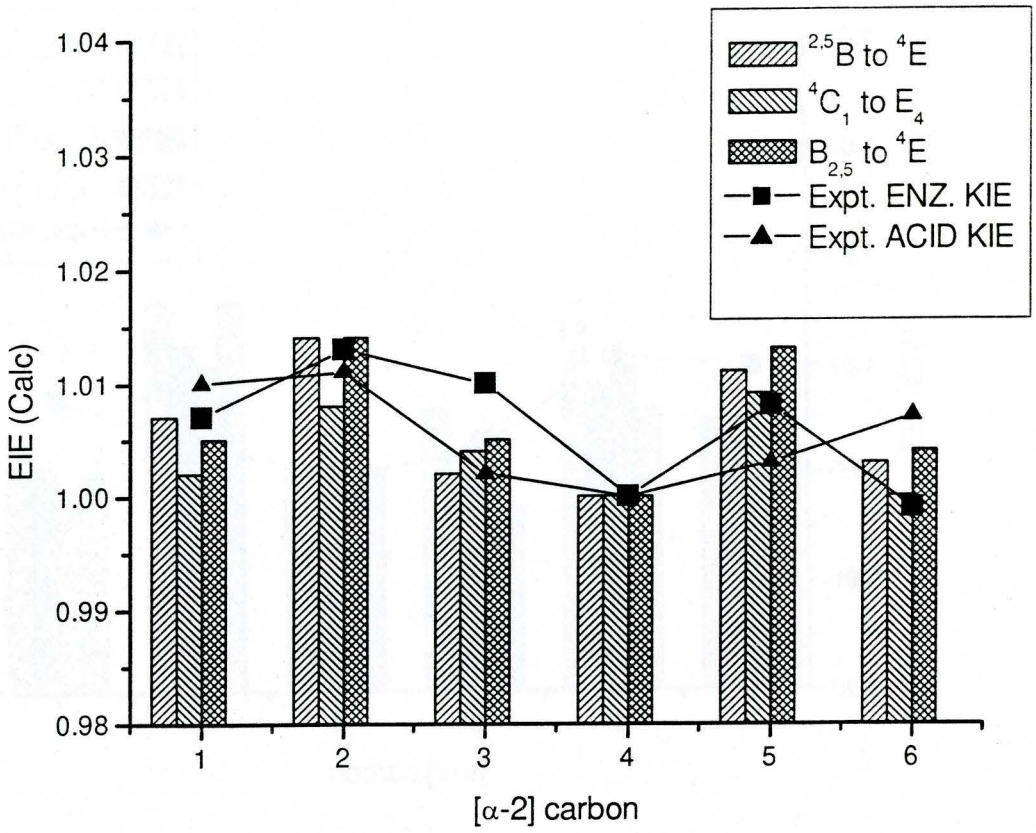

Figure 25. Calculated EIE using the E_4 oxocarbenium ion shows increases in the EIE at C2 and C3 compared to previous calculations, which used ^3E and E_3 oxocarbenium ion structures.

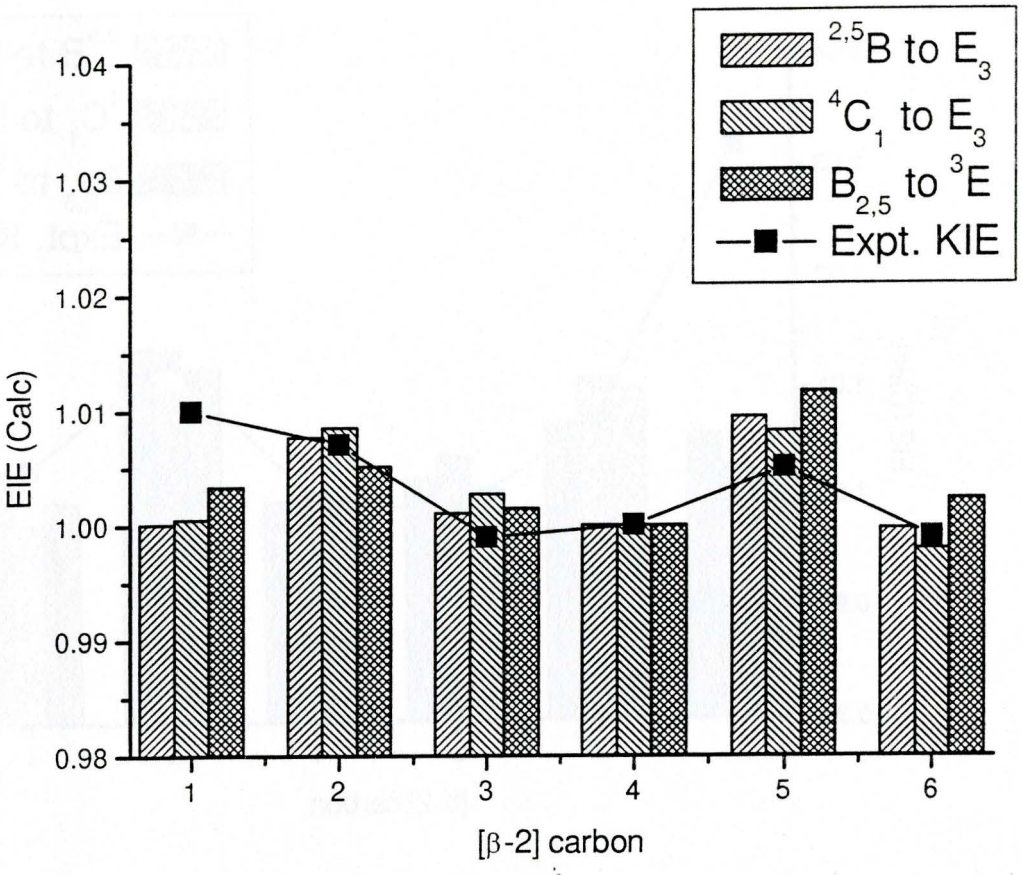

Figure 26. Comparison of experimental ^{13}C KIEs (lines and symbols) to calculated ^{13}C EIE (bars) for acid catalyzed hydrolysis of **β-2**.

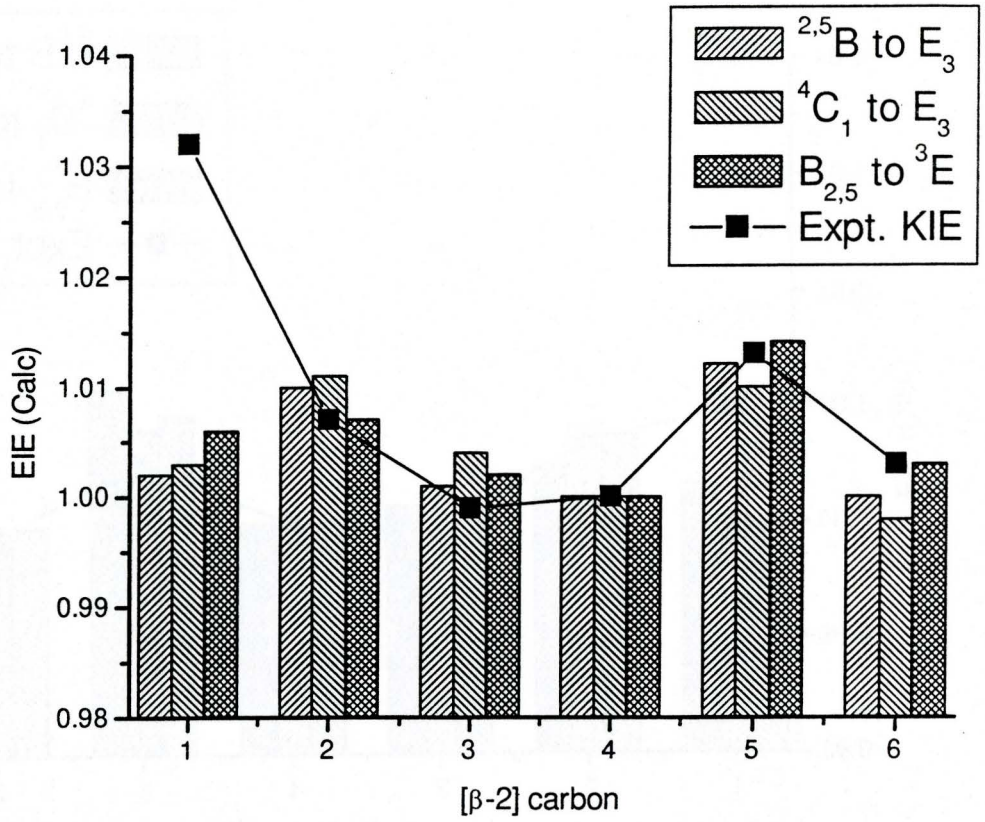

Figure 27. Comparison of experimental ^{13}C KIEs (lines and symbols) and calculated ^{13}C EIE (bars) for β-glucosidase catalyzed **β-2** hydrolysis.

The α-methyl glucoside reactions show significant similarities and differences between the acid catalyzed, enzyme catalyzed and the calculated EIEs. As described above, both enzyme and acid catalyzed reactions are $D_N{}^*A_N$, and match the low EIE value, further supporting a highly dissociative mechanism and a transition state that is closer to the intermediate than the reactant state in reaction space. The differences in the KIEs and EIEs are notable at C2 and C3 (Figure 23).

The difference in calculated EIEs for the C2 and C3 to the experimental KIEs was greater that at the other carbons. Therefore, attempts were made to improve the agreement, with some success. Two other ring conformations were attempted, including an envelope (E_4) for the oxocarbenium (Figure 25) and small increases in the EIE at C2 and C3 were observed. A skewed structure ($^1S_3$) was also attempted. The skew conformation, gave increases in the calculated C2 and C3 EIEs, and appeared to give the best fit to the experimental KIEs (Figure 23). This observation coincides with the results of Bennet and Sinnot[84] who found that the skew conformation best fit the KIEs measured on the acid catalyzed hydrolysis of α-methyl glucoside.

Secondary ^{13}C KIEs provided some ring conformational information for the transition states. For the **β-2** (Figure 26 and Figure 27), there was little difference in the calculated ^{13}C EIE with differing ring conformations. For the **α-2**, the calculated EIEs for the $^1S_3$ conformation agree best in a qualitative way with the experimental KIEs because the other conformations were more different at C2 and C3.

4.3.2 ^2H EIEs

The calculated ^2H EIEs show larger differences in value depending on the conformations of the methyl glucosides used. When ^2H KIE are measured, then the values will allow the determination of the TS

structures in greater detail. The major source of the conformational information is the ^{2}H2 KIE, which results from hyperconjugation to the positively charged p-orbital on the anomeric carbon. There is a $\cos^2$ dependence of the KIE on the dihedral angle (ω) of the p-orbital and the C-H bond of C2. The maximum KIE will result when the dihedral angle is 0° or 180° and at a minimum at 90°.[84]

$$ln(KIE_{expt}) = ln(KIE_{max})\cos^2\omega \quad (8)$$

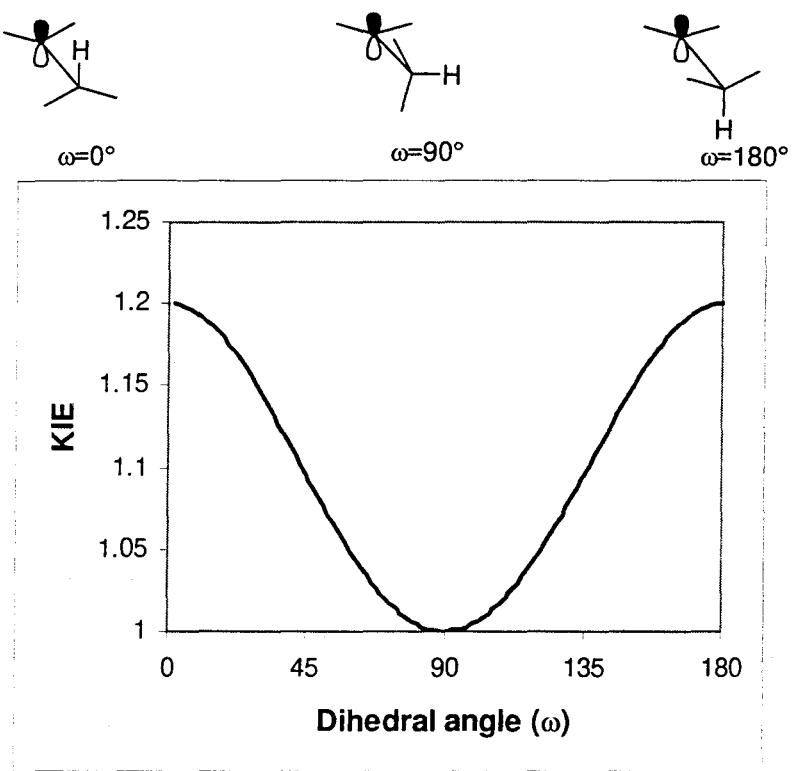

Figure 28. The β-secondary ^{2}HKIE depends on dihedral angle (ω). A maximum value of 1.2 was arbitrarily chosen.

4.4 Commitment to catalysis

External commitment of catalysis occurs when an enzyme becomes so efficient at catalyzing a reaction that the first irreversible step of the reaction becomes binding of the enzyme to the substrate. This means that KIEs measured by competitive methods will only reflect substrate binding and will have no information on the chemical step of the reaction. Commitment becomes a problem when enzymes approach diffusion-rate-limiting efficiency and is unlikely for the present system because the **α-2** and **β-2** are low-activity substrates for the glucosidases.

Because the K_M values were so large, the pulse-chase method normally used to determine external commitment to catalysis was not possible[8]. The method requires enzyme concentrations approaching K_M of the substrate, which is impossible to achieve in this case, where K_M = 61 or 440 mM (Table 11 and Table 12).

Based on steady-state kinetic constants, it is possible to argue that external commitment to catalysis for both the α-glucosidase and β-glucosidases with **α-2** and **β-2** would be negligible and also make statements about the first irreversible step of the reaction. The steady state kinetic parameters, K_M, k_{cat} and k_{cat}/K_M were determined for β-glucosidase and recombinant α-glucosidase (Table 11 and Table 12). These enzymes are known to operate by double-displacement

mechanisms, with an enzyme bound intermediate (Figure 8). As the second step of the mechanism involves deglycosylation of this intermediate, the identity of the aglycone would have no effect on the deglycosylation rate, which is identical for both the methyl glucoside and *p*-nitrophenyl glucoside reactions. Therefore, any differences in the steady-state kinetics of these two substrates result from the binding and/or the glycosylation step.

For **β-2**, the K_M determined for the methyl-glucoside was 180 times larger than for that of the *p*-nitrophenyl glucoside, a good substrate for the enzyme. By definition, K_M is the substrate concentration at which the reaction rate is ½ V_{max} but is also the apparent dissociation constant. K_M can be larger, smaller, or equal to K_s, the true dissociation constant for enzyme-substrate binding (9).

$$E \bullet S \underset{}{\overset{K_s}{\rightleftharpoons}} E + S \qquad (9)$$

K_M is larger than the dissociation constant (K_s) only in the case where enzyme-substrate association becomes rate-limiting and k_{cat}/K_M approaches 10^7-10^8 $M^{-1}s^{-1}$; far larger than what is seen for methyl glucoside hydrolysis (Table 11 and Table 12).[106] K_M can be less than K_s under a variety of circumstances, such as when the rate-limiting step occurs after the first irreversible step of the reaction. Because the present

reactions did not follow Brigs-Haldane kinetics, it was safe to assume that K_M was either less than K_s, or equal to it. As K_M was 180-200 times higher for **α-2** and **β-2** than *p*-nitrophenyl glucoside, K_s is also likely much higher.

^{18}O KIEs measured on the β-glucosidase catalyzed hydrolysis of β-*p*-nitrophenyl glucoside show that the C-O bond is being broken at the transition state, indicating that the chemical step is the first-irreversible step.[91] The first implication is that the binding of aryl glucoside is not the first-irreversible step, and as binding of the **β-2** is poorer, binding is not the first-irreversible step for **β-2** either. The second implication is that the glycosylation step of reaction is the first irreversible step. Since the k_{cat}/K_M (V/K) for methyl glucoside was 3500 fold smaller than for the *p*-nitrophenyl glucoside, the energetic barrier for the first-irreversible step of **β-2** should be higher by the same factor. This further increases the likelihood that the first chemical step is the first irreversible step for methyl glucoside. Furthermore, the large primary ^{13}C KIE (1.032) would only occur if the KIE reflected the chemical step.

Hydrolysis of **α-2** was unlikely to have external commitment to catalysis, simply because the K_M was high, indicating a fast dissociation of enzyme bound intermediate. In addition, the $^{13}C2$ KIEs measured on the **α-2** hydrolysis are similar for both the acid and enzyme catalysis reactions, which also supports a lack of commitment to catalysis. The

changes in vibrational environment at C2 likely result from the formation of the oxocarbenium ion-like TS.

Hosie and Sinnott[99] found that the leaving group ^{18}O KIE was suppressed in α-*p*-nitrophenyl-glucoside hydrolysis and concluded that it was a result of a partially rate limiting conformational change from a chair to a boat conformation (an example of internal commitment to catalysis). In addition, there was an inverse α-secondary ^{2}H KIE, which would not occur if the chemical step is the rate-limiting step. Presumably, **α-2** is also starting from the chair conformation.

p-Nitrophenol is a much better leaving group than methanol. Methyl glucoside hydrolysis requires harsh acidic and high temperature to promote hydrolysis, whereas some aryl-glucosides spontaneously hydrolyze at 25°C.[107]

Commitment to catalysis is more likely for the *p*-nitrophenyl-glucosides because *p*-nitrophenol is better leaving group, meaning that the energetic barrier for hydrolysis may be small enough to make binding and conformational changes the first irreversible steps. As V/K was 4000 times smaller for **α-2** hydrolysis than for *p*-nitrophenyl-glucoside hydrolysis, the energetic barrier at the first-irreversible step must be greater by the same factor. This can suggest that either the conformational change is 4000-fold slower for **α-2** or a more likely

explanation is that the C-O bond cleavage is much slower in the case of the methyl glucoside because the activation energy is higher, a result of the worse leaving group. However, internal commitment cannot be definitively discounted.

In order to more fully address the question of commitment in the case of methyl glucoside hydrolysis, the α-secondary ^{2}H KIE should be measured. The α-secondary ^{2}H KIE on the chemical step will be large and normal as predicted in the calculated EIE (Table 21 and Table 23) and is also well established in the literature.[28-31,85,89]

4.5 NMR measurements and methods

The measurement of KIEs with precisions as high as ±0.001 to 0.005 demands rigorous analytical techniques that afford a high level of reproducibility and small errors on detection. To this end, the quantitation of isotopes by scintillation counting is usually performed with successive measurements, over a period of days. By recording many measurements on the same sample, the confidence intervals on the experimental KIE are narrowed to less than 0.5%.

Likewise, the NMR data in this study was acquired in blocks, i.e. 16 successive spectra of 256 scans rather than 1 spectrum of 4096 scans. The reasoning behind this practice was to allow (a) statistical analyses on

the acquisition and (b) the removal of any outlying data that could skew the isotope ratios.

Peak intensity (height) was investigated as a means of quantifying the peaks. Using intensity had a number of potential advantages, including simplicity in data analysis and would be less affected by peak overlap with baseline impurities. It was found, however, that the peak quantitation was affected by the manner in which the spectra were processed. Specifically, the value of LB used in the exponential multiplication function changed the value of the KIE. LB is a variable that affects peak width and, it turned out, changes peak intensity non-uniformly throughout the spectrum.

In the Diels-Alder reactions of isoprene, low values of LB exaggerated KIEs, making normal KIEs larger and inverse KIEs more inverse. KIEs only approached the literature KIE values when large LBs (~15-20 Hz) were used, but this caused broad, overlapping peaks. When quantitating the peaks by area, it was found that the KIEs did not vary as a function of LB, meaning that a low LB could be used, affording narrow peaks with excellent peak resolution.

Gaussian transformation was used in this study because the Gaussian peak shape is much narrower at the baseline compared with the Lorentzian line shapes that result from an exponential window function.

Gaussian line shapes have been used for measurement of ^2H KIEs by NMR[10]. Minimizing the amount of peak overlap is essential to proper peak quantitation at a 0.1% accuracy level, which is needed when isotope effects are less than 1%. Narrow peaks were achieved with small values of GB and small negative values of LB. The values of LB and GB are constrained by the fact that when large values were used, baseline artifacts appeared that could affect peak quantitation.

^2H NMR

In the initial ^2H spectrum of **β-2** the ring deuteron peaks were broad and barely visible (Figure 18). The broadening was a result of solution viscosity and the fact that deuterium is a quadropolar nucleus, having inherently broad peaks. Increasing the temperature to 56°C, the boiling point of acetone, in a sealed NMR tube improved signal to noise and peak resolution (Figure 19). The improved peak resolution was a result of decreased viscosity near the boiling point of acetone, the sample solvent. The sample viscosity affects T_2, the spin-spin relaxation time, which relates to peak width.

There is a balance to be attained in sample preparation: between high enough sample concentration for a strong signal and sample viscosity at high concentrations that decreases resolution. Further

improvements in signal to noise are required before high precision isotope effects can be measured on ^{2}H.

4.6 Method development

A purification scheme was developed to isolate residual **α-2** or **β-2** after the reaction had been taken to 90% completion. The product glucose was oxidized to gluconic acid with glucose oxidase (GOD), then separated by anion exchange chromatography, with **α-2** and **β-2** being eluted without retention on the column.

The acid-catalyzed reactions were performed in 2 M $HClO_4$ to reproduce the conditions of Bennet and Sinnott.[84] Before enzymatic oxidation of the glucose, the perchloric acid was removed by neutralization by KOH, precipitating $KClO_4$, which has an aqueous solubility of 100mM. This simplified the anion exchange purification of the residual methyl glucoside.

4.6.1 Methyl glucoside reactions

The acid-catalyzed reactions changed colour during the course of the reaction becoming yellow or dark amber. This was likely due to condensation reactions involving the aldehyde functionality of glucose. Polyalcohols such as inositol and sorbitol gave no colour change when incubated under the same conditions as **2** hydrolysis. No ^{13}C peaks

attributed to condensation were visible in the reaction mixture. Nonetheless, such reactions could have created errors in calculating the extent of reaction if it relied on quantitating product glucose formation. To eliminate this potential source of error, an internal standard was used. Succinic acid was chosen because there was no peak overlap in the ^{13}C spectrum with methyl glucoside or glucose. It is symmetrical, allowing comparatively small amounts to be used in the reaction while still achieving a good NMR signal. Finally, succinate, was easily removed by anion exchange chromatography.

4.6.2 GOD reactions

The idea of using the glucose oxidase (GOD) reaction to remove the glucose from the reaction was originally inspired from Houben *at al.* in which GOD was used to remove the glucose from wheat, allowing the determination of pentosan content by HPLC[108]. Early small scale reactions showed that an initial reaction pH of 8.5 helped the oxidation to go to completion as the pH would drop over the course of the reaction with the production of gluconic acid. If the pH dropped too low, then the enzyme would precipitate out of solution. Also, Houben *et al.* reported that O_2 can become limiting over the course of the reaction, despite the enzymatic regeneration of O_2 from H_2O_2 by catalase. As a result, small scale reactions were more effective when reacted in larger volume containers that left a significant amount of head space.

A greater challenge was encountered when attempts were made to scale up the GOD reaction. The reactions did not go to completion despite the modification of a number of parameters. Bubbling air into the solution seemed to have no effect on the reaction, but caused foaming of the solution and the precipitation of the enzyme. The methanol product or methyl glucoside in solution did not seem to effect the reaction either. It was found, however, that the addition of 0.5 mL of H_2O_2 to the solution seemed to "jump-start" the reaction though the rapid production of O_2 by catalase. Catalase is a diffusion rate-limited enzyme and reacted quickly with the peroxide to produce bubbles of oxygen gas. This seemed to "oxygenate" the solution sufficiently, to drive the reactions to completion. A reaction involving H_2O_2 and glucose (but no enzymes) showed no oxidation of glucose to gluconic acid.

4.7 Conclusions

Natural abundance ^{13}C kinetic isotope effects were successfully measured for the acid catalyzed and glucosidase catalyzed hydrolyses of α and β-methyl glucosides using NMR spectroscopy. The validity of the results is shown in the fact that (1) experimental primary ^{13}C KIEs of the acid catalyzed reactions match well with the literature values[84] and (2) secondary ^{13}C KIEs match well with the calculated EIEs. As well, the

Diels-Alder reaction of isoprene was used to further validate quantitative NMR measurements.

The primary ^{13}C KIE for β-glucosidase hydrolysis of **β-2** shows it involves nucleophilic assistance and is therefore an A_ND_N reaction. The α-glucosidase reaction has a small primary ^{13}C KIE indicating a $D_N{}^*A_N$ mechanism, although internal commitment due to a ring conformational change cannot be discounted and may suppress the KIE.

Large secondary ^{13}C KIEs were measured at C2 and C5, and correspond well with the calculated EIEs. The calculated EIE using the $^1S_3$ conformation best matches the isotope effects for the **α-2** hydrolysis reactions. All the calculated ^{13}C EIEs are similar for **β-2** hydrolysis, regardless of the ring conformations used.

Progress towards the measurement of the ^2H KIEs hinges on the ability to obtain a large enough natural abundance ^2H signal and therefore depends on sample concentration and viscosity. Acquiring ^2H spectra at elevated temperatures greatly improves the broadness and resolution of the ring deuteron peaks. However, better signal-to-noise and resolution are still needed to obtain high precision ^2H KIEs.

Calculated EIEs were used in an attempt to obtain conformational information from measured ^{13}C KIEs. The ^{13}C EIEs show little difference

in value as a function of ring conformation. Calculated ^{2}H EIEs show variation between methyl glucoside conformations and can be used to determine the TS structure when ^{2}H KIEs are measured.

4.8 Future Work

The measurement of ^{2}H KIEs will allow a more accurate determination of the TS structure in the glucosidase catalyzed hydrolysis of **α-2** and **β-2**. The ^{2}H EIEs have already been calculated here for three ring conformations and will be compared to the experimental ^{2}H KIEs. Also, all the ^{13}C and ^{2}H KIEs can be used with Bond Order Vibrational Analysis (BOVA) to computationally determine the TS in atomic detail. Measuring ^{2}H KIEs on **2** will depend, however, on the ability to improve the signal to noise and the resolution of the ring deuterons. High temperature NMR along with improved instrumentation (higher field strength and a ^{2}H probe) will likely be required.

Having determined the TS structure, the design and synthesis of glucosidase inhibitors will follow. The inhibitors will have a wide range of possible applications including the treatment of HIV and cancer.

The method of measuring ^{13}C KIEs developed here for glucosidase reactions is easily extendable to allow measurement of KIEs on other glycosidases such as mannosidases and galactosidases. This will provide

a more general understanding of glycosidase catalysis as a whole. As well, comparison of the results to available protein sequences will allow an understanding of the enzyme mechanism as it relates to it primary amino acid sequence.

Appendices:

Appendix 1. ^{1}H NMR spectrum of α-methyl glucoside in D_2O. (200MHz).

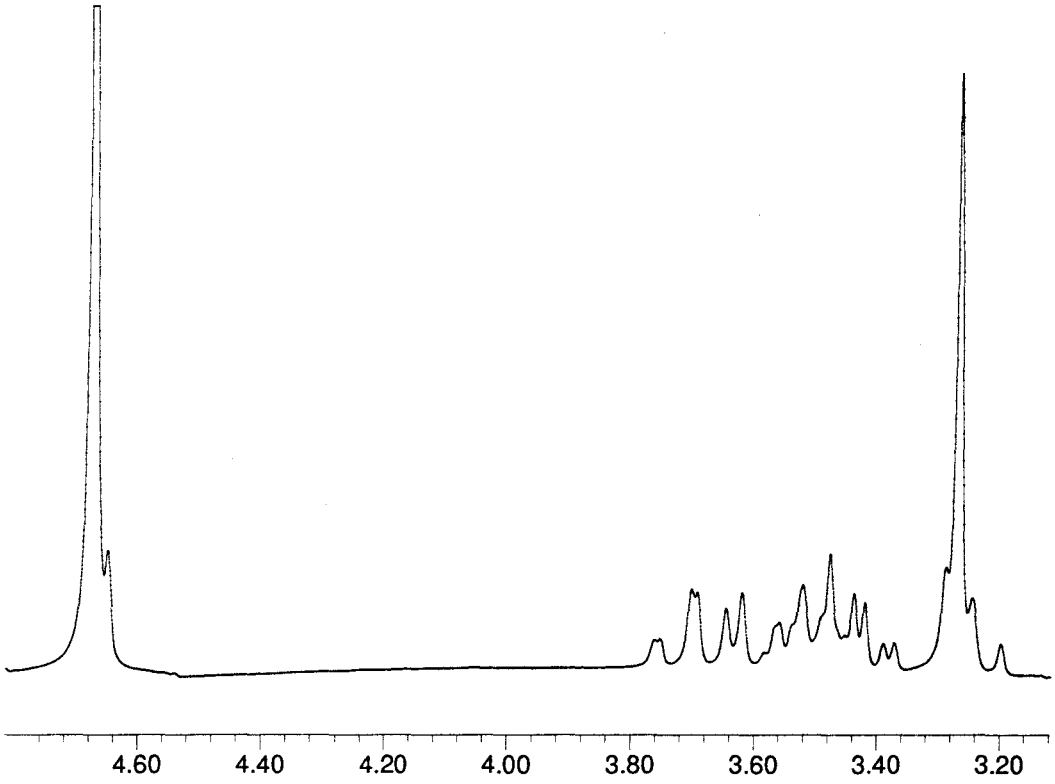

Appendix 2. $^{1}H,^{13}C$, COSY and HSQC NMR spectra for peracetylated α-methyl
glucoside.(600MHz)

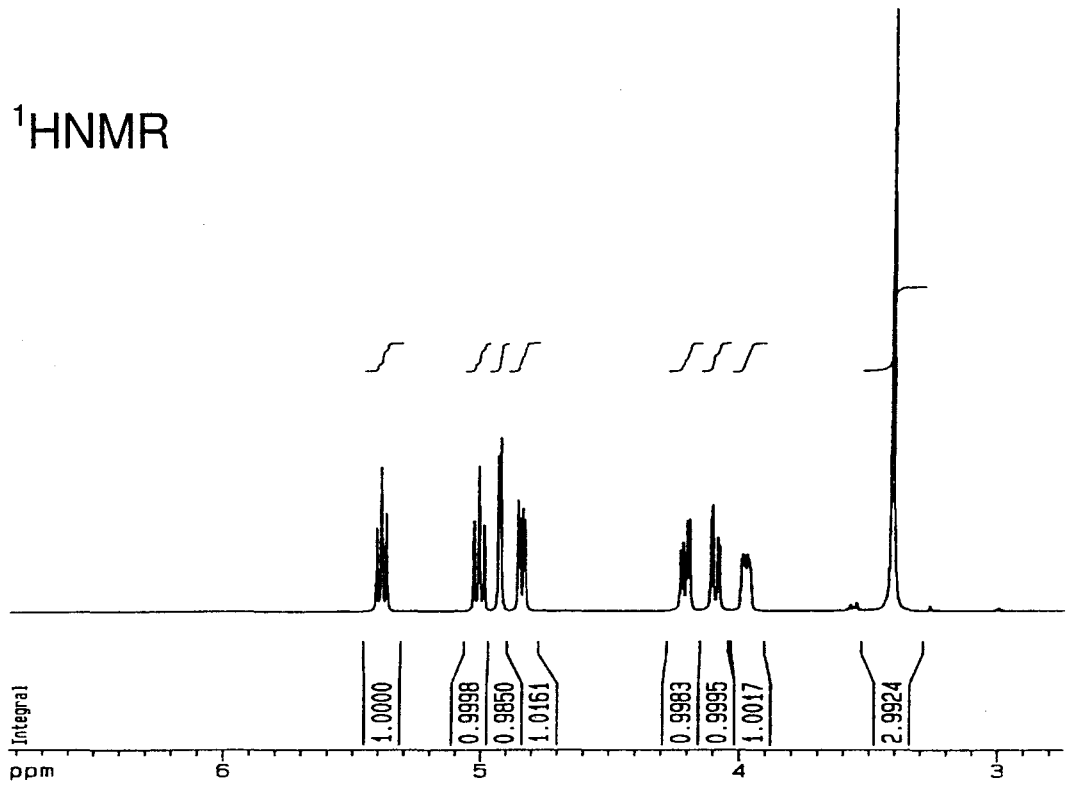

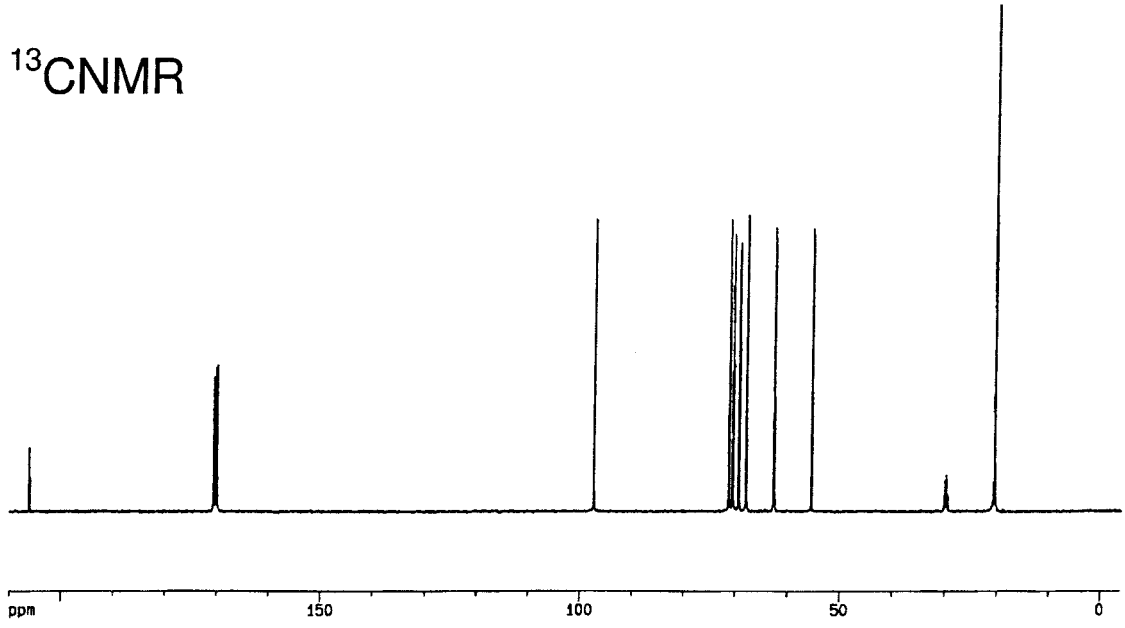
^{13}CNMR
ppm
150
100
50
0

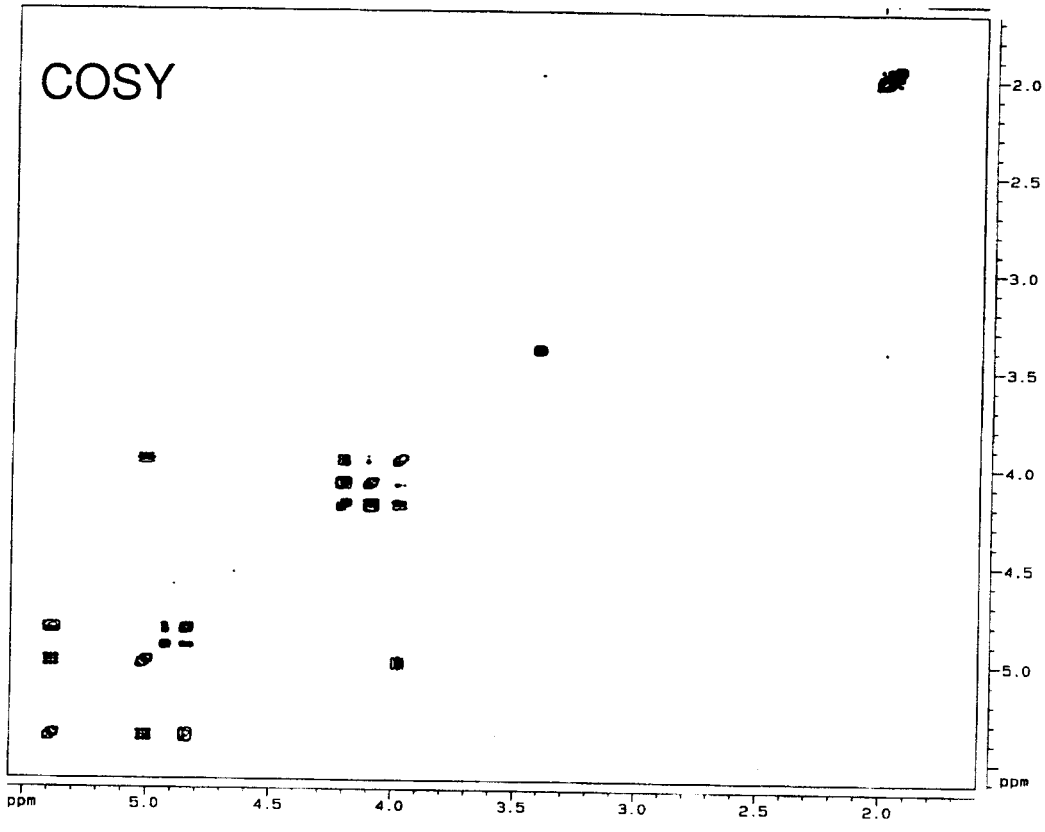
COSY
2.0
2.5
3.0
3.5
4.0
4.5
5.0
ppm
ppm
5.0
4.5
4.0
3.5
3.0
2.5
2.0

HSQC

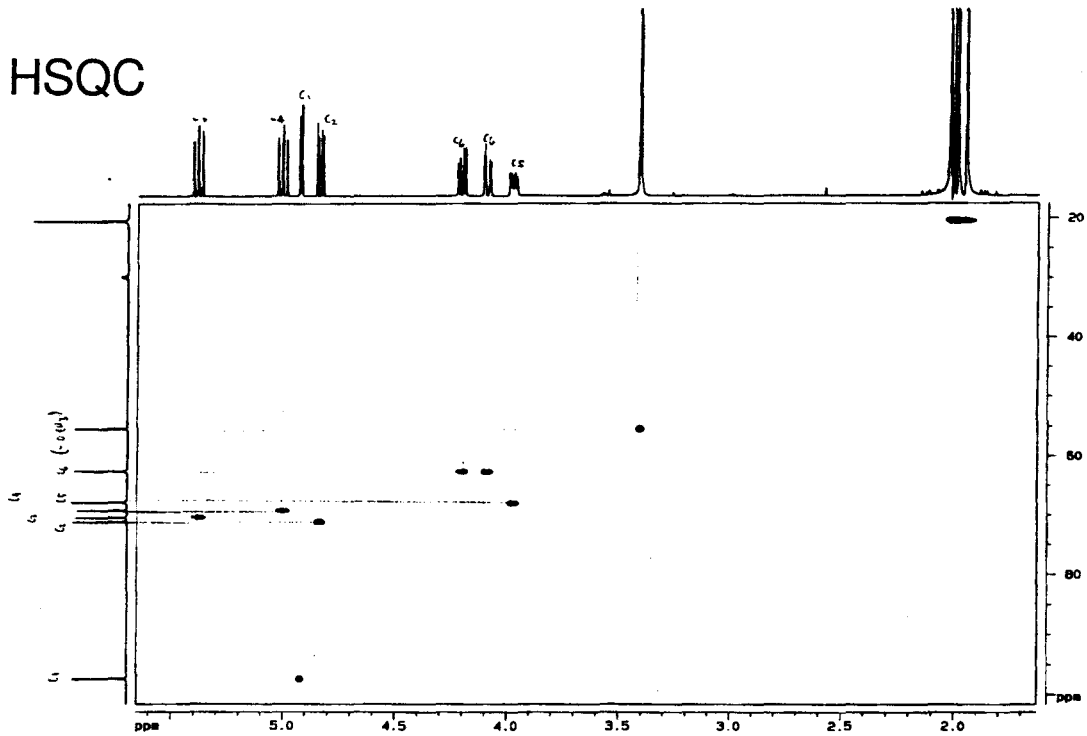

Appendix 3. ^{1}H,^{13}C, COSY and HSQC NMR spectra for peracetylated β-methyl glucoside.

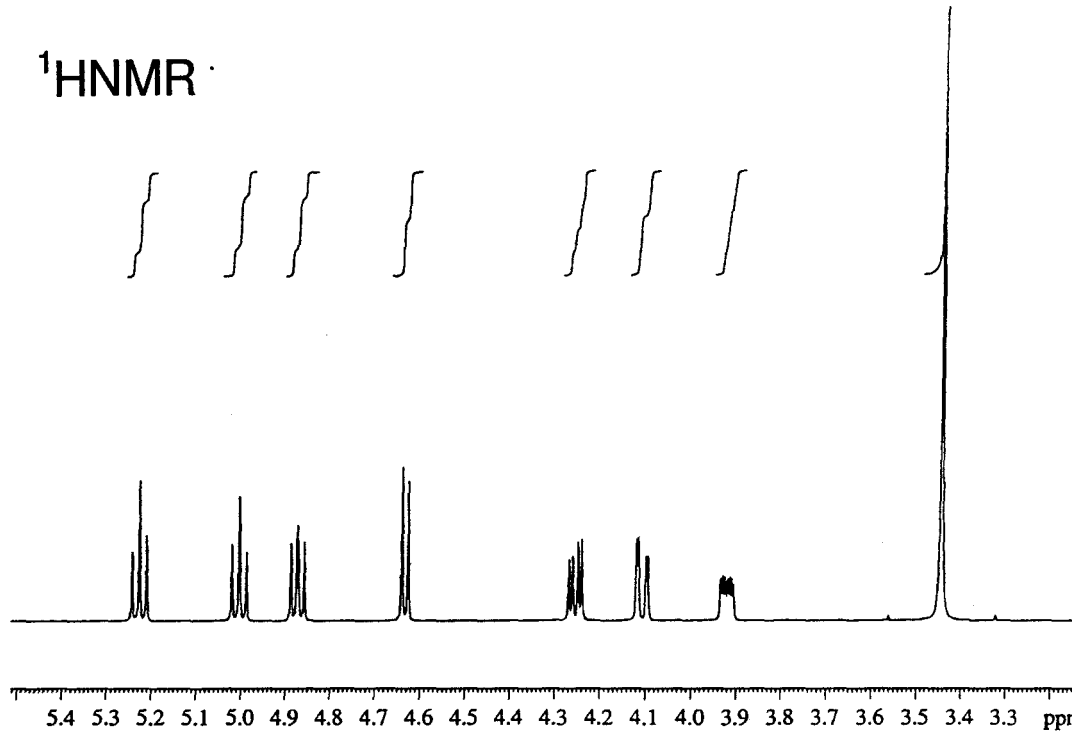

^{13}CNMR

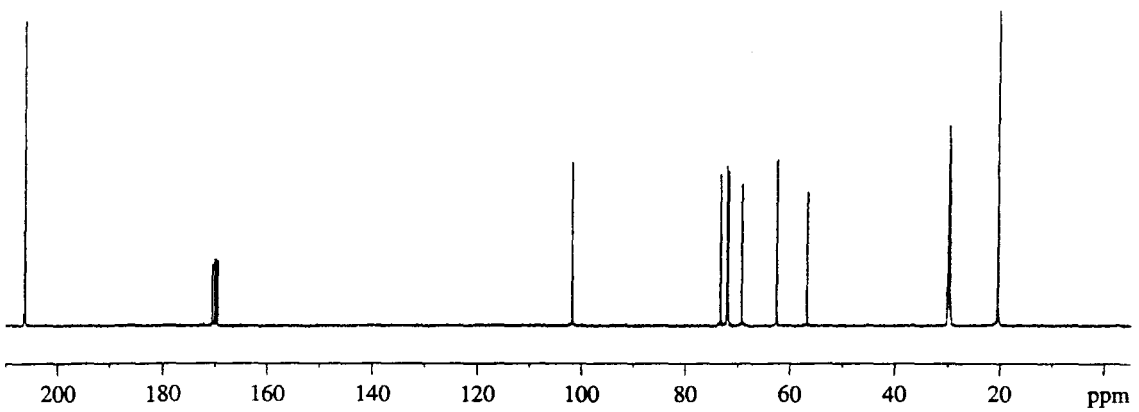
200
180
160
140
120
100
80
60
40
20
ppm

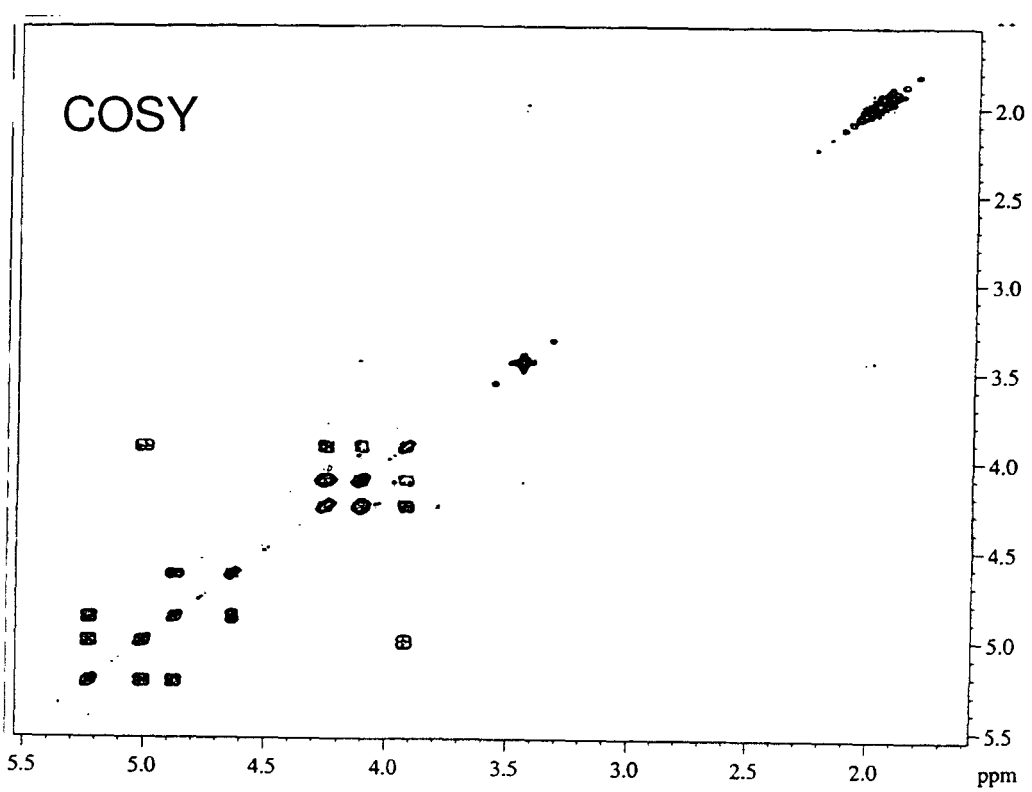
COSY
2.0
2.5
3.0
3.5
4.0
4.5
5.0
5.5
5.5
5.0
4.5
4.0
3.5
3.0
2.5
2.0
ppm

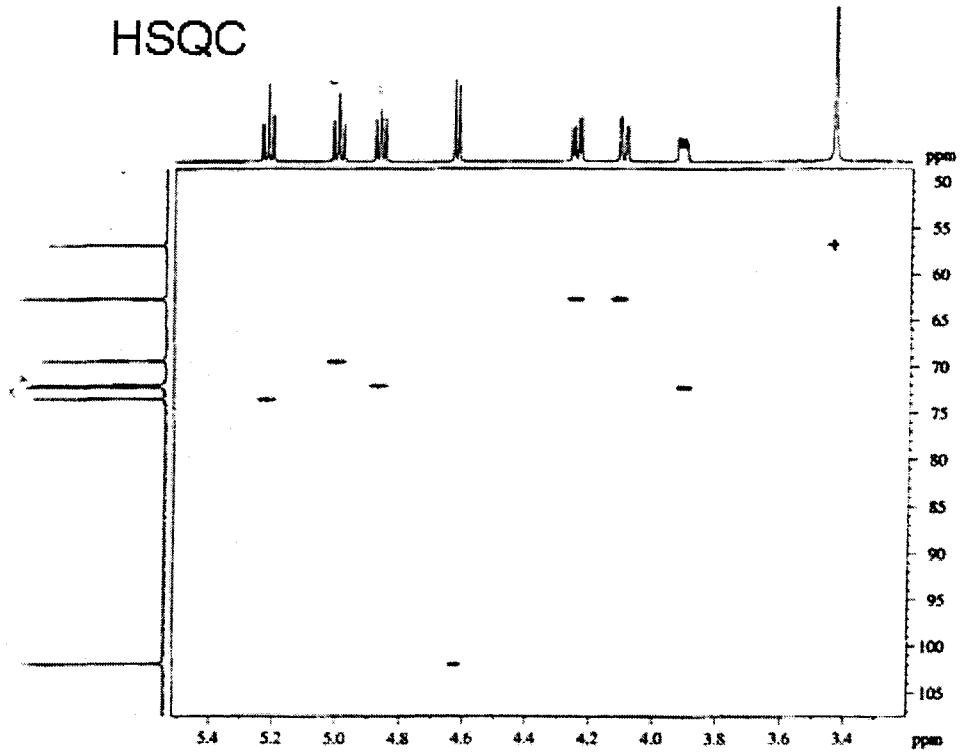
HSQC
ppm
50
55
60
65
70
75
80
85
90
95
100
105
5.4
5.2
5.0
4.8
4.6
4.4
4.2
4.0
3.8
3.6
3.4
ppm

Appendix 4. ^{13}C spectrum of a typical sample following the glucose oxidase reaction showing the residual methyl-glucoside.

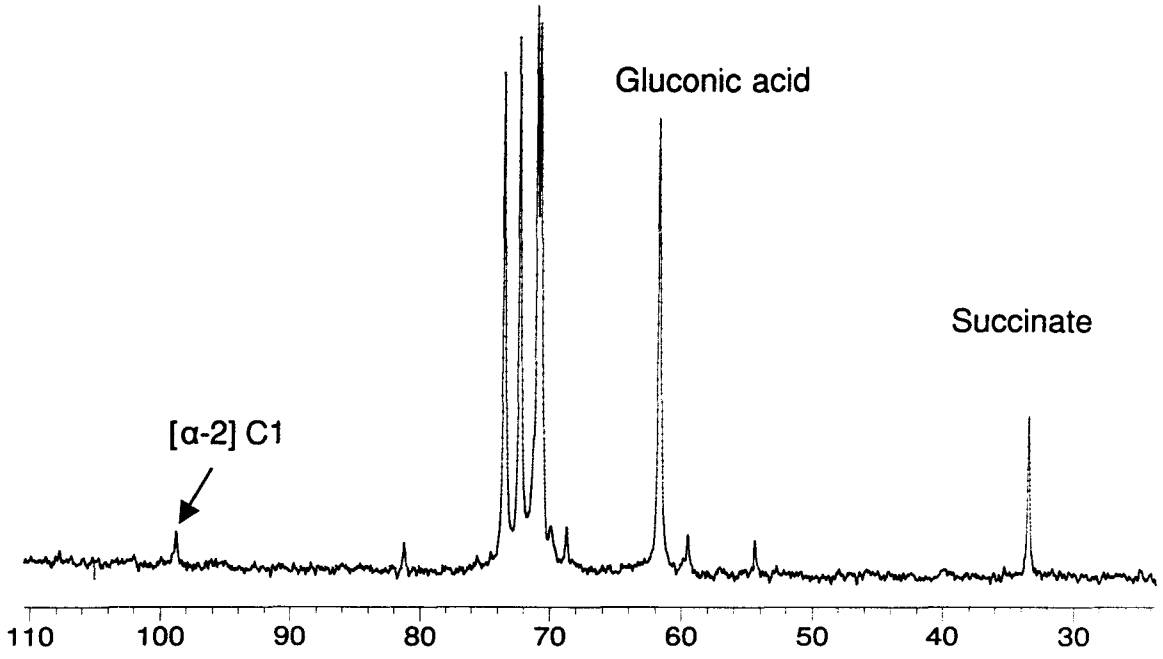

Appendix 5. ^{13}C spectra of the unlabled and labeled syntheses of the deuterium labeled methyl glucosides (CD3-glucoside) showing both the α and β anomers. The methyl carbons (54-56ppm) are split by the presence of deuterium in the labeled material. Shown also are the ^{1}H and ^{2}H spectra for the labeled product.

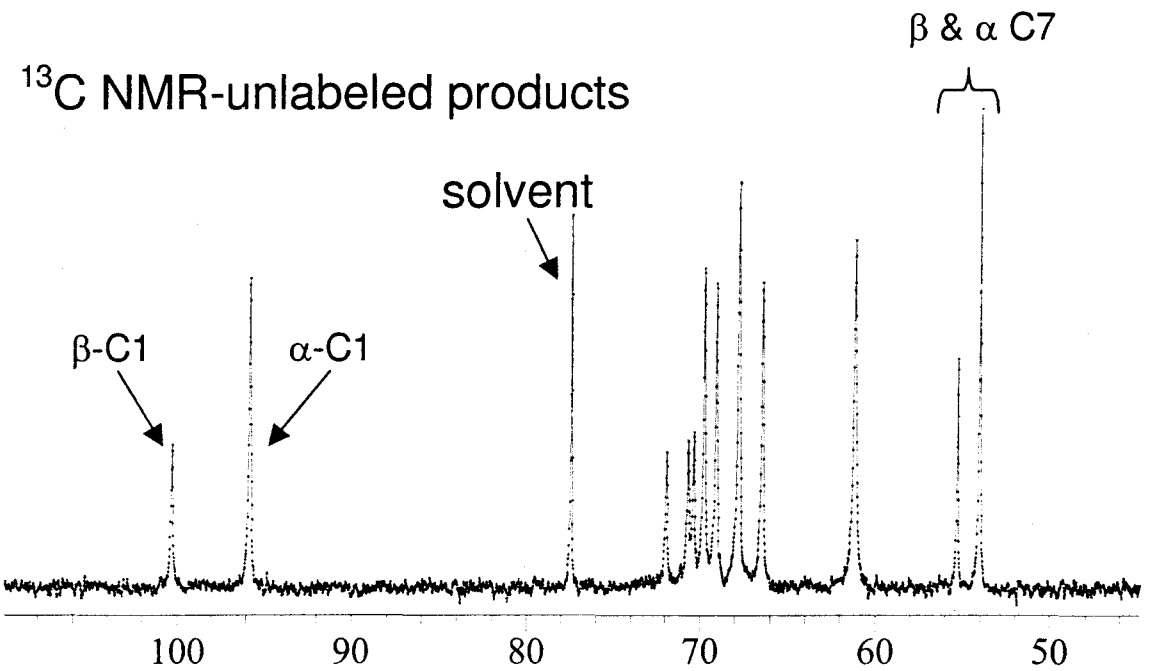

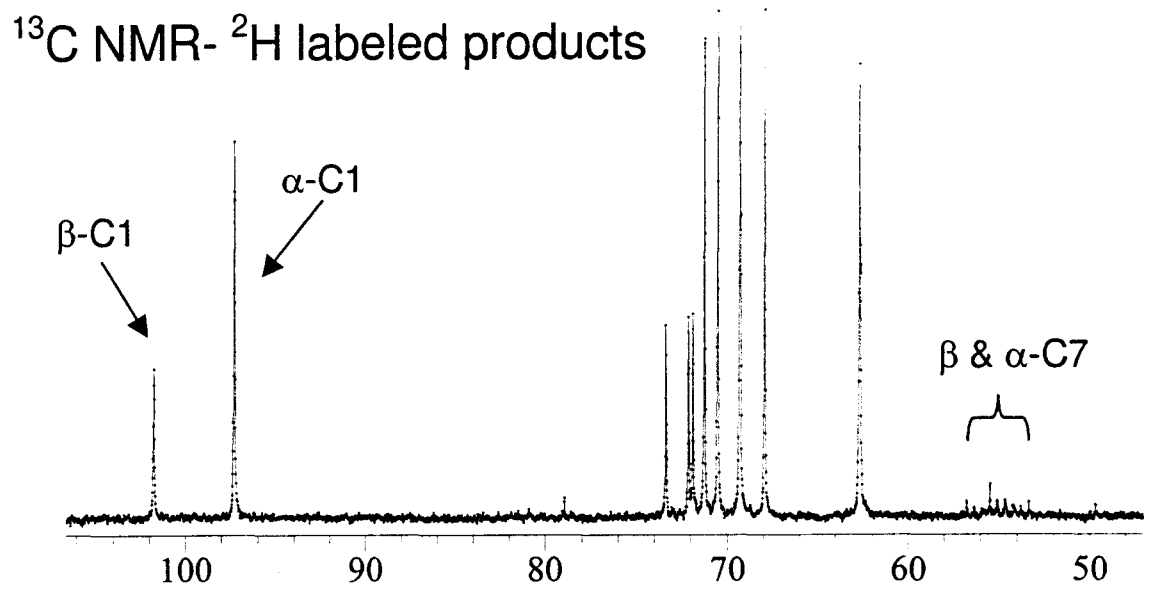
^{13}C NMR- ^{2}H labeled products
β-C1
α-C1
β & α-C7
100
90
80
70
60
50

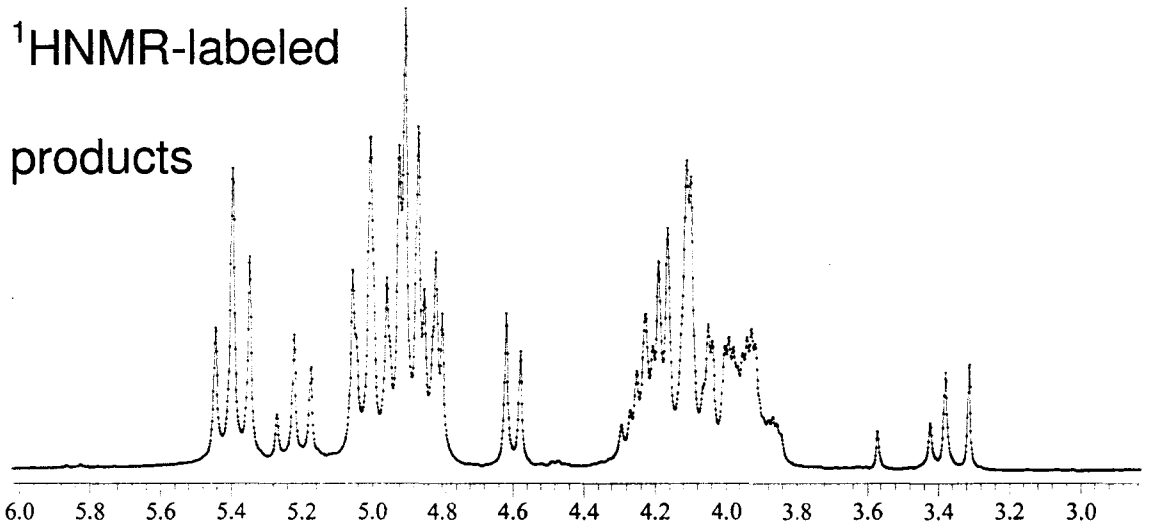
^{1}HNMR-labeled
products
6.0
5.8
5.6
5.4
5.2
5.0
4.8
4.6
4.4
4.2
4.0
3.8
3.6
3.4
3.2
3.0

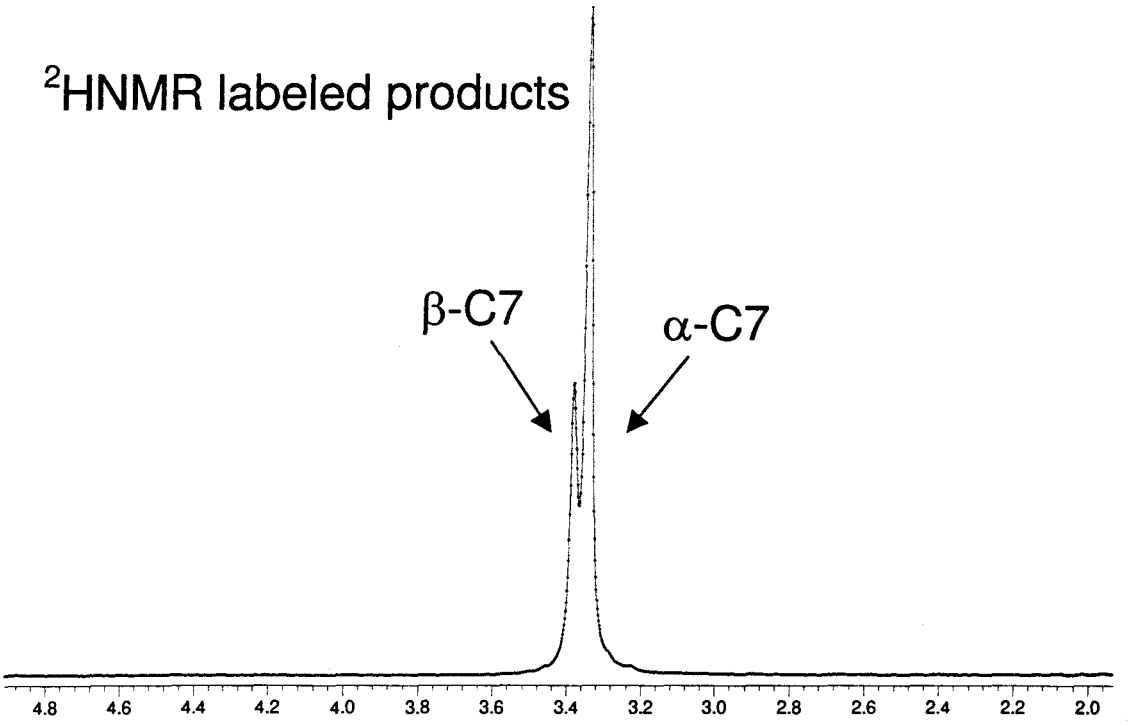
^{2}HNMR labeled products
β-C7
α-C7
4.8
4.6
4.4
4.2
4.0
3.8
3.6
3.4
3.2
3.0
2.8
2.6
2.4
2.2
2.0

Appendix 6. Code for the AU program, used to convert 2D NMR serial files to 1D processed data.

```
/* Author: Jason Lee */
/* this program splits a 2D longterm AQ into 1D spectra and */
/* saves the spectra as increasing proc #s */
/* works on dataset of 16 spectra, can be changed for more or
less
at loops "times(#)"*/
/* the program will work on more than one (successive) data set*/
/* peak intensities saved as (ascii) files, user defined*/
/* peak data is summarized in file pp.all, ftp to lab computer */
/* for now, LB must be changed in the code */
/* start program on 2D spectrum, or else it will not work*/
/* peak output code copied from AU multi_integ */

int tprocno, i4;
int iii, pparmod;
char printname[256], dummystr[256], ppresult[256];
char ppallresult[256];
FILE *fpnt, *fpnt2;

GETCURDATA;
/*getfloat("enter LB you wish to use:",f1);*/
GETINT("enter the number of datasets to be processed:",i3);
(void) strcpy (printname, "JLpeak");
GETSTRING("enter filename for peakpick output files:",
printname);

tprocno=procno+1;
i1=1;
i2=1;
i4=1;   /* while statement loopcounter*/

while(i4<=i3){

SETCURDATA;

RPROCNO(2); /* increases proc number to first 1d spectrum */

            /* open file pp.all */
(void) sprintf (ppallresult,
"%s/data/%s/%s/%s/%d/pdata/%d/pp.all",
   disk, user, type, name, expno, procno);
fpnt2=fopen(ppallresult, "wt");

TIMES(16)
{
  SETCURDATA;
  STOREPAR("CURPRIN", printname);
  /* sets output as filename, see edo */

  CPR_exec("lb -.06", WAIT_TERM);
  CPR_exec("gb .01", WAIT_TERM);
```

```
   CPR_exec("si 256k", WAIT_TERM);
   /*(void) sprintf (text,"lb %f",f1);*/
   /*CPR_exec(text, WAIT_TERM);*/
   (void) sprintf (text,"gfp %d",i1);
                          /*stores "ef #" as string variable
"text"*/
   SETCURDATA;
   CPR_exec(text, WAIT_TERM);     /*executes string variable
"text"*/
   /* CPR_exec("apks", WAIT_TERM); */
   VIEWDATA;
   CPR_exec("f1p 120", WAIT_TERM); /* sets limits for pp */
   CPR_exec("f2p 50", WAIT_TERM);
   CPR_exec("cy 1000", WAIT_TERM); /*sets largest peak to 1000cm*/
   CPR_exec("mi 100", WAIT_TERM);  /* sets min. intensity to
100cm*/
   CPR_exec("pp", WAIT_TERM);     /* writes peakpick to file */

    /* file output code follows */

   (void) sprintf (ppresult, "%s/data/%s/%s/%s/%d/pdata/%d/%s",
disk,
   user, type, name, expno, procno, printname);
   fpnt=fopen(ppresult, "r");

   for (iii = 0; iii < 4; iii++)
     fgets(dummystr, 120, fpnt);
   (void) sprintf (dummystr, "\n%s\n", ppresult);
   fputs (dummystr, fpnt2);

   while (fgets(dummystr,120, fpnt) != NULL)
     fputs (dummystr, fpnt2);
   fclose (fpnt);

   IPROCNO;
   i1++;
}
END;

fclose (fpnt2);   /*close pp.all*/

RPROCNO(2);
IEXPNO;
i1=1;
i2=1;
i4++;
VIEWDATA;

}

QUITMSG("processing is complete");
```

Appendix 7. Raw area data obtained for all acid catalyzed and enzyme catalyzed reactions

alpha acid catalyzed

Trial1

unreacted **Carbon**

Spectrum	1	2	3	4	5	6	7
1	1.049	1.015	1.032	1.025	1.071	1.000	1.142
2	1.044	1.011	1.031	1.029	1.069	0.995	1.142
3	1.046	1.020	1.028	1.026	1.073	0.999	1.141
4	1.047	1.018	1.030	1.031	1.078	1.001	1.141
5	1.049	1.021	1.034	1.033	1.078	1.005	1.138
6	1.053	1.022	1.036	1.031	1.078	1.008	1.143
7	1.053	1.024	1.034	1.034	1.078	1.011	1.145
8	1.052	1.028	1.039	1.036	1.085	1.010	1.143
9	1.053	1.025	1.039	1.037	1.083	1.010	1.146
10	1.051	1.027	1.036	1.038	1.083	1.009	1.144
11	1.056	1.026	1.043	1.035	1.084	1.007	1.145
12	1.053	1.029	1.043	1.038	1.082	1.005	1.147
13	1.053	1.028	1.039	1.042	1.082	1.011	1.150
14	1.057	1.028	1.039	1.041	1.082	1.007	1.143
15	1.057	1.027	1.039	1.039	1.086	1.008	1.153
16	1.057	1.028	1.039	1.044	1.087	1.011	1.144
Average	1.052	1.024	1.036	1.035	1.080	1.006	1.144
stddev	0.004	0.005	0.004	0.006	0.005	0.005	0.004
95% CI	0.002	0.003	0.002	0.003	0.003	0.003	0.002
% CI in ave.	0.212	0.276	0.224	0.288	0.268	0.255	0.172

reacted **Carbon**

Spectrum	1	2	3	4	5	6	7
1	1.046	1.026	1.032	1.005	1.077	1.000	1.133
2	1.046	1.020	1.026	1.004	1.080	0.991	1.129
3	1.051	1.022	1.031	1.010	1.082	1.000	1.131
4	1.051	1.027	1.030	1.014	1.087	1.001	1.131
5	1.053	1.028	1.031	1.012	1.081	0.996	1.130
6	1.048	1.025	1.029	1.011	1.077	0.994	1.125
7	1.048	1.020	1.029	1.011	1.078	0.994	1.128
8	1.044	1.023	1.031	1.012	1.083	0.997	1.128
9	1.049	1.018	1.028	1.006	1.082	0.994	1.128
10	1.051	1.026	1.035	1.010	1.081	0.992	1.130
11	1.045	1.026	1.030	1.013	1.080	0.998	1.132
12	1.056	1.028	1.034	1.014	1.079	0.997	1.130
13	1.048	1.030	1.036	1.015	1.086	1.003	1.131
14	1.050	1.029	1.034	1.017	1.080	1.001	1.132
15	1.053	1.026	1.033	1.022	1.082	1.005	1.132
16	1.058	1.037	1.032	1.014	1.087	1.001	1.142
Average	1.050	1.026	1.031	1.012	1.081	0.998	1.131

Trial 2

unreacted	Carbon						
Spectrum	**1**	**2**	**3**	**4**	**5**	**6**	**7**
1	1.000	0.984	0.994	0.976	1.030	1.002	1.047
2	0.999	0.975	0.989	0.971	1.023	0.997	1.038
3	1.000	0.983	0.991	0.980	1.034	1.002	1.045
4	1.003	0.983	0.987	0.974	1.026	1.000	1.045
5	0.999	0.982	0.990	0.973	1.028	0.998	1.046
6	0.995	0.982	0.992	0.974	1.033	1.005	1.044
7	1.006	0.985	0.994	0.978	1.031	1.004	1.044
8	1.002	0.989	0.994	0.975	1.030	1.004	1.049
9	0.995	0.981	0.993	0.972	1.032	0.997	1.045
10	1.000	0.981	0.989	0.978	1.032	1.000	1.045
11	0.988	0.975	0.979	0.968	1.021	0.989	1.034
12	0.981	0.967	0.974	0.959	1.013	0.983	1.026
13	0.979	0.969	0.973	0.958	1.015	0.987	1.028
14	0.987	0.969	0.976	0.960	1.018	0.985	1.032
15	0.990	0.974	0.984	0.963	1.020	0.993	1.034
16	1.002	0.990	0.994	0.979	1.034	1.008	1.054
Average	0.995	0.979	0.987	0.971	1.026	0.997	1.041
stddev	0.008	0.007	0.008	0.007	0.007	0.008	0.008
95% CI	0.004	0.004	0.004	0.004	0.004	0.004	0.004
% CI in ave.	0.430	0.380	0.406	0.397	0.364	0.402	0.413

reacted	Carbon						
Spectrum	**1**	**2**	**3**	**4**	**5**	**6**	**7**
1	1.000	1.004	1.006	0.958	1.038	0.993	1.072
2	1.033	1.019	1.022	0.988	1.064	1.016	1.104
3	1.039	1.040	1.038	1.003	1.079	1.038	1.108
4	1.038	1.048	1.050	1.010	1.079	1.043	1.119
5	1.048	1.045	1.050	1.006	1.092	1.042	1.125
6	1.052	1.046	1.052	1.009	1.095	1.052	1.120
7	1.056	1.056	1.052	1.011	1.092	1.057	1.123
8	1.062	1.047	1.052	1.011	1.094	1.057	1.134
9	1.065	1.057	1.061	1.014	1.091	1.058	1.124
10	1.060	1.051	1.058	1.011	1.096	1.060	1.127
11	1.062	1.065	1.061	1.024	1.106	1.053	1.133
12	1.066	1.065	1.073	1.030	1.108	1.062	1.146
13	1.083	1.066	1.070	1.022	1.107	1.071	1.144
14	1.075	1.071	1.073	1.032	1.104	1.069	1.145
15	1.075	1.066	1.076	1.028	1.117	1.068	1.139
16	1.083	1.072	1.070	1.034	1.104	1.075	1.140
Average	1.056	1.051	1.054	1.012	1.092	1.051	1.125
stddev	0.021	0.019	0.019	0.019	0.019	0.021	0.019
95% CI	0.011	0.010	0.010	0.010	0.010	0.011	0.010
% CI in ave.	1.077	0.944	0.963	0.997	0.947	1.080	0.898

beta acid catalyzed

Trial1

unreacted **Carbon**

Spectrum	1	3	5	2	4	6	7
1	1.040	1.020	1.041	1.013	1.010	1.000	1.133
2	1.045	1.010	1.048	1.012	1.018	1.000	1.133
3	1.052	1.020	1.063	1.023	1.013	1.002	1.135
4	1.044	1.018	1.050	1.008	1.018	0.993	1.122
5	1.038	1.026	1.056	1.011	1.004	1.000	1.126
6	1.054	1.024	1.042	1.018	1.005	1.005	1.124
7	1.043	1.031	1.059	1.017	1.017	1.002	1.132
8	1.049	1.030	1.062	1.021	1.008	1.000	1.128
9	1.051	1.024	1.058	1.017	1.013	0.998	1.129
10	1.046	1.026	1.058	1.012	1.017	1.006	1.129
11	1.051	1.016	1.054	1.014	1.012	0.999	1.125
12	1.042	1.025	1.054	1.014	1.013	1.001	1.127
13	1.045	1.029	1.052	1.023	1.015	1.002	1.131
14	1.043	1.031	1.063	1.013	1.010	0.996	1.126
15	1.040	1.024	1.048	1.017	0.995	0.990	1.139
16	1.042	1.030	1.038	1.009	1.012	1.002	1.128
Average	1.045	1.024	1.053	1.015	1.011	1.000	1.129
stddev	0.005	0.006	0.008	0.005	0.006	0.004	0.004
95% CI	0.003	0.003	0.004	0.002	0.003	0.002	0.002
% CI in ave.	0.245	0.304	0.403	0.238	0.325	0.219	0.210

reacted **Carbon**

Spectrum	1	3	5	2	4	6	7
1	1.076	1.026	1.073	1.033	1.015	1.000	1.144
2	1.081	1.026	1.070	1.044	1.018	1.003	1.141
3	1.073	1.026	1.072	1.038	1.014	1.008	1.133
4	1.072	1.019	1.076	1.033	1.021	1.012	1.144
5	1.070	1.021	1.080	1.030	1.000	1.000	1.141
6	1.076	1.022	1.072	1.033	1.011	1.000	1.130
7	1.083	1.027	1.063	1.035	1.022	1.004	1.140
8	1.081	1.018	1.078	1.028	1.009	0.999	1.138
9	1.070	1.019	1.070	1.033	1.004	0.999	1.133
10	1.073	1.017	1.066	1.037	1.006	1.005	1.129
11	1.080	1.016	1.068	1.038	1.015	0.997	1.130
12	1.070	1.024	1.070	1.029	1.017	0.993	1.141
13	1.068	1.019	1.075	1.036	1.016	1.004	1.129
14	1.063	1.021	1.069	1.021	1.001	0.996	1.137
15	1.074	1.018	1.065	1.037	1.016	0.992	1.140
16	1.070	1.015	1.061	1.032	0.999	1.002	1.128
Average	1.074	1.021	1.070	1.034	1.012	1.001	1.136
stddev	0.005	0.004	0.005	0.005	0.008	0.005	0.006
95% CI	0.003	0.002	0.003	0.003	0.004	0.003	0.003
% CI in ave.	0.268	0.203	0.265	0.274	0.399	0.273	0.271

Trial 2

unreacted	Carbon						
Spectrum	**1**	**3**	**5**	**2**	**4**	**6**	**7**
1	1.000	0.993	1.021	0.969	0.964	0.984	1.059
2	1.004	0.987	1.018	0.971	0.964	0.984	1.061
3	1.005	0.990	1.015	0.970	0.964	0.987	1.053
4	0.997	0.986	1.012	0.964	0.956	0.989	1.052
5	1.002	0.990	1.019	0.965	0.962	0.980	1.048
6	1.001	0.990	1.013	0.961	0.965	0.983	1.046
7	1.001	0.988	1.015	0.968	0.964	0.985	1.054
8	0.997	0.984	1.020	0.966	0.967	0.987	1.056
9	0.995	0.982	1.009	0.965	0.966	0.991	1.050
10	1.006	0.983	1.017	0.969	0.963	0.983	1.051
11	0.996	0.985	1.017	0.964	0.963	0.982	1.054
12	0.995	0.988	1.016	0.960	0.963	0.987	1.048
13	0.994	0.982	1.013	0.962	0.960	0.987	1.051
14	1.002	0.987	1.011	0.961	0.959	0.992	1.048
15	1.002	0.978	1.013	0.969	0.964	0.981	1.057
16	1.004	0.986	1.018	0.966	0.963	0.990	1.057
Average	1.000	0.986	1.015	0.966	0.963	0.986	1.053
stddev	0.004	0.004	0.004	0.003	0.003	0.004	0.004
95% CI	0.002	0.002	0.002	0.002	0.001	0.002	0.002
% CI in ave.	0.205	0.201	0.184	0.193	0.150	0.191	0.224

reacted	Carbon						
Spectrum	**1**	**3**	**5**	**2**	**4**	**6**	**7**
1	1.000	0.960	1.010	0.960	0.938	0.958	1.026
2	1.004	0.969	1.011	0.966	0.946	0.958	1.024
3	1.006	0.972	1.013	0.957	0.942	0.965	1.031
4	0.998	0.964	1.013	0.960	0.947	0.959	1.029
5	1.005	0.968	1.013	0.956	0.942	0.956	1.025
6	1.003	0.965	1.011	0.962	0.949	0.955	1.027
7	1.000	0.967	1.004	0.956	0.946	0.954	1.030
8	1.005	0.975	1.008	0.957	0.951	0.963	1.024
9	1.006	0.968	1.015	0.959	0.953	0.958	1.030
10	1.007	0.962	1.015	0.960	0.951	0.965	1.029
11	1.006	0.971	1.005	0.968	0.955	0.964	1.025
12	1.005	0.972	1.019	0.962	0.955	0.964	1.027
13	1.011	0.969	1.017	0.961	0.944	0.965	1.029
14	1.011	0.971	1.019	0.967	0.953	0.965	1.033
15	1.002	0.970	1.011	0.960	0.952	0.961	1.027
16	1.006	0.962	1.017	0.968	0.949	0.964	1.030
Average	1.005	0.968	1.012	0.961	0.948	0.961	1.028
stddev	0.003	0.004	0.005	0.004	0.005	0.004	0.003
95% CI	0.002	0.002	0.002	0.002	0.003	0.002	0.001
% CI in ave.	0.184	0.229	0.240	0.223	0.286	0.218	0.134

alpha enzyme catalyzed

Trial1

unreacted

	Carbon						
Spectrum	**1**	**2**	**3**	**4**	**5**	**6**	**7**
1	1.000	0.976	0.994	0.982	1.031	1.002	1.069
2	1.004	0.980	0.996	0.983	1.034	0.998	1.070
3	1.009	0.980	1.001	0.984	1.035	1.006	1.068
4	1.011	0.984	1.000	0.989	1.036	1.006	1.068
5	1.008	0.986	1.002	0.991	1.041	1.004	1.070
6	1.008	0.988	1.001	0.988	1.038	1.001	1.073
7	1.011	0.983	1.000	0.992	1.037	1.004	1.071
8	1.007	0.987	1.005	0.987	1.042	1.006	1.070
9	1.012	0.985	1.002	0.987	1.039	1.004	1.072
10	1.014	0.984	0.996	0.991	1.040	1.009	1.072
11	1.008	0.987	1.001	0.989	1.035	1.004	1.070
12	1.014	0.985	1.005	0.994	1.042	1.009	1.074
13	1.014	0.992	1.003	0.994	1.040	1.007	1.075
14	1.012	0.991	1.002	0.995	1.041	1.006	1.072
15	1.009	0.988	1.004	0.990	1.036	1.003	1.074
16	1.014	0.990	1.001	0.991	1.039	1.003	1.073
Average	1.010	0.985	1.001	0.989	1.038	1.005	1.071
stddev	0.004	0.004	0.003	0.004	0.003	0.003	0.002
95% CI	0.002	0.002	0.002	0.002	0.002	0.002	0.001
% CI in ave.	0.206	0.233	0.168	0.211	0.161	0.157	0.110

reacted

	Carbon						
Spectrum	**1**	**2**	**3**	**4**	**5**	**6**	**7**
1	1.000	0.977	0.966	0.954	1.018	0.991	1.048
2	0.997	0.983	0.964	0.955	1.016	0.992	1.045
3	1.002	0.981	0.967	0.957	1.019	0.988	1.049
4	1.004	0.982	0.970	0.953	1.022	0.995	1.054
5	1.003	0.984	0.968	0.955	1.018	0.993	1.050
6	1.002	0.982	0.969	0.956	1.018	0.999	1.052
7	1.002	0.979	0.968	0.955	1.019	0.995	1.046
8	1.001	0.980	0.973	0.959	1.016	0.993	1.051
9	0.999	0.985	0.975	0.959	1.019	0.994	1.049
10	1.007	0.986	0.966	0.956	1.022	0.995	1.051
11	1.004	0.981	0.969	0.956	1.021	0.994	1.048
12	1.006	0.979	0.968	0.963	1.015	0.995	1.053
13	1.006	0.981	0.971	0.960	1.020	0.998	1.054
14	1.006	0.983	0.972	0.961	1.021	0.999	1.053
15	1.008	0.987	0.974	0.961	1.022	0.992	1.054
16	1.009	0.981	0.975	0.958	1.022	0.992	1.051
Average	1.004	0.982	0.970	0.957	1.019	0.994	1.051
stddev	0.003	0.003	0.003	0.003	0.002	0.003	0.003
95% CI	0.002	0.001	0.002	0.002	0.001	0.002	0.001
% CI in ave.	0.171	0.147	0.192	0.161	0.129	0.155	0.137

Trial 2

unreacted **Carbon**

Spectrum	1	2	3	4	5	6	7
1	1.048	1.018	1.028	1.020	1.069	1.000	1.127
2	1.047	1.019	1.028	1.018	1.070	0.997	1.128
3	1.050	1.020	1.027	1.021	1.069	0.999	1.130
4	1.048	1.019	1.031	1.021	1.071	0.997	1.128
5	1.049	1.018	1.027	1.015	1.070	0.997	1.130
6	1.049	1.017	1.027	1.020	1.070	0.997	1.128
7	1.049	1.016	1.025	1.019	1.068	0.998	1.128
8	1.050	1.017	1.026	1.017	1.070	0.997	1.128
9	1.047	1.018	1.026	1.017	1.070	0.997	1.131
10	1.048	1.022	1.026	1.022	1.069	0.995	1.128
11	1.048	1.018	1.028	1.019	1.070	0.996	1.128
12	1.049	1.018	1.031	1.023	1.069	0.999	1.129
13	1.049	1.020	1.028	1.020	1.070	1.001	1.128
14	1.050	1.020	1.030	1.019	1.070	1.001	1.130
15	1.047	1.019	1.029	1.020	1.069	1.000	1.130
16	1.053	1.025	1.032	1.025	1.075	1.001	1.130
Average	1.049	1.019	1.028	1.020	1.070	0.998	1.129
stddev	0.001	0.002	0.002	0.003	0.001	0.002	0.001
95% CI	0.001	0.001	0.001	0.001	0.001	0.001	0.001
% CI in ave.	0.073	0.109	0.102	0.133	0.073	0.106	0.055

reacted **Carbon**

Spectrum	1	2	3	4	5	6	7
1	1.055	1.015	1.007	1.015	1.066	1.000	1.130
2	1.049	1.014	1.009	1.014	1.065	0.993	1.134
3	1.053	1.012	1.009	1.011	1.065	0.994	1.126
4	1.052	1.012	1.007	1.015	1.064	0.996	1.130
5	1.054	1.017	1.008	1.012	1.065	0.997	1.132
6	1.055	1.018	1.012	1.017	1.063	0.997	1.125
7	1.052	1.018	1.011	1.019	1.062	0.996	1.128
8	1.056	1.020	1.013	1.015	1.065	0.998	1.132
9	1.058	1.020	1.012	1.021	1.065	0.998	1.130
10	1.054	1.018	1.013	1.019	1.068	1.001	1.132
11	1.057	1.019	1.015	1.017	1.069	0.997	1.132
12	1.060	1.015	1.014	1.017	1.065	0.996	1.130
13	1.057	1.019	1.014	1.021	1.066	0.997	1.136
14	1.056	1.021	1.013	1.020	1.067	0.998	1.129
15	1.054	1.018	1.011	1.019	1.064	0.999	1.135
16	1.056	1.018	1.010	1.019	1.067	0.999	1.130
Average	1.055	1.017	1.011	1.017	1.065	0.997	1.131
stddev	0.003	0.003	0.002	0.003	0.002	0.002	0.003
95% CI	0.001	0.002	0.001	0.002	0.001	0.001	0.002
% CI in ave.	0.133	0.148	0.130	0.165	0.089	0.112	0.143

Trial 3

unreacted **Carbon**

Spectrum	1	2	3	4	5	6	7
1	1.000	0.983	0.996	0.982	1.032	1.007	1.049
2	0.998	0.980	0.991	0.979	1.027	0.997	1.040
3	1.005	0.984	0.991	0.979	1.029	1.000	1.042
4	0.997	0.974	0.992	0.982	1.026	0.997	1.040
5	0.992	0.970	0.985	0.972	1.021	0.989	1.037
6	0.993	0.975	0.986	0.975	1.023	0.992	1.039
7	0.998	0.976	0.986	0.977	1.027	0.994	1.037
8	1.000	0.978	0.991	0.981	1.027	0.998	1.039
9	0.998	0.977	0.990	0.977	1.027	0.996	1.044
10	1.003	0.979	0.992	0.979	1.023	0.995	1.040
11	0.997	0.976	0.991	0.980	1.025	1.000	1.036
12	0.995	0.976	0.990	0.978	1.026	0.998	1.040
13	1.000	0.976	0.989	0.976	1.030	0.996	1.043
14	0.997	0.981	0.988	0.982	1.028	0.993	1.039
15	0.996	0.976	0.990	0.980	1.031	0.996	1.045
16	0.995	0.973	0.991	0.975	1.029	0.996	1.037
Average	0.998	0.977	0.990	0.978	1.027	0.997	1.040
stddev	0.003	0.004	0.003	0.003	0.003	0.004	0.003
95% CI	0.002	0.002	0.001	0.002	0.002	0.002	0.002
% CI in ave.	0.168	0.194	0.147	0.156	0.148	0.206	0.168

reacted **Carbon**

Spectrum	1	2	3	4	5	6	7
1	1.000	0.974	1.000	0.965	1.022	1.007	1.048
2	1.012	0.993	1.008	0.973	1.032	1.021	1.062
3	1.008	0.997	1.019	0.977	1.032	1.025	1.060
4	1.007	0.995	1.013	0.975	1.034	1.027	1.059
5	1.009	0.995	1.013	0.984	1.029	1.021	1.057
6	1.006	0.989	1.022	0.981	1.033	1.022	1.056
7	1.012	0.992	1.010	0.982	1.030	1.023	1.058
8	1.014	0.985	1.011	0.980	1.035	1.025	1.056
9	1.008	0.995	1.012	0.975	1.034	1.019	1.055
10	1.006	0.996	1.017	0.984	1.034	1.023	1.060
11	1.010	0.984	1.014	0.979	1.042	1.024	1.062
12	1.010	0.994	1.012	0.983	1.035	1.029	1.056
13	1.008	0.991	1.015	0.974	1.032	1.020	1.062
14	1.007	0.995	1.016	0.982	1.032	1.022	1.052
15	1.011	0.995	1.023	0.975	1.036	1.026	1.061
16	1.014	0.996	1.013	0.986	1.038	1.032	1.056
Average	1.009	0.992	1.014	0.978	1.033	1.023	1.058
stddev	0.004	0.006	0.005	0.006	0.004	0.005	0.004
95% CI	0.002	0.003	0.003	0.003	0.002	0.003	0.002
% CI in ave.	0.186	0.334	0.280	0.300	0.222	0.280	0.202

beta enzyme catalyzed

Trial1

unreacted

	Carbon						
Spectrum	**1**	**3**	**5**	**2**	**4**	**6**	**7**
1	1.051	1.028	1.060	1.010	1.015	1.000	1.125
2	1.046	1.028	1.064	1.011	1.013	1.006	1.120
3	1.045	1.030	1.058	1.009	1.015	1.004	1.123
4	1.044	1.024	1.058	1.009	1.014	1.010	1.123
5	1.048	1.022	1.059	1.009	1.014	1.005	1.123
6	1.046	1.026	1.052	1.011	1.016	0.999	1.125
7	1.040	1.024	1.059	1.015	1.015	1.003	1.120
8	1.043	1.025	1.054	1.010	1.012	1.001	1.122
9	1.047	1.023	1.059	1.003	1.008	1.007	1.122
10	1.040	1.025	1.056	1.011	1.014	1.006	1.119
11	1.045	1.029	1.058	1.011	1.014	0.997	1.117
12	1.045	1.029	1.060	1.007	1.011	1.005	1.123
13	1.045	1.025	1.058	1.004	1.011	1.001	1.125
14	1.043	1.022	1.059	1.007	1.013	1.006	1.119
15	1.041	1.023	1.062	1.013	1.016	1.001	1.123
16	1.044	1.028	1.060	1.008	1.017	1.000	1.122
Average	1.045	1.026	1.059	1.009	1.014	1.003	1.122
stddev	0.003	0.003	0.003	0.003	0.002	0.003	0.002
95% CI	0.002	0.001	0.001	0.002	0.001	0.002	0.001
% CI in ave.	0.148	0.137	0.140	0.161	0.125	0.184	0.109

reacted

	Carbon						
Spectrum	**1**	**3**	**5**	**2**	**4**	**6**	**7**
1	1.117	1.016	1.069	1.018	1.013	1.000	1.126
2	1.114	1.012	1.071	1.016	1.007	1.004	1.123
3	1.117	1.017	1.072	1.016	1.011	0.999	1.127
4	1.117	1.018	1.067	1.015	1.007	0.999	1.124
5	1.116	1.019	1.069	1.017	1.009	0.996	1.128
6	1.113	1.017	1.074	1.018	1.008	1.004	1.130
7	1.119	1.015	1.080	1.026	1.012	1.001	1.126
8	1.121	1.021	1.076	1.017	1.015	1.001	1.122
9	1.121	1.022	1.074	1.020	1.014	0.998	1.127
10	1.113	1.017	1.074	1.025	1.013	1.001	1.124
11	1.119	1.022	1.078	1.028	1.011	1.004	1.126
12	1.121	1.024	1.077	1.020	1.016	1.002	1.128
13	1.119	1.019	1.079	1.023	1.013	1.004	1.127
14	1.120	1.021	1.079	1.025	1.017	1.002	1.130
15	1.122	1.023	1.079	1.024	1.019	1.005	1.127
16	1.123	1.019	1.074	1.023	1.012	1.006	1.124
Average	1.118	1.019	1.074	1.021	1.012	1.002	1.126
stddev	0.003	0.003	0.004	0.004	0.003	0.003	0.002
95% CI	0.002	0.002	0.002	0.002	0.002	0.001	0.001
% CI in ave.	0.153	0.170	0.192	0.215	0.181	0.142	0.104

Trial 2

unreacted	Carbon						
Spectrum	1	3	5	2	4	6	7
1	1.000	0.983	0.996	0.982	1.032	1.007	1.049
2	0.998	0.980	0.991	0.979	1.027	0.997	1.040
3	1.005	0.984	0.991	0.979	1.029	1.000	1.042
4	0.997	0.974	0.992	0.982	1.026	0.997	1.040
5	0.992	0.970	0.985	0.972	1.021	0.989	1.037
6	0.993	0.975	0.986	0.975	1.023	0.992	1.039
7	0.998	0.976	0.986	0.977	1.027	0.994	1.037
8	1.000	0.978	0.991	0.981	1.027	0.998	1.039
9	0.998	0.977	0.990	0.977	1.027	0.996	1.044
10	1.003	0.979	0.992	0.979	1.023	0.995	1.040
11	0.997	0.976	0.991	0.980	1.025	1.000	1.036
12	0.995	0.976	0.990	0.978	1.026	0.998	1.040
13	1.000	0.976	0.989	0.976	1.030	0.996	1.043
14	0.997	0.981	0.988	0.982	1.028	0.993	1.039
15	0.996	0.976	0.990	0.980	1.031	0.996	1.045
16	0.995	0.973	0.991	0.975	1.029	0.996	1.037
Average	0.998	0.977	0.990	0.978	1.027	0.997	1.040
stddev	0.003	0.004	0.003	0.003	0.003	0.004	0.003
95% CI	0.002	0.002	0.001	0.002	0.002	0.002	0.002
% CI in ave.	0.168	0.194	0.147	0.156	0.148	0.206	0.168

reacted	Carbon						
Spectrum	1	3	5	2	4	6	7
1	1.000	0.974	1.000	0.965	1.022	1.007	1.048
2	1.012	0.993	1.008	0.973	1.032	1.021	1.062
3	1.008	0.997	1.019	0.977	1.032	1.025	1.060
4	1.007	0.995	1.013	0.975	1.034	1.027	1.059
5	1.009	0.995	1.013	0.984	1.029	1.021	1.057
6	1.006	0.989	1.022	0.981	1.033	1.022	1.056
7	1.012	0.992	1.010	0.982	1.030	1.023	1.058
8	1.014	0.985	1.011	0.980	1.035	1.025	1.056
9	1.008	0.995	1.012	0.975	1.034	1.019	1.055
10	1.006	0.996	1.017	0.984	1.034	1.023	1.060
11	1.010	0.984	1.014	0.979	1.042	1.024	1.062
12	1.010	0.994	1.012	0.983	1.035	1.029	1.056
13	1.008	0.991	1.015	0.974	1.032	1.020	1.062
14	1.007	0.995	1.016	0.982	1.032	1.022	1.052
15	1.011	0.995	1.023	0.975	1.036	1.026	1.061
16	1.014	0.996	1.013	0.986	1.038	1.032	1.056
Average	1.009	0.992	1.014	0.978	1.033	1.023	1.058
stddev	0.004	0.006	0.005	0.006	0.004	0.005	0.004
95% CI	0.002	0.003	0.003	0.003	0.002	0.003	0.002
% CI in ave.	0.186	0.334	0.280	0.300	0.222	0.280	0.202

Appendix 8. Raw fractionation factors for the calculated EIEs.

13C EIEs

25°C **fractionation factors**

ground-state

carbon	alpha-25B	alpha-4C1	alpha-B25	alpha-1S3
1	1.16710028	1.16729172	1.16519393	1.16502761
2	1.16808004	1.16683109	1.16774854	1.16668389
3	1.16065309	1.16800252	1.16403093	1.16710416
4	1.16164547	1.16744931	1.16185022	1.16489327
5	1.16166026	1.16534799	1.16441614	1.16182438
6	1.1501401	1.15247935	1.15129375	1.15045806

oxocarbenium

carbon	alpha-25B	alpha-4C1	alpha-B25	alpha-1S3
1	1.16350807	1.1631392	1.15992682	1.16219178
2	1.1610847	1.15246625	1.15965474	1.15360977
3	1.16470028	1.1605795	1.16512079	1.16305318
4	1.16208075	1.16416606	1.16293466	1.16812515
5	1.14409575	1.15061491	1.15148991	1.14694149
6	1.15108334	1.15189354	1.15096484	1.1494616

80°C

ground-state

carbon	alpha-25B	alpha-4C1	alpha-B25	alpha-1S3
1	1.12790203	1.12798918	1.12636265	1.12633349
2	1.1289418	1.127932	1.1285844	1.12790663
3	1.12315248	1.1289447	1.12574984	1.12835042
4	1.12386423	1.1285244	1.12409678	1.12653114
5	1.12390246	1.12675582	1.12617952	1.12408327
6	1.11641641	1.11805641	1.11729201	1.11672842

oxocarbenium

carbon	alpha-25B	alpha-4C1	alpha-B25	alpha-1S3
1	1.12684445	1.1265184	1.12396635	1.12579724
2	1.123691	1.11700134	1.12259287	1.1179444
3	1.12638801	1.1232052	1.12672214	1.12519234
4	1.12426856	1.12593766	1.12493611	1.12919785
5	1.11038033	1.11529893	1.11606213	1.1126849
6	1.11714592	1.11766732	1.11711092	1.11598759

25°C **fractionation factors**

ground-state

carbon	Beta-25B	Beta-4C1	Beta-B25
1	1.16621299	1.16964149	1.1641467
2	1.16847331	1.1685126	1.16479744
3	1.16687964	1.16828826	1.16575261
4	1.16285534	1.16768965	1.16113311
5	1.16057466	1.16594138	1.16518621
6	1.14993221	1.15267614	1.15152431

oxocarbenium

carbon	Beta-25B	Beta-4C1	Beta-B25	E4
1	1.16524698	1.16317759	1.15980712	1.162259
2	1.15843096	1.1524976	1.15971601	1.1555
3	1.16661618	1.16056169	1.16598931	1.161493
4	1.16405784	1.16416214	1.16367213	1.165212
5	1.14818778	1.15061335	1.15115723	1.152437
6	1.15153909	1.15189396	1.15070801	1.15031

80°C

ground-state

carbon	Beta-25B	Beta-4C1	Beta-B25
1	1.12721356	1.12996817	1.12563015
2	1.12926079	1.12933094	1.12632957
3	1.12804911	1.12913573	1.12710819
4	1.1248327	1.12870837	1.12352072
5	1.12301476	1.12719479	1.12673493
6	1.1162492	1.11821506	1.11748545

oxocarbenium

carbon	Beta-25B	Beta-4C1	Beta-B25
1	1.1281226	1.1265488	1.12386619
2	1.12170677	1.11702632	1.12263746
3	1.12790988	1.12319138	1.12739896
4	1.12590154	1.12593487	1.12552022
5	1.11356913	1.11529779	1.11578933
6	1.11759873	1.11766764	1.11691547

2H EIEs

25°C **fractionation factors**

ground-state

proton	alpha-25B	alpha-4C1	alpha-B25	alpha-1S3
1	13.54439824	13.12887836	13.48179498	12.8454579
2	12.6761663	12.70308552	12.73027965	13.06567072
3	12.78950621	12.62162636	12.84286813	12.53624861
4	13.06219927	12.73372813	12.30475717	12.77135148
5	13.08455646	12.63023815	12.85734451	13.259251
6	12.00476623	12.11398161	12.01016082	11.97274521
6	12.03969749	11.80425152	11.95936634	11.75255699

oxocarbenium

proton	alpha-25B	alpha-4C1	alpha-B25	alpha-1S3
1	10.97054715	10.81407528	11.20714035	10.88892282
2	12.784300	11.3620993	12.98743473	11.48336029
3	12.85972572	12.8051906	12.88280523	12.33929223
4	13.27485313	13.2274808	12.99671683	12.50802411
5	13.06434551	13.3972716	13.37455774	12.65044346
6	12.23080948	12.2403324	12.23210927	11.97541245
6	11.78119295	11.9056558	12.69664218	12.64268801

80°C

ground-state

proton	alpha-25B	alpha-4C1	alpha-B25	alpha-1S3
1	8.07911045	7.86711022	8.04588615	7.73470362
2	7.65514073	7.66889654	7.67955698	7.8624412
3	7.71466447	7.63381893	7.7395213	7.59799301
4	7.85019083	7.68907836	7.46267483	7.70991382
5	7.86224502	7.63158863	7.75512099	7.96137073
6	7.35943623	7.41738008	7.36464054	7.35144248
6	7.3817576	7.25922374	7.33918783	7.23989926

oxocarbenium

proton	alpha-25B	alpha-4C1	alpha-B25	alpha-1S3
1	6.8660187	6.78733455	6.98439351	6.82770692
2	7.720996	7.01243116	7.82144627	7.07370945
3	7.75498936	7.72571886	7.76475389	7.49960195
4	7.95465939	7.92535367	7.82421751	7.57643305
5	7.86245602	8.02304563	8.01243228	7.66726313
6	7.48029503	7.31288349	7.47227336	7.35721137
6	7.247163	7.48198703	7.70989657	7.69754686

2H EIEs

25°C **fractionation factors**

ground-state

proton	Beta-25B	Beta-4C1	Beta-B25
1	13.46811862	12.32752144	11.28197006
2	12.3942964	12.42338644	11.5091783
3	12.3539682	12.38826735	11.64603491
4	13.28501563	12.79565616	11.2319034
5	12.99737055	12.27626915	11.46221373
6	11.90095751	12.15043567	10.71377578
6	12.1027023	11.82509892	10.6573853

oxocarbenium

proton	Beta-25B	Beta-4C1	Beta-B25
1	10.96275624	10.814329	11.22015941
2	10.28918875	11.35528288	12.97815744
3	12.54505355	12.80640431	12.92755933
4	12.6481356	13.22846031	12.99184538
5	12.8568484	13.39587997	13.27059024
6	12.05941358	12.2401172	12.6801786
6	12.36287937	11.90511911	12.22153923

80°C

ground-state

proton	Beta-25B	Beta-4C1	Beta-B25
1	8.04124494	7.46704135	7.63558195
2	7.51754646	7.53717229	7.77474985
3	7.49257418	7.5111682	7.84911192
4	7.96432988	7.72071226	7.61806621
5	7.81867969	7.4488226	7.74098633
6	7.30965789	7.43541376	7.36586001
6	7.4145762	7.26960894	7.33510159

oxocarbenium

proton	Beta-25B	Beta-4C1	Beta-B25
1	6.86012415	6.78746625	6.99083838
2	6.44968719	7.00892444	7.81647485
3	7.59473162	7.72639557	7.78836512
4	7.64140456	7.92584191	7.82108192
5	7.76065544	8.02236549	7.96018476
6	7.38785019	7.31262262	7.46712452
6	7.54288205	7.48187784	7.70327213

Appendix 9. Data for the enzyme kinetics.

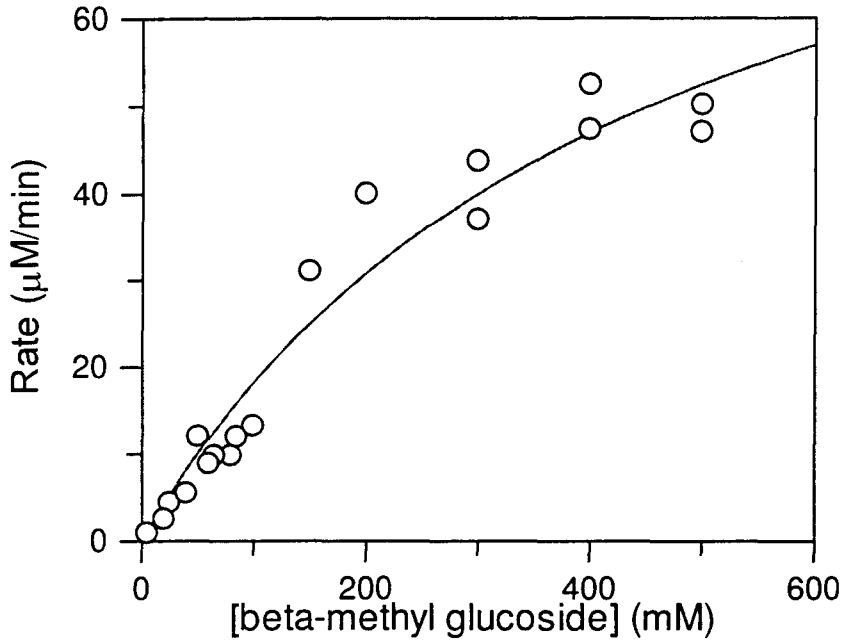

Parameter	Value	Std. Error
Vmax	98.7227	17.5181
Km	440.9230	135.7749

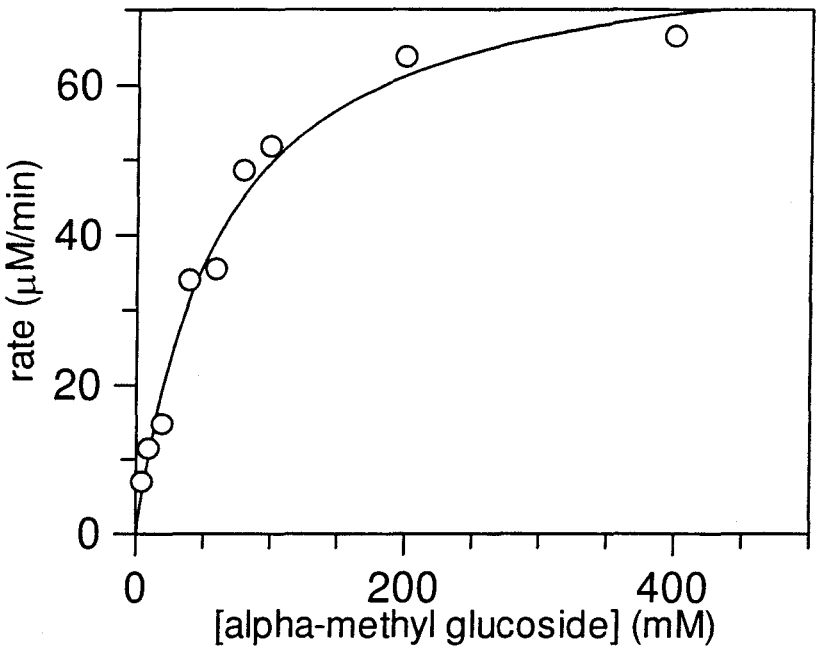

Parameter	Value	Std. Error
Vmax	80.0487	4.3798
Km	61.2765	9.2036

Appendix 10. Raw data for the T1 experiments.

delay time	C1	C2	C3	C4	C5	C6	C7
0.01	-16.501	-16.498	-16.131	-16.377	-16.892	-14.613	-19
0.05	-13.972	-13.658	-13.298	-13.449	-13.92	-9.716	-19
0.1	-9.933	-9.813	-9.432	-9.587	-10.043	-3.848	-19
0.2	-1.687	-1.448	-1.238	-1.241	-1.641	7.405	-19
0.5	14.21	14.29	14.16	14.6	14.58	19	-5.778
1	18.48	18.41	18.04	18.45	19	17.57	9.3
3	18.47	18.34	17.97	18.43	19	17.27	15.9
5	18.55	18.32	18.01	18.53	19	17.31	18.88
8	17.63	17.56	17.19	17.56	18.02	16.36	19

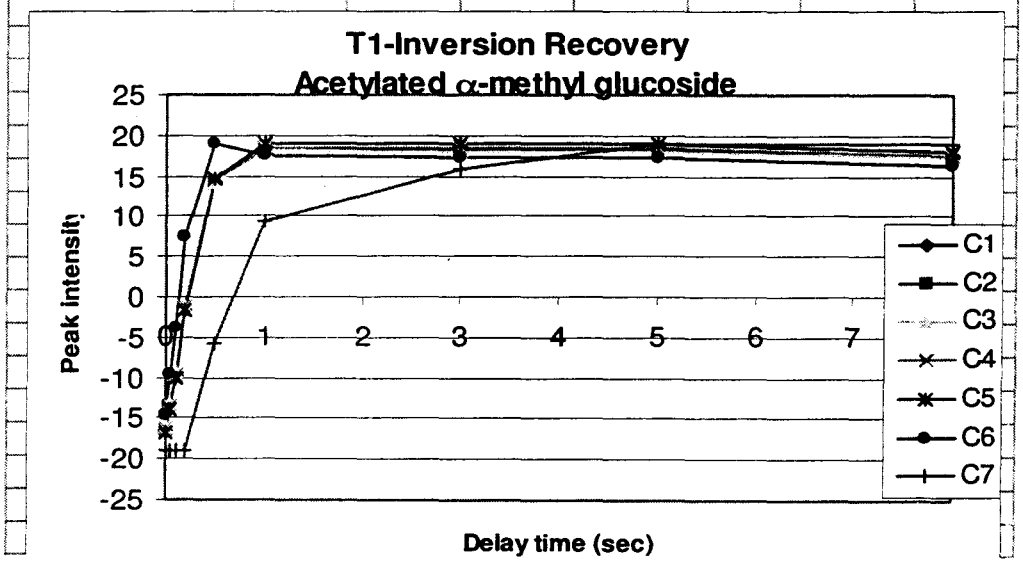

delay time (s)	C1	C2	C3	C4	C5
0.1	-32415498	-43574663	-64514924	-62164553	
1	-30886530	-40894565	-58139851	-56708800	1429007
5	-18603790	-21283508	-26161664	-26067649	20036992
10	-4265885	-1211480	6705624	5456121	37942554
20	14337937	24153103	39175158	37245392	56858483
30	24246948	36358459	53578385	51171741	66105706
40	28926936	42485041	60722055	58261822	71068274
60	35533905	48761852	66617474	64082088	74423877
90	38744750	51227487	67178057	64726204	74518609
120	40139380	52156297	67597759	65387357	75077732

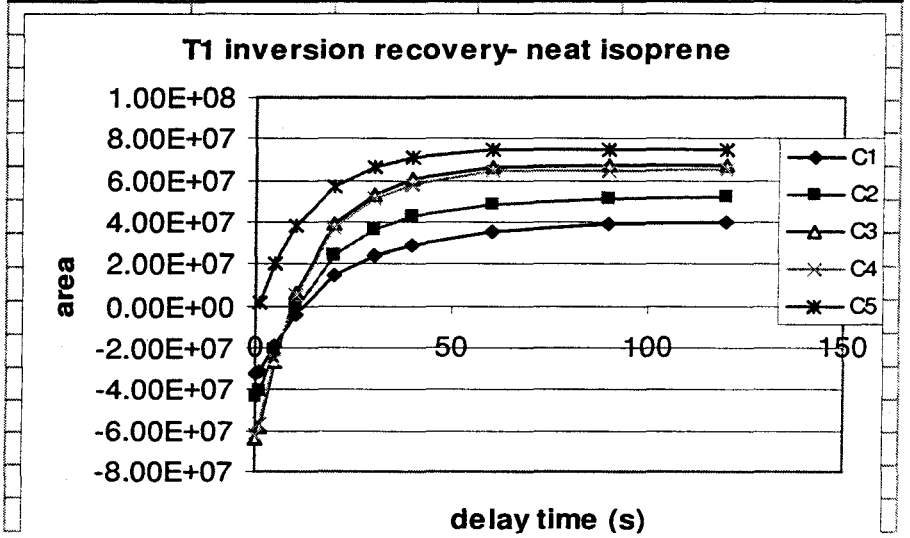

5 References:

[1] Johnston, H.S. *Gas Phase Reaction Rate Theory.* (1966) Ronald Press, Co., New York.

[2] Harris, D.C and Bertolucci, M.D. *Symmetry and Spectroscopy an Introduction to Vibrational and Electronic Spectroscopy.* (1978) Dover publications Inc. New York.

[3] Bigeleisen, J.; Goeppert, M. *J. Phys. Chem.* (1947) 15, 126.

[4] Bigeleisen, J.; Wolfsberg, M. *Adv. Chem. Phys.* (1958) 1, 15.

[5] Berti, P.J. and Tanaka, K.S.E. *Adv. Phys. Org. Chem.* (2002) 37, 239.

[6] Ferscht, A.R. *Structure and Mechanism in Protein Science.* (1999) *W.H. Freeman and Co, USA.*

[7] Rose, I.A.; O'Connell, E.L; Litwin, S; Bar Tana, J. *J. Biol. Chem.* (1974) 249, 5163.

[8] Rose, I.A. *Methods Enzymol.* (1980) 64, 47.

[9] Martin, G.J. and Martin M.L., *Tetrahedron Lett.* (1981) 22, 3525.

[10] Grant, D.M; Curtis, J.; Croasmun, W.R.; Dalling, D.K.; Wehrli, F.W.; Wehrli, S.; *J. Am. Chem. Soc.* (1982) 104, 4492.

[11] Pascal, R.A., Jr.; Baum, M.W.; Wagner, C.K.; Rodgers, L.R. *J. Am. Chem. Soc.* (1984) 106, 5377.

[12] Pascal, R. A., Jr.; Baum, M.W.; Wagner, C. K.; Rodgers, L.R.; Huang, D.S. *J. Am. Chem. Soc.* (1986) 108, 6477.

[13] Zhang, B.L., *Mag. Res. Chem.* (1988) 26, 955.

[14] Zhang, B.L.; Pionnier, S. *J. Phys. Org. Chem.* (2001) 14, 239.

[15] Zhang, B.L.; Wu, W.X.; Gao, Z.H.; Sun, X.Y. *Acta Chim. Sin.* (1986) 44, 437.

[16] Singleton, D.A.; Thomas, A.A. *J. Am. Chem. Soc. (*1995) 117, 9357.

[17] Singleton, D. A.; Schulmeier, B. E.; Hang, C.; Thomas, A. A.; Leung, S.-W.; Merrigan, S. R. *Tetrahedron* (2001) 57, 5149.

[18] Singleton, D. A.; Merrigan, S.R. *J. Am. Chem. Soc.* (2000) 122, 11035.

[19] Singleton, D. A.; Hang, C. *J. Am. Chem. Soc.* (1999) 121, 11885.

[20] Meyer, M.P.; DelMonte, A.J.; Singleton, D.A. *J. Am. Chem. Soc.* (1999) 121, 10865.

[21] Singleton, D.A.; Szymanski, M.J. *J. Am. Chem. Soc.* (1999) 121, 9455.

[22] Singleton, D.A.; Hang, C.; Szymanski, M.J.; Greenwald, E.E. *J. Am. Chem. Soc.* (2003) 125, 1176.

[23] Friebolin, H. *Basic One- and Two-Dimensional NMR Spectroscopy* (1993) VCH, Germany.

[24] Evilia, R.F. *Anal. Lett.* (2001) 34, 2227.

[25] Griffiths, L ; A.M. Irving. *Analyst* (1998) 123, 1061.

[26] Kraut, J. *Science* (1988) 242, 533.

[27] Messing, Rita B.; Phebus, Lee; Fisher, Laurel A.; Lytle, Loy D. *Psychopharmacology Communications* (1976) 1, 511.

[28] Berti, P.J.; Blanke, S.R.; Schramm, V.L. *J. Am. Chem. Soc.* (1997) 119, 12079.

[29] Scheuring, J.; Berti, P.J.; Schramm, V.L. *J. Am. Chem. Soc.* (1998) 37, 2748.

[30] Chen, X.-Y.; Berti, P.J.; Schramm, V.L. *J. Am. Chem. Soc.* (2000) 122, 1609.

[31] Chen, X.-Y.; Berti, P.J.; Schramm, V.L. *J. Am. Chem. Soc.* (2000) 122, 6527.

[32] Bruner, M; Horenstein, B. A. *Biochemistry.* (1998) 37, 289.

[33] Cleland, W. W. Protein Pept. Lett. (2000) 7, 305.

[34] Weiss, P.M.; Gavva, S.R.; Harris, B.G.; Urbauer, J.L.; Cleland, W. W.; Cook, P. F. *Biochemistry* (1991) 30(23), 5755.

[35] Grissom, C. B.; Cleland, W. W. *Biochemistry* (1985) 24(4), 944.

[36] Hermes, J.D.; Roeske, C. A.; O'Leary, M.H.; Cleland, W. W. *Biochemistry* (1982) 21, 5106.

[37] Kline, P.C.; Rezaee, M.; Lee, T. *Anal. Biochem.* (1999) 275(1), 6-10.

[38] Rising, K.A.; Schramm, V. L. *J. Am. Chem. Soc.* (1997) 119(1), 27.

[39] Werner, R.M.; J.T. Stivers., Biochemistry (2000) 39, 14054.

[40] Tanaka, K.S. E.; Chen, X.-Y.; Ichikawa, Y.; Tyler, P.C.; Furneaux, R.H.; Schramm, V.L.;. *Biochemistry* (2001) 40, 6845.

[41] Miles, R.W.; Tyler, P.C.; Furneaux, R.H.; Bagdassarian, C.K.; Schramm, V.L.; *Biochemistry* (1998) 37, 8615.

[42] Evans, G.B.; Furneaux, R.H.; Gainsford, G.J.; Hanson, J.C.; Kicska, G.A.; Sauve, A.A.; Schramm, V.L.; Tyler, P.C.; *J. Med. Chem.* (2003) 46, 155.

[43] Wolfenden, R.; Lu, X.; Young, G.; *J.Am. Chem Soc.* (1998) 120, 6814-6815.

[44] Radzicka, A.; Wolfenden, R.; *Science* (1995) 267, 90-93.

[45] Radzicka, A.; Wolfenden, R.; *J. Am. Chem. Soc.* (1996) 118, 6105-6109.

[46] Ege, S. *Organic Chemistry.* 3rd ed. (1994) D.C. Heath and Co., Toronto.

[47] Jeffery, G.A.; Pople, J.A.; Radom, L. *Carbohyd. Res.* (1972) 25, 117.

[48] Wolfe, A; Whangbo, W-H; Mitchell, D.J. *Carbohyd. Res.*(1979) 69, 1.

[49] Van-Catledge, F.A. *J. Am. Chem. Soc. (1974) 96, 5693.*

[50] Williams, J.F.A . *Tetrahedron* (1962) 18, 1477.

[51] Delongchamps, P. *Tetrahedron* (1975) 31, 2463.

[52] Perrin, C.L. *Acc. Chem. Res.* (2002), 35, 28.

[53] Henrissat, B.I; Bairoch, A. *Curr.Opin.Struct. Biol.* (1997) 7, 637-644.

[54] Sinnott, M.L. *Chem Rev.* (1990) 90, 1171.

[55] Zechel, D.; Withers,S.G. *Acc. Chem. Res.* (2000) 33, 11-18.

[56] Hehre, E.J. *Carbohydrate Research* (2001) 331, 347.

[57] Withers, S.G. *Carbohydrate polymers* (2001) 44, 325-337.

[58] Vasella, A; Davies, G.J.; Bohm, M. *Curr. Opin. Chem. Biol.*, (2002) 6, 619-629.

[59] Hecht, S.M. *Bioorganic chemistry: Carbohydrates*; Oxford University press: New York, 1999.

[60] Winchester, B.G.; Fleet, G.W. *Glycobiology* (1992) 2, 199.

[61] Humphries, M.J.; Matsumoto, K.; White, S.L.; Olden, K. *Cancer Res.* (1986) 46. 5216.

[62] Rowe, P.M. *The Lancet.* (1999),354 402.

[63] Karpas, A.; Fleet, G.W.J.; Dwek, R.A.; Petursson, S.; Namgoong, S.K.; Ramsden, N.G.; Jacob, G.S.; Rademacher, T.W. . *Proc. Natl. Acad. Sci.* USA. (1988) 85, 9229.

[64] Asano, N.; Nash, R.J.; Molyneux, R.J. ; Fleet, G.W.J. *Tetrahedron.* (2000) 11, 1645.

[65] Heightman, T.D ; A.T. Vasella. *Agnew. Chem. Int. Ed.* (1999) 38, 750-770.

[66] Pistia-Brueggeman , G. ; R.I. Hollingsworth. *Tetrahedron,* (2001) 57, 8773.

[67] Bols, M.; Lillelund, V.H.; Jensen, H.H.; Liang,X. *Chem. Rev.* (2002) 102, 515.

[68] Tanaka, K.S.E. ; A.J. Bennet. *Can J. Chem.* (1998) 76, 431.

[69] Tanaka, K.S.E.; Winters, S.G.; Batchelor, R.J.; Einstein, F.W.B.; Bennet, A.J. J. *Am. Chem. Soc.* (2001) 123, 998.

[70] He, S.and S.G. Withers. *J. Biol. Chem.* (1997) 272, 24864.

[71] Barrett,T; Suresh, C.G.; Tolley,S.P.; Dodson,E.J.; Hughes, M.A. *Structure* (1995) 3, 951.

[72] Withers,S.G.; Warren, R.A.J; Street, I.P.; Rupitz, K; Kempton, J.B.; Aebersold, R. *J. Am. Chem. Soc.* (1990) 112, 5887.

[73] Wang, Q.; Graham, R.W.; Trimbur, D.; Warren, R.A.J.; Withers, S.G. *J. Am. Chem. Soc.* (1994) 116, 11594

[74] Koshland, D.E. *Biol. Rev.* (1953) 28, 416-436.

[75] White, A. ; Rose, D.R. *Curr. Opin. Struct. Biol.* (1997) 7, 645.

[76] Gutherie, R.D. ; Jencks, W.P. *Acc. Chem Res.*(1989) 22, 343.

[77] Young, P.R.; W.P. Jencks. *J. Am. Chem. Soc.* (1977) 99, 8238.

[78] Amyes, T.L.; W.P. Jencks. *J. Am. Chem. Soc.* (1989) 111, 7888.

[79] Melander, L.; Saunder, W.H. *Reaction Rates of Isotopic Molecules;* (1980), Wiley Interscience, New York.

[80] Berti, P.J. *Methods in Enzymology.* (1999) 308, 355.

[81] Poirier, R.A.; Wang, Y. ; K.C Westaway. *J. Am. Chem. Soc.* (1994) 116, 2526.

[82] Matsson, O.; Westaway, K. C. *Adv. Phys. Org. Chem.* (1998) 31, 143-248.

[83] Sunko, D.E., Szele, I ; Hehre, W.J. *J. Am. Chem. Soc.* (1977) 99, 5000.

[84] Bennet, A.J.; Sinnot, M.L. *J. Am. Chem. Soc.* (1986) 108, 7287.

[85] Zhang, Y; Bommuswamy, J.; Sinnott, M.L. *J. Am. Chem. Soc.* (1994) 116, 7557.

[86] Huang, X.; Tanaka, K.S.E.; Bennet, A, J. *J. Am. Chem. Soc.* (1997) 119, 11147.

[87] Indurugalla, D.; Bennet, A.J. *J. Am. Chem. Soc.* (2001) 123, 10889.

[88] Rosenberg, S.; Kirsch, J.F. *Biochemistry*, (1981) 20, 3189.

[89] Tanaka,Y.; Tao,W.; Blanchard, J.S.; Hehre, E.J.; *J. Biol. Chem.* (1994) 269, 32306.

[90] Calculated from the ^{14}C from the Swain-Schaad relationship $(^{13}CKIE)^{1.89} = (^{14}CKIE)$

[91] Rosenberg, S.; Kirsch, J.F. *Biochemistry*, (1981) 20, 3196.

[92] Parkin,D.W.; Horenstein,B.A.; Abdulah,D.R.; Estupinan,B.; Schramm, V.L. *J. Biol. Chem.* (1991) 266, 20658-20665.

[93] Laemmli, U.K. *Nature.* (1970) 227, 680-685.

[94] Saunders, M.; Laidig, K.E.; Wolfsberg, M. *J. Am. Chem. Soc.* (1989) 111, 8989-8994.

[95] Becke, A.D. *Phys. Rev.* A (1988) 38, 3098.

[96] Perdew, J.P.; Wang, Y. *Phys Rev.* B 1992. 45. 13244.

[97] Hansen, S.U.; Plesner I.W.; Bols, M. *CHEMBIOCHEM.* (2000) 1, 177-180

[98] Dale, M.P.; Ensley, H.E.; Kern, K. ; Sastry, K. A. R.; Byers, L. D. *Biochemistry*, (1985) 24, 3530

[99] Hosie, L. ; Sinnott, M.L. *Biochem. J.* (1985) 226, 437.

[100] Homer, J. ; Valdivieso Cedeno, E.R. *J. Chem. Soc. Faraday Trans. 2* (1983) 79, 1021.

[101] Blake, C.C.; Johnson, L.N.; Mair, G.A.; North, A.C.; Phillips, D.C.; Sarma,V.R. *Proc. Roy. Soc.* (1967) 167, 378.

[102] Philips, D.C. *Proc. Natl. Acad. Sci. U.S.* (1967) 57,484

[103] Horenstein, B.A. *J. Am. Chem. Soc.* (1997) 119, 1101.

[104] Singleton, D.A.; Merrigan, S.R.; Kim, B.J.; Beak, P.; Phillips, L.M.; Lee, J.K.; *J. Am. Chem. Soc.* (2000) 122, 3296.

[105] Krishnamurthy, V.V.; Surya Prakash, G. K.; Iyer, P.S. ; Olah, G.A. *J. Am. Chem. Soc.* (1985) 107, 5015.

[106] Ferscht, A.R. *Structure and Mechanism in Protein Science* (1999) W.H. Freeman and Company, New York.

[107] Cocker, D.; M.L. Sinnott. *J. Chem. Soc. Perkin 2.* (1975) 13, 1391.

[108] Houben, R.; de Ruijter, C.F.; Brunt, K. *J. Cereal. Sci,* (1997) 26, 37.